Identifying Geologically Meaningful U-Pb Dates in Fossil Teeth

by

Stephanie Nichols

A thesis submitted in partial fulfillment of the requirements for the degree of

Master of Science

Department of Earth and Atmospheric Sciences
University of Alberta

Abstract

Dating attempts on fossil material have thus far yielded mixed results. While successes have been reported on single specimens, most fossils are thought to have experienced a complex history that obscures a simple determination of age. For this thesis, transects along the cross-sections of 14 fossil alligorid teeth from the Arroyo Chijuillita Member of the Nacimiento Formation, New Mexico, and tyrannosaur and crocodilian teeth from the Dinosaur Park Formation, Alberta were analysed for their trace elements and U-Pb isotope composition using laser ablation ICP-MS. The reliability of this method is supported by good agreement in the TIMS (61.5±1.6 Ma) and laser ablation ICP-MS (64.9±3.6 Ma) dates for a targeted tooth region.

The cross-sectional profile of Y concentration in fossil teeth was found to be a good indicator of the extent of post-fossilisation alteration: the highest-gradient Y profiles (Patterns 1 and 2: 2-3 orders of magnitude variation) tend to indicate preservation of pristine geochemical profiles where meaningful fossilisation dates can be obtained, while lower Y gradients (Patterns 3-4) are associated with progressive disturbance of the fossilisation-age signature. In the Arroyo Chijuillita Member, the U-Pb system preserved in the fossil teeth analyzed can be considered a mixing between the fossilisation-age, low-Y center of a Pattern 2 sample (64.2±5.4 Ma) and a Pattern 4 sample preserving an alteration age (25.7±2.1 Ma) corresponding to the end of large-scale volcanic activity in the Four Corners region. In the Dinosaur Park Formation, the U-Pb data yield a date of 71.8±9.4 Ma from a Pattern 1 sample at low $^{238}U/^{206}Pb$ and altered analyses skewing towards higher $^{238}U/^{206}Pb$ values. Disturbed dates are ~49 Ma, possibly related to the last pulse of Rocky Mountain formation, and ~33 Ma, which has not been tied to a known geological event. A simple geochemical screen using Y profiles can be used to monitor the extent of post-fossilisation alteration. Using this geochemical screen, regions of bioapatite that preserve U-Pb fossilisation and post-fossilisation alteration dates can be discerned.

Preface

  This thesis is a collaborative work by Stephanie Nichols, building on the work of Dr. Larry Heaman at the University of Alberta. The New Mexico samples were collected by Dr. Thomas Williamson (New Mexico Museum of Natural History and Science), and the Alberta samples by Dr. Phil Currie (University of Alberta). Some data included in this thesis was collected by Larry Heaman. The section on the New Mexico geological setting specific to the samples was contributed by Thomas Williamson. The literature review, broader geological setting, and data analysis are my original work, with the guidance of Larry Heaman.

  This thesis includes acknowledgement of those who've contributed samples, skill and support, and a general introduction discussing the basis of this investigation. This is followed by the main thesis, which will be submitted for publication to Geochimica et Cosmochimica Acta, and appendices addressing aspects of the data not fully explored in the main thesis. These include the geochemical similarities between Y and the REE in fossil teeth, the possibility of using Sr isotopes as a paleodiet indicator, the possibility of preserving *in vivo* geochemical signatures, and applying the method developed in the body of the thesis to two additional teeth from different units.

Acknowledgements

Table of Contents

List of Acronyms

AB: Alberta

DPF: Dinosaur Park Formation

DPP: Dinosaur Provincial Park

IDTIMS: Isotopic Dilution Thermal Ionization Mass Spectrometry

LA ICP-MS: Laser Ablation Inductively Coupled Plasma Mass Spectrometer

NM: New Mexico

SHRIMP: Sensitive High-Resolution Ion Microprobe

SJB: San Juan Basin

TIMS: Thermal Ionization Mass Spectrometry

List of Tables

List of Figures

1 Introduction

During permineralization of fossil vertebrates, bioapatite is converted from hydroxlapatite to fluoroapatite, pore spaces are filled, and trace element enrichment occurs. However, the fossilisation of teeth is still inadequately understood (Kohn, 2008). The standard model of fluid infiltration from the exterior edges of the tooth inward is increasingly being questioned: it has been postulated that the first stage of trace element uptake occurs from the center of the tooth outward, while any later uptake would need to occur from the edges inward due to the extensive filling of pore space that occurs in the first stage (Kohn, 2008; Kohn & Moses, 2013). Most studies have reported that the concentration of trace elements generally decreases from the edge of a sample to the center (e.g. Toyoda and Tokonami, 1990; Trueman et al., 1999; Herwartz et al., 2011), however that is not always observed (Kowal-Linka et al., 2014). There is some debate in the literature as to which mechanism(s) control this trace element uptake, with most of the work being done on bone (e.g. Millard and Hedges, 1996; Toyoda & Tokonami, 1990; Kohn & Moses, 2013; Herwartz et al., 2011). The implications of these mechanisms are also debated. Some studies have concluded that fossils record an early diagenetic signature (e.g. Trueman et al., 1999), and others suggest this is outside the realm of possibility (e.g. Kowal-Linka et al., 2014).

There have been numerous attempts at radiogenic isotope dating of fossils, with use of the U-Pb (e.g. Sano and Terada, 1999; Romer, 2001; Sano and Terada, 2001; Sano et al., 2006; Fassett et al., 2011) and Lu-Hf systems (e.g. Herwartz et al., 2011) being the most common. A small (2 mm^2) fresh-water shark tooth was dated using a SHRIMP (Sensitive High-Resolution Ion Microprobe) instrument, resulting in a $^{238}U/^{206}Pb$ isochron date of 266±18 Ma (Sano and Terada, 1999). The host sedimentary sequence is Early Permian (256 – 290 Ma); the U-Pb date is thus similar to the age of deposition (Sano and Terada, 1999). In another study, a conodont micro-fossil yielded a $^{238}U/^{206}Pb$ isochron date of 323±36 Ma; this was found to be in good agreement with the Carboniferous age of the strata, but specific age information on this unit is not reported (Sano and Terada, 2001).

Similarly, an Allosaurid tooth yielded a Tera-Wasserburg concordia intercept date of 115±10 Ma; however, the depositional age of the host strata (the Hasandong Formation, Korea) is poorly constrained (Sano et al., 2006). In situ U-Pb dating by laser ablation ICP-MS was successfully preformed on two dinosaur bones near the Cretaceous-Paleogene interface. The Cretaceous bone yielded a date of 73.6±0.9 Ma, in agreement with the $^{40}Ar/^{39}Ar$ date derived from a proximal ash bed (73.04±0.25 Ma). A second bone from above the Cretaceous-Paleogene boundary gave a date of 64.8±0.9 Ma (Fassett et al., 2011), a finding that has caused much discussion (Koenig et al., 2012; Renne & Goodwin, 2012; Ludwig, 2012).

While there have been numerous studies examining either the geochemistry or geochronology of bioapatite, there have been few attempts to combine the two datasets. An important exception is Kocsis et al. (2010), where they reported young Lu-Hf dates, and therefore interpreted open-system behavior with regards to REE and/or Hf in bone.

In this study, the trace element geochemistry and the U-Pb geochronology are compared for fossil teeth from the Arroyo Chijuillita Member of the Nacimiento Formation in New Mexico and from the Dinosaur Park Formation in Alberta. This dual geochemistry plus geochronology approach is used to explore the relationship between trace element geochemistry and U-Pb dates. We seek to determine whether there is an element or group of elements that are good indicators of the presence and extent of post-fossilisation alteration, and whether different teeth from the same unit variably preserve geochemical evidence for the same fossilisation and post-fossilisation processes. We also seek to identify differences in fossilisation and post-fossilisation geochemical signatures between the Alberta and New Mexico samples, that can be attributed to broader geological events in these areas. Elucidating the relationship between the trace element and the isotopic compositions of bioapatite may allow for the derivation of meaningful fossilisation and alteration U-Pb dates, laying the groundwork for a better understanding of the underlying fossilisation and post-fossilisation processes.

2 Geological Setting

The formation of the Cordillera throughout the Jurassic and Cretaceous periods caused lithospheric loading and downwarping, resulting in the formation of the Western Interior Basin and the Western Interior Seaway (Cant and Stockmal, 1989). This foreland basin extended from the Canadian Arctic to the Gulf of Mexico and from western British Columbia to Saskatchewan (Lehman, 1987). The Western Canadian Sedimentary Basin covers much of Western Canada from the Rocky Mountains to the Canadian Shield and includes deposition of the Belly River Group in Alberta's Dinosaur Provincial Park (Figure 1a). The San Juan Basin is a late Campanian to Eocene segment of the Western Interior Basin in the Four Corners region of New Mexico (Figure 1b).

In Campanian time, the Western Interior Seaway covered much of Western Canada and Western to Midwestern United States (Figure 1c). By the end of the Cretaceous, the Western Interior Seaway was separated into north and south embayments (Figure 1d); continental sedimentary deposits thus dominated the basin at this time (Lehman, 1987). Cordilleran thrusting continued until ~50 Ma (Figure 1e; Panǎ et al., 2015), and magmatism in the Western Plains migrated southward with time, with magmatism at ~52 Ma in Montana (Figure 1e), and in Colorado and New Mexico between ~38 and 23 Ma (Figure 1f).

3 Local Geology

The age of the fossils recovered from the Arroyo Chijuillita Member of the Nacimiento Formation and the Dinosaur Park Formation of the Belly River Group are constrained by the age of the host units. The post-depositional geological history of the region is relevant to this study as well, because disturbance of the fossilisation-age U-Pb signature is thought to occur through interaction with fluids (Millard and Hedges, 1996), which will result in secondary dates younger than the age of fossilisation (Romer, 2001). It is thus possible that tectonic, magmatic and fluid flow events might alter the geochemistry and geochronology of fossil teeth.

3.1 Nacimiento Formation

3.1.1 Stratigraphy

The San Juan Basin was formed in response to the Laramide orogeny, with deposition occurring relatively consistently throughout the late Mesozoic and early Cenozoic eras. Although some of the stratigraphy is disputed, the major units, in ascending stratigraphic order, are the 1) Pictured Cliffs sandstone, 2) Fruitland Formation, 3) Kirtland Formation, 4) Ojo Alamo Sandstone, 5) Nacimiento Formation, and 6) San Jose Formation (Figure 1b; Baltz, 1967). The Pictured Cliffs sandstone is a shoreline-facies medium-grained unit representing a regression event (Baltz, 1967). The Fruitland Formation is dominated by coal and shale, and represents a deltaic environment proximal to the Western Interior Seaway. The Fruitland Formation transitions upsection into alluvial floodplains with high-sinuous, then low-sinuous streams through the Kirtland Formation (Williamson and Brusatte, 2014). The Naashoibito member is often considered part of the Kirtland Formation, and comprises a basal conglomerate, purple and grey mudstones representing paleosols, and clay-rich white sandstones (Williamson and Brusatte, 2014). The Ojo Alamo sandstone is a coarse-grained, trough-crossbedded unit representing paleochannel facies (Sikkink, 1987), and rests conformably below the Nacimiento Formation.

The Nacimiento Formation has been subdivided into three members by Williamson and Lucas (1993); in ascending order, they are 1) the Arroyo Chijuillita Member, 2) the Ojo Encino Member, and 3) the Escavada Member (Figure 1b). The Arroyo Chijuillita Member is a finer-grained unit dominated by organic-rich mudstone and siltstone, with occasional sandstone lenticulars. The environment is interpreted as an alluvial floodplain: the local abundance of crocodilians and Champosaurus fossils are in agreement with this interpretation (Williamson, 1996). The Ojo Encino Member contains siltstone and organic-rich mudstone sequences, but is distinguished from the Arroyo Chijuillita Member by a higher proportion of sandstone, including a thick basal sheet (Williamson, 1996). The Escavada Member is

4

dominated by coarse-grained sandstone, with thin layers of organic-rich mudstone that may represent paleosols (Williamson, 1996).

3.1.2 Age constraints on samples

The Nacimiento Formation is composed of alluvial floodplain deposits that were deposited in riverine and overbank environments (Williamson, 1996). Locality L-646 is from Mammalon Hill in Betonnie-Tsosie Arroyo, from a locality in the lower part of the Arroyo Chijuillita Member, Nacimiento Formation (Figure 1b; see Sinclair and Granger, 1914, plate XXVI; Williamson, 1996). Locality L-646 is about 11 m above the base of the Nacimiento Formation and was included in Fossil Horizon A of Williamson (1996, section M, fig. A2), the lowest horizon of the Nacimiento Formation that yields vertebrate fossils (Figure 1b).

This fossil horizon is low within a zone of normal magnetic polarity originally correlated to C28n (e.g., Lindsay et al., 1981; Lindsay et al., 1978), but this correlation was later found to be incorrect and was later correlated with C29n by Butler and Lindsay (1985), a correlation followed by most subsequent workers (e.g., Williamson, 1996; Lofgren et al., 2004; Fassett, 2009). The reversal at the base of this normal polarity zone is not preserved at Betonnie-Tsosie Wash (e.g., Lindsay et al., 1981). However, the fossil horizon containing L-646 is thought to be correlative with the lowest fossil level of the BDNZ, a location where a lowest fossil horizon is superposed by a higher fossil horizon yielding a late Puercan mammal assemblage (Lofgren et al., 2004; Williamson, 1996). In the BDNZ area, the lowermost fossil horizon is near the base of the normal polarity zone correlated with C29n. The reversal between C29r and C29n is near the base of the Nacimiento Formation, above the earliest Paleocene Ojo Alamo Sandstone (Peppe et al., 2014; Williamson et al., 2014).

Recently, a bentonite bed was identified immediately above the lowest fossil vertebrate horizon in De-na-zin Wash of the BDNZ (Heizler et al., 2013; Peppe et al., 2014; Williamson et al., 2014). Preliminary analysis indicates a radiometric date of 65.69±0.03 Ma based on $^{40}Ar/^{39}Ar$ from data

obtained from sanidine crystals (Mason et al., 2013a, b). Based on correlation between the lowest fossil vertebrate horizons of the BDNZ and Betonnie-Tsosie Wash, this age is also thought to closely constrain the age of the Arroyo Chijuillita Member samples.

3.1.3 Post-depositional history of the region

Thrusting associated with the Sevier orogeny persisted sporadically after the deposition of the Arroyo Chijuillita member until ~ 50 Ma, and deformation associated with the Laramide orogeny continued until ~ 45 Ma, and sporadically afterwards until ~ 37 Ma (Chapin, 2012 and references therein). Mineralization of the Colorado Mineral belt is thought to have occurred in large part in the middle Cenozoic between 43 and 37 Ma (Chapin, 2012). A molybdenum-rich intrusive system of leucocratic alkali-feldspar granite and granite porphyry was emplaced between 33 and 24 Ma at Climax, Colorado, about 600 km from the field area (Wallace and Booksrom, 1993; Chapin, 2012).

Major volcanic fields are present within 300 km to the North, East and South of field area (Figure 1f). Magmatism in the region in the middle Cenozoic was caused by rollback of part of the Farallon plate and inception of the Rio Grande Rift (Chapin et al., 2004). The two important volcanic fields are the San Juan volcanic field, part of the Southern Rocky Mountain volcanic field to the north, and the Mogollon-Datil volcanic field to the south (Figure 1f).

The Southern Rocky Mountain Volcanic Field covers an area of several hundred square kilometers to the north-east of the San Juan Basin, in southwestern Colorado (Figure 1). Activity in this volcanic field began at 38 Ma and ended at 23 Ma, with early activity beginning in central Colorado and moving southward with time (Lipman et al., 2007). The San Juan volcanic region is about 170 km north-east of the field area; it became active at 35 Ma (Lipman et al., 1970), with large eruptions beginning at 29 Ma (Lipman, 1975) and activity ending at 26.9 Ma (Lipman and McIntosh, 2006b). The Questa-Latir volcanic locus is about 200 km east by north-east from the field area and was active between 28 and 25 Ma (Lipman et al., 1986), with the Amalia Tuff dated at 25.1 Ma (Lipman et al., 2007). The only eruption

younger than the Amalia Tuff in the Southern Rocky Mountain volcanic field is the 23.0 Ma Sunshine

Peak Tuff (Lipman et al., 2007), which is about 215 km north of the field area.

The other significant volcanic complex is the Mogollon-Datil volcanic field: the northern-most

caldera of this field lies about 250 km south of the field area (Figure 1f), where activity extends from

about 36 to 24 Ma (McIntosh et al., 1992).

3.2 Belly River Group

3.2.1 Stratigraphy

The Belly River Group in Alberta comprises three formations (Figure 1a); in ascending

stratigraphic order they are 1) the Foremost Formation, 2) the Oldman Formation, and 3) the Dinosaur

Park Formation (Figure 1a; Eberth and Hamblin, 1993). The Foremost Formation overlies the Pakowki

Formation and represents the lower portion of the regressional period of the formation (Eberth and

Hamblin, 1993). The Oldman Formation is a south to southwesterly-thickening nonmarine alluvial unit

representing the upper portion of this regressional period. The Dinosaur Park Formation is a north to

northwesterly-thickening alluvial, estuarine and paralic facies unit, representing the transgressional

phase of the Belly River Group (Eberth and Hamblin, 1993).

The Dinosaur Park Formation is bounded at the base by a discontinuity with the Oldman

Formation (Eberth and Hamblin, 1993). This is considered to represent a change in sediment dispersal in

the basin: the Oldman Formation's material originates from the Crowsnest re-entrant, while the

Dinosaur Park Formation represents deposition of material from the Peace re-entrant (Eberth and

Hamblin, 1993). The Dinosaur Park Formation consists of relatively immature fine sandstone and clay-

dominated fine units (Koster et al., 1987). Sandstone units range from 2- to 20-m-thick and are 100's of

meters in lateral extent. The dominant lithofacies present are trough cross-stratified sandstone, inclined

heterolithic stratification and inclined bedded sandstone (Eberth and Hamblin, 1993). Sandstone units

are interpreted as paleochannel facies, with paleocurrent data suggesting a highly sinuous south-east

trending river system (Koster et al., 1987). The massive mudstone units range in thickness from 2-6 m, and are interpreted as overbank facies.

3.2.2 Age constraints on samples

White to green bentonite layers occur in association with mudstone and represent altered volcanic ash beds; $^{40}Ar/^{39}Ar$ dating of sanidine crystals from bentonite beds provide important geochronological constraints on ages of deposition within the Dinosaur Park Formation. The Dinosaur Park Formation samples are isolated tyrannosaur and crocodilian teeth collected from two microvertebrate sites (catalogue numbers 55269 and 55408) in Dinosaur Provincial Park, Alberta (Figure 1a). Both are positioned stratigraphically between bentonite horizons III and V, with the 55269 site about 3.3 km east by south from the 55408 site (Figure 1a). Weighted means of the $^{40}Ar/^{39}Ar$ dates derived in the 1990s – 2000s produced the following dates, reported by (Eberth et al., 2013): Bentonite horizon III, the Plateau Tuff is dated at 76.4±0.4 Ma, while bentonite horizon V, the Lethbridge Coal Zone Tuff is dated at 76.1±0.5 Ma. The fossils analyzed in this study are thus assumed to have fossilised at about 76 Ma.

3.2.3 Post-depositional history of the region

Important geological events in the region occurring after the ~76 Ma deposition of the Dinosaur Park Formation include continued uplift of the Rocky Mountains, magmatism in Montana, lithostatic rebound and drying of the Western Interior Seaway. Uplift of the Rocky Mountains occurred in several pulses from the mid- to late-Jurassic to the early Eocene; the Rundle fault was active around 72 Ma, and the McConnell fault around 54 – 52 Ma (Figure 1c, 1e; Pană et al., 2015). After this time, extension in the region lead to lithospheric rebound (Pană et al., 2015), although it has also been suggested that uplift was associated with delamination of cold mantle lithosphere and replacement by hot asthenosphere (e.g. Mix et al., 2011). This uplift may have caused regional drying in the latest Eocene-Oligocene (Fan et al., 2014), although a eustatic drop in sea level of ~100 m occurs at this time as well (Gradstein et al.,

2012). Magmatism in northern Montana/southern Alberta occurred between 52 and 49 Ma (Figure 1e;

Hearn et al., 1978).

4. Analytical Techniques

4.1 Sample collection and preparation

The Arroyo Chijuillita Member samples are from a batch of isolated alligatorid teeth (New Mexico Museum of Natural History [NMMNH] P-38627) collected from NMMNH localities L-646 and L-4546. The teeth were recovered from a bulk sample that was collected and processed using underwater screenwashing methods (see Cifelli et al., 1996). Isolated teeth were picked from the resulting concentrate. The teeth include morphologies ranging from conical teeth, likely representing anterior maxillary and mandibular teeth to relatively small, blunt, and rugose teeth of the posterior part of the upper and lower dentition. These teeth are typical of alligatorids from the lower Nacimiento Formation and likely represent the alligatorid Navajosuchus navajovius (Simpson, 1930). Teeth from the Dinosaur Park Formation are isolated tyrannosaur and crocodilian teeth collected individually from two microvertebrate sites.

In order to compare the geochemistry between fossilised and unfossilised teeth, three unfossilised teeth from 1-3 American Alligators at the Toronto Zoo were acquired from their pen. The origin of the alligators is unknown. In preparation for analysis, fossilised and unfossilised teeth samples were photographed, cut along the cross-section, and set in epoxy mounts between 0.7 and 1.5 cm thick. The mounts were then polished and photographed (Figure 2).

4.2 Trace element analysis

In situ trace element analysis using the quadrupole thermo iCAP Laser Ablation Inductively Coupled Mass Spectrometry (LA ICP-MS) was performed on the cross-section of the teeth samples at the Radiogenic Isotope Facility at the University of Alberta, Edmonton. The laser is a New Wave UP-213. The standard used was NIST 612, which is frequently used as a standard for trace element analysis of bioapatite (e.g. Koenig et al, 2009; Suarez et al, 2010). The standard was measured 4 to 5 times before

and after each set of analyses, as well as periodically (after every 10-15 points) over the course of the

sampling. The fossil teeth were lased with a spot size of 60 μm at a repetition rate of 10 Hz, with a 15 s

delay to record background signals, 5 s warm-up, a 40 s acquisition time, and a 60 s wash between

analyses. The data were processed using the software Iolite (Paton et al. 2011), with a Ca content of

38.89 weight % assumed, based on the stoichiometric concentration of Ca in fluoroapatite. Changing the

assumed Ca content of bioapatite by several weight percent was found to only change the concentration

of trace elements by <5 ppm. Spots were analyzed along linear transects through approximately the

center of the teeth at roughly equal intervals, with some small deviations to avoid cracks and veins. Spot

intervals varied between teeth from 200 μm to 500 μm.

The same procedure was applied to the modern American alligator teeth acquired from the

Toronto Zoo. The concentration of Y and rare earth elements (REE) determined for these teeth was

largely near the technique detection limit; sample MT-B was selected for further analysis. Trace element

data of this tooth were obtained using *in situ* laser ablation coupled with sector field inductively coupled

plasma-mass spectrometry (LA-SF-ICP-MS) at the Arctic Resources Laboratory, University of Alberta. The

laser ablation used was a Resolution M-50 193nm excimer laser system connected, via Nylon tubing, to

a sector-field ICP-MS Thermo Element XR. The mass spectrometer was operated in low mass resolution

mode (M/ΔM=ca. 300). Sample MT-B was ablated using 235 μm craters and a 10 Hz repetition with the

laser energy at the target (fluence) regulated at ~4 J/cm^2. An analysis comprised 30 s of background gas

collection followed by 60 s of ablation. Ablated aerosols were entrained in a He cell gas flow (600

mL/min) and subsequently mixed with N_2 (2 mL/min) and Ar (0.8 mL/min) prior to entering the ICP-MS

torch. The ICP-MS was operated at 1300 W and a torch depth of 3.7 mm. Argon and helium gas flow,

torch position and focusing potentials were optimized in order to achieve optimal signals on Co, La and

Th and low oxide production rates (ThO/Th<0.2). The resulting data were normalized using the software

Iolite (Paton et al. 2011) with Durango apatite, the composition of which was taken from Simonetti et al. (2008).

3.3 U-Pb dating by laser ablation ICP-MS

Uranium-lead isotopes were measured with a Nu Plasma I Multi-Collector ICP Mass Spectrometer at the University of Alberta, in Edmonton. The fossil teeth were lased with a New Wave UP 213 nm laser, standard supercell cell design, using a spot size of 80 µm, a repetition rate of 10 Hz, and a fluence of around 1.90 J/cm^2. The spots selected for U-Pb analysis mirror, and were taken in close proximity to, the spots selected for trace element analysis. At the edges of some teeth, elevated Pb signals triggered an automatic shut-down of the SEM detectors. Several analyses of Durango apatite were conducted at the beginning of each session, and after every set of approximately 10 unknown analyses afterwards. Blank corrections were applied periodically during each session.

Common Pb correction was applied to the data using the ^{207}Pb method. The lack of meaningful spread in the Durango U-Pb analyses necessitated an assumption on the ^{207}Pb/^{206}Pb composition of Durango apatite; for consistency, a ^{207}Pb/^{206}Pb value of 0.8377 as reported in Chew et al. (2011) is assumed for this calculation for consistency. For the unknown samples, the ^{207}Pb/^{206}Pb intercept on a Tera-Wasserburg plot of the uncorrected data was used in the correction as the best estimate for the common Pb composition. This composition ranged from 0.818 to 0.886.

A fractionation correction factor was calculated for each session by comparing the average ^{206}Pb*/^{238}U values of the common-Pb corrected Durango analyses to the weighted average ^{206}Pb*/^{238}U value (0.005148) for the same Durango apatite measured using thermal ionization mass spectrometry (TIMS) by Heaman (2014). This fractionation correction factor was then applied to the common-Pb corrected ^{206}Pb*/^{238}U ratios for unknown analyses; this fractionation correction was also applied to the ^{238}U/^{206}Pb ratios not corrected for common Pb, producing good agreement in age with the weighted average common-Pb corrected age (Figure 3). The ^{207}Pb/^{206}Pb ratio is not well-constrained by the

Durango standard; although no correction is possible, the fractionation effect is considered negligible within the uncertainties of the dates achieved in this study. The resulting data were plotted on a Tera-Wasserburg diagram using the Isoplot 4 software (Ludwig, 2008), using a ^{238}U decay constant of 1.55125×10^{-10} yr^{-1}, and ^{238}U/^{235}U value of 137.88 (Jaffey et al., 1971).

3.4 U-Pb dating by isotope dilution thermal ionization mass spectrometry

In order to verify that the dates acquired using laser ablation ICP-MS and the corrections applied to them were accurate, five IDTIMS analyses were acquired on sample AL-D from the De-na-zin Member, San Juan Basin, New Mexico. This sample was selected because of its large size and relatively homogeneous ICP-MS age profile compared to other teeth samples. Chips were removed from one area of the tooth with homogeneous colouration using a NuPlasma Micromill. The five tooth fragments were weighed with a UTM-2 Mettler ultramicrobalance and then dissolved in separate Savillex dissolution vessels after adding a combination of 6.2 N HCl and a measured amount of ^{205}Pb-^{235}U tracer solution. The samples were heated on a hotplate (120°C) for ~48 hours. Uranium and lead were purified using anion exchange chromatography and followed closely the HBr technique employed for perovskite reported by Heaman and Kjarsgaard (2000).

The purified U and Pb were dissolved in a silicic acid-phosphoric acid mixture and loaded onto outgassed, zone-refined Re filaments. The U and Pb isotopic compositions were measured using a VG354 thermal ionization mass spectrometer operating in single Daly photomultiplier mode. The isotopic data were corrected for mass discrimination, blank (5pg Pb, 1pg U) and spike contribution. The quoted errors in the IDTIMS analyses were determined by numerically propagating 14 known sources of analytical uncertainty.

The IDTIMS U-Pb results were consistent, and summarized in Table 1. Uranium concentrations average 55.9±6.3 ppm, which is at the low end of the range reported for a dinosaur tooth by Sano and

Terada (2006), and lower than reported by Romer (2001) for a dinosaur bone by two orders of

magnitude. An average radiogenic Pb proportion of 14.8% was measured for AL-D, and a Th/U of 0.159.

The ^{206}Pb/^{238}U ratios averaged at 0.009676±143, and ^{207}Pb/^{235}U ratios varied between 0.041603 and

0.077151, with uncertainties between 12.5% and 22.9%. These data yield a weighted mean ^{206}Pb/^{238}U

date of 61.5±1.6 Ma (n = 5, MSWD = 0.36; Figure 4a).

3.5 IDTIMS and LA ICP-MS date comparison and implications for uncertainties

In order to most directly compare the IDTIMS results to laser ablation ICP-MS results, 30

analyses were acquired around the full circumference of the microdrill pit in the manner described

above (Table 2a). The ^{238}U/^{206}Pb ratio normalized by the above method (Table 2b) and plotted on the

Tera-Wasserburg diagram produces a date of 64.9±3.6 Ma (n=30, MSWD = 0.32; Figure 4b). This is

within uncertainty of the 61.5±1.6 Ma IDTIMS date. This agreement within analytical uncertainty

between the laser ablation ICP-MS and IDTIMS dates indicates that laser ablation ICP-MS dates are

reliable and accurate once the correction procedure above is applied.

The uncertainty in the average Durango apatite analyses acquired during the session and the

uncertainty in the accepted Durango values were propagated into the normalized U-Pb data. For most

sessions, Durango apatite analyses were within uncertainty of each other, and a single average was used

to normalize the U-Pb sample data. For one session, the Durango analyses drifted towards higher

^{206}Pb*/^{238}U values over the course of the session; a moving average taking into account analyses

acquired before and after each tooth was then used for normalization.

5. Results

5.1 Characterization of Teeth

The preservation of a fossilisation U-Pb signature is most likely to occur in samples that have experienced the least post-fossilisation alteration. Alteration is thought to occur from the edges inward, or along cracks in the fossil. The teeth analyzed in this study have a wide range of colours and textures. The interiors of Arroyo Chijuillita Member teeth vary in colour from black to tan to orange-brown (Figure 2a, b), with concentric zonation preserved in AL-A and AL-B and dark, wedge-shaped radial patterns variably present in AL-B, AL-C, and AL-A (Figure 2a) from locality L-646. Major cracks are absent from these teeth (Figure 2a).

Samples AL-E, AL-G, and AL-F from locality L-4546 are entirely black in colour, with complex networks of cracks occasionally running in broadly concentric patterns, and with variable sand in-filling of the center of the teeth (Figure 2b). Sample AL-D is also from the San Juan Basin, but from the De-na-zin Member of the Kirtland Formation; its coloration is dominantly orange-brown, with patches of black and tan (Figure 2b).

Dinosaur Park Formation teeth show a similar range of colour and texture to the Arroyo Chijuillita Member teeth. Most teeth preserve fine concentric zonation, and like the Arroyo Chijuillita samples, dark radial wedge-shaped patterns are variably present in all samples from both localities (Figure 2c, d). Significant dark patches are present in T408-B, T408-C, and T408-D (Figure 2c). Sample T408-B is cut by numerous visible cracks, and two visible cracks cut T408-C.

The modern, unfossilised teeth are much more homogeneous in colour and much lighter, but concentric zonation and darker radial patterns similar to those found in fossilised teeth are present (Figure 2e).

5.2 Geochemistry of Modern Teeth

In order to understand the degree of trace element enrichment during fossilisation and post-fossilisation alteration, the trace element concentrations of bioapatite before fossilisation must be understood. The *in vivo* trace element concentrations and profiles of fossil alligatorid fossil teeth are unknown, therefore we have selected modern alligator teeth as the best proxy available. For this reason, three fresh American Alligator teeth (Figure 2e) obtained from the Toronto Zoo were analyzed for their trace element composition (Table 3). Rare earth element concentrations were below detection limits on the LA-ICP-MS instrument used, so were measured again using LA-SF-ICP-MS (Table 4).

We assume that these modern alligator teeth give a close approximation to the original *in vivo* concentrations of the fossil alligatorid and crocodilian teeth analysed in this study. They may also give a first approximation for the *in vivo* trace element content of the tyrannosaur teeth. Laser ablation ICP-MS transects acquired along the cross-section revealed that most trace elements (e.g. Y, REE) are below detection limits in unfossilised teeth; this is true for a large proportion of analyses acquired using LA-SF-ICP-MS as well. There are significant concentrations of Sr and Zn; the ranges obtained in this study for modern alligator teeth (Sr about 200 ppm, Zn about 30 ppm) are similar to those reported previously for other modern wildlife (e.g. Kohn et al, 1999; Kohn et al, 2013). Selected trace element profiles across one of these teeth (MT-A) are shown in Figure 5; this sample is the only one to have concentrations of Pb and U significantly above detection limits.

The results of a comparison between the fresh and the fossil teeth are largely unsurprising; concentrations of all trace elements are significantly more elevated in fossil teeth (Table 3, Table 4, Table 5). Concentrations of Sr are about 300 ppm in unfossilised teeth versus about 2000 ppm in most of the fossil teeth, whereas concentrations of Pb are about 0.1 ppm in fresh teeth versus 3-30 ppm in fossil teeth. Concentrations of Y and REE are largely below detection limit in unfossilised teeth.

16

5.3 Trace Element Profiles in Fossil Teeth

The concentration of trace elements measured varied significantly both across individual fossil teeth and between fossil teeth samples, as is summarized for selected elements in three teeth in Figure 6. Trace element data is presented in Table 5. Most studies report that fossils have elevated trace element concentrations at the edges, decreasing gradually towards the center (e.g. Trueman et al., 1999; Herwartz et al., 2011). The teeth analyzed in this study are much more diverse; both the absolute concentrations and the trace element profile vary from tooth to tooth.

Concentrations of Sr are relatively consistent for most samples, both within individual teeth and between the teeth, at about 1 000 - 3 000 ppm (Figure 6). Some samples from the Dinosaur Park Formation were anomalous in their low-Sr concentrations (20 to 60 ppm). The Sr concentrations for these samples are even lower than the Sr concentrations in unfossilised teeth.

The elements Y and La behave similarly (Figure 6) and vary substantially between and within samples (Figure 6). Concentrations of Y vary within some teeth by orders of magnitude, while in others the concentration is consistent at high (several thousand parts per million) or low (2-50 ppm) concentrations. Elemental Pb concentration for teeth analyzed in the Arroyo Chijuillita Member fall between 0.1 ppm and ~1000 ppm, and between about 0.03 ppm and 5 ppm for the Dinosaur Park Formation (Figure 6). Uranium varies between 10 ppm and 700 ppm in teeth from the Arroyo Chijuillita Member, and 0.1 ppm and 18 ppm in teeth from the Dinosaur Park Formation. Profiles for U, Pb, and Sr are not as consistent or well-developed as profiles for Y and the REE in the same samples, and consistently have shallower gradients.

For every tooth analyzed, the profile for the REE, as well as Zr, were analogous to the profile of Y (see Appendix I). As the absolute concentrations of each REE varied within individual samples, and the trace element profiles for Y and the REE are identical, for simplicity's sake Y will be used to represent the behaviour of this group of trace elements.

17

The elements Sr, Pb and U do not mirror this pattern for all teeth (Figure 6), tending to have a flatter profile than Y and the REE; this can be explained by higher diffusivities for Sr, U and Pb in bioapatite than Y and the REE (e.g. Millard and Hedges, 1996; Kohn and Moses, 2013). This is consistent with the diffusivity experiments of Kohn and Moses (2013) on fresh cow bone, which found that Y and REE have the lowest diffusivities (< 8 x 10^{-15} cm^2/s), U and Pb have intermediate diffusivities (~ 1 x 10^{-14} cm^2/s), and Sr has high diffusivity (> 1 x 10^{-12} cm^2/s). The high diffusivity of Sr has implications for attempts to use Sr as a paleodiet or migration indicator (see Appendix II).

Concentrations of Zn appear to be similar between fresh and fossil teeth (~10 – 30 ppm), and Rb concentrations appear to be lower in the fossil samples (<0.2 ppm in fossilised samples compared to ~0.4 – 6 ppm in unfossilised teeth). Concentrations of Ti measured for this study appear to be controlled by molecular interference with Ca and Ar. The implications of the similarity in Zn concentration between fossilised and unfossilised samples, and possibility of preserving *in vivo* signatures in general, are addressed in Appendix III.

Although no two teeth are exactly alike, the fourteen teeth analyzed in this study can be broadly classified into four general types of patterns based on the Y profile (Figure 7). The boundaries between these patterns are gradational:

Pattern 1: Sample T408-C defines a unique pattern, with an elevated Y concentration at the center of the tooth, decreasing gradually and relatively smoothly towards the edges (in blue in Figure 7a). The Y concentration reaches a maximum of ~ 3000 ppm, and a minimum of ~100 ppm. The very center of the tooth, likely representative of the central tubule, shows a dip in concentration (~ 1350 ppm).

Pattern 2: Sample AL-C defines a second unique pattern; it shows a dramatic decrease in Y concentration from the edges of the tooth to the center (Figure 7b). The Y concentration in AL-C ranges from ~4600 ppm to ~10 ppm.

Pattern 3: These samples are transitional between the Patterns 1 and 2 samples and Pattern 4 samples. Among the Arroyo Chijuillita Member samples, one sample shows a decrease in Y concentration from the edges of the tooth to the center, as in AL-C, but have Y profiles that are less flattened than those of the Pattern 4 samples AL-B, AL-E, AL-F, and AL-G (represented by the green bar in Figure 7b). In the Dinosaur Park Formation, there is one transitional sample: T408-B has a similar profile to Pattern 1 sample T408-C at one end of the tooth, but progressively becomes more similar to the Pattern 4 samples in terms of Y concentration and profile on the other side (represented by the green bar in Figure 7a).

Pattern 4: These samples make up the bulk of the tooth population analysed in this study. Concentrations are relatively flat at elevated (Y > 3000 ppm in the San Juan Basin, Figure 7b) or at low concentrations (Y < 100 ppm in the Dinosaur Park Formation, Figure 7a). The Y profile can be constant across the sample, have a slight trend, or be scattered: in any case, the Y profile has a low gradient compared to the other patterns. Concentrations are either very low compared to a Pattern 1 sample for the same unit, or high compared to a Pattern 2 sample.

Samples from the Dinosaur Park Formation have variable concentration ranges between teeth (Figure 7a); all T408 teeth were from the same microsite, and yet two of the tyrannosaur teeth had low Y concentrations (Pattern 4: ~0.5 to ~45 ppm), whereas one showed more elevated Y concentrations (Pattern 1: ~92 to ~ 3000 ppm for T408-C), and another had elevated concentrations at one end of the sample, transitioning into low concentrations at the other end (Pattern 3: ~22 to ~2373 ppm for T408-B).

This suggests that even within a single bone bed, indeed, within a single sample, trace element alteration may be quite heterogeneous.

5.4 U-Pb Geochronology

Uranium-Pb LA-ICPMS age spot analyses are placed close to those selected for trace element analyses; the data for the Durango apatite standard is given in Table 6, and the raw data for the fossil teeth are presented in Table 7. Normalized U-Pb isotopic data for select teeth are reported in Table 8.

Significant variation was measured in both $^{238}U/^{206}Pb$ and $^{207}Pb/^{206}Pb$ between and within some teeth. In the Arroyo Chijuillita Member of the Nacimiento Formation, all analyses from three teeth have low $^{238}U/^{206}Pb$ (< 5), and $^{207}Pb/^{206}Pb$ values of approximately 0.831: this represents a significant common Pb component. Three teeth analyzed from this unit preserve significant ranges in in their 238U/206Pb and 207Pb/206Pb compositions: AL-A (5-27 and 0.67-0.83, respectively), AL-B (2-15 and 0.79-0.84, respectively) and AL-C (5-30 and 0.63-0.82, respectively). For AL-B and AL-C, variation towards higher $^{238}U/^{206}Pb$ and lower $^{207}Pb/^{206}Pb$ is relatively consistent, but for AL-A several analyses appear to plot below the general trend.

For fossils collected in the Dinosaur Park Formation, analyses from most teeth have low $^{238}U/^{206}Pb$ (< 5), and $^{207}Pb/^{206}Pb$ values approaching 0.850. Only one tooth (T408-B) has high $^{238}U/^{206}Pb$ ratios (25-62) and $^{207}Pb/^{206}Pb$ ratios less than 0.70; analyses in this sample have $^{238}U/^{206}Pb$ ratios as high as 62 and $^{207}Pb/^{206}Pb$ ratios as low as 0.52. The outer edges of one tooth (T408-C) could not be analyzed because elevated Pb content tripped the ion counter detectors.

None of the teeth approximated the known stratigraphic age when all $^{206}Pb/^{238}U$ analyses are considered; however, a correlation was observed between a sample's Y profile and its U-Pb date. The Pattern 1 sample preserves a fossilisation U-Pb signature towards the edges of the tooth (Figure 8a), while the Pattern 2 sample preserves the age of fossilisation in the center of the tooth (Figure 8b).

Among the Pattern 2 samples, AL-A produces an imprecise date within uncertainty of the fossilisation age (Figure 8c), and T408-B records a secondary date. In the case of the Pattern 4 teeth, there is no apparent screening of the data that would reproduce the stratigraphic ages. The dates that result from these teeth either cluster about the value for common Pb or are younger than the stratigraphic age of the sample (Figure 8d).

With minor data screening, meaningful fossilisation dates were obtained from the teeth with high Y gradients (Patterns 1 and 2). For Pattern 1 sample T408-C from the Dinosaur Park Formation, considering all analyses, the resulting date is 42.9±5.1 Ma (n =20, MSWD = 6.8; Figure 8a). However, when the low-^{238}U/^{206}Pb portion of the array is isolated, it yields a date of 75±14 Ma (n=6, MSWD = 1.2; Figure 8a), within uncertainty of the known depositional age of the host Dinosaur Park Formation strata (~76 Ma). Including into this selection a single point of higher ^{238}U/^{206}Pb, the date becomes 71.8±9.4 Ma (n=7, MSWD = 1.06; Figure 8a). This analysis narrows the uncertainty on the date, but may be skewing the calculation towards a younger date. In either case, the limited spread in the U-Pb data limits the precision on this date; additional analyses acquired on this region may produce more spread, and thus a more precise date.

The disturbed regions of T408-C from the Dinosaur Park Formation, Alberta have higher ^{238}U/^{206}Pb ratios than those portions of the tooth that record the ~75 Ma date (Figure 8a); this is most likely caused by post-fossilisation alteration associated with two significant cracks. These cracks likely acted as preferential channels for post-fossilisation fluid flow. Pattern 3 sample T408-B is transitional between Pattern 1 sample T408-C and the Pattern 4 samples of the same unit in terms of the Y profile (Figure 7). When all U-Pb analyses are considered, a date of 34.4±4.4 Ma is obtained (n=15, MSWD=10.4). However, this date may be misleading; there may be a mixture of two approximately parallel data trends, both preserving dates closer to 31 Ma, or a distinction between the low ^{238}U/^{206}Pb values (< 40) and the high ^{238}U/^{206}Pb values (> 40) measured in two spots.

21

Pattern 4 teeth in the Dinosaur Park Formation preserve Y concentrations that are very low

compared to all other teeth analysed (Y = 2 – 50 ppm), and Sr concentrations lower even than those

measured for the unfossilised teeth (Sr < 60 ppm). These teeth produce two distinct dates at ~49 Ma

and ~33 Ma. Samples T408-A and C269-D record dates of 48.0±6.3 Ma (n=11, MSWD=1.4) and 49.5±6.3

Ma (n=12, MSWD=4.4), respectively. Samples T408-D and C269-C record dates of 33.8±5.2 when outlier

analyses are excluded (n=7, MSWD=8.5) and 33.4±6.2 Ma (n=13, MSWD=4.8; Figure 8d), respectively.

When calculated together, T408-A and C269-C record a date of 33.4±3.3 Ma (n=20, MSWD=5.4).

A similar pattern is observed for teeth from the Arroyo Chijuillita Member. For Pattern 2 sample

AL-C, when all analyses are considered, a date of 57.6±4.7 Ma is obtained (n=26, MSWD = 74; Figure 8b);

this is younger than the 65.7 Ma depositional age of the host strata (Mason et al., 2013a, b). However,

when only the low-Y central region of AL-C, and a point adjacent with higher Y concentration and nearly

identical isotopic composition, is considered the resulting U-Pb date produced is 64.2±5.4 Ma (n=7,

MSWD = 1.7; Figure 8b). We interpret the 64.2±5.4 Ma date to be an accurate estimate for the time of

tooth fossilisation, overlapping within uncertainty of the 65.7 Ma depositional age of the host

stratigraphic unit (Mason et al., 2013a, b).

Pattern 3 sample AL-A has a Y profile intermediate in both concentration and shape to Pattern 2

sample AL-C and Pattern 4 sample AL-B (Figure 7). When all analyses are considered, the U-Pb date is

59±12 Ma, with an MSWD = 73 (Figure 8c). Pattern 4 sample AL-B has a relatively flat and elevated Y

profile, peaking sharply at the center of the sample. The date produced for this tooth when all analyses

are considered is 33.1±3.4 Ma (n=27, MSWD = 7.8; Figure 9). When the two outliers with lower

$^{207}Pb/^{206}Pb$ ratios are excluded, a date of 25.7±2.1 Ma results (n=25, MSWD = 5.3).

The relative shape of the cross-sectional Y profile can thus be used to classify fossil teeth into

four types of patterns, which appear to be correlated with the preservation and alteration of

fossilisation U-Pb signatures. Investigations of two teeth from two other units are in agreement with this finding, suggesting that this method may be broadly applicable (Appendix II).

6. Discussion

Uranium-Pb dating of fossils has produced mixed results. There are examples of success in dating single specimens, such as an Early Permian shark tooth (Sano and Terada, 1999), a Carboniferous conodont (Sano and Terada, 2001), and Cretaceous-Paleogene dinosaur bones (Fassett et al., 2011). However, Romer (2001) elucidates the potential challenges involved in direct U-Pb dating of fossils, and is not optimistic about the potential to obtain meaningful fossilisation dates. While a number of issues, such as radiogenic Pb input and post-fossilisation element mobility, may disturb a fossilisation-age U-Pb signature (Romer, 2001), the higher spatial resolution of laser ablation ICP-MS analysis compared to bulk fossil analysis allows for the potential to identify discreet domains that may preserve the fossilisation signature.

Based on previous studies, there are clearly examples where geochronological studies of bioapatite have been successful and others that have failed, but there is currently no way to evaluate, in the absence of known depositional dates for the host strata, whether a fossil radiometric date is geologically meaningful. Post-fossilisation alteration in fossil material poses many challenges to direct dating (e.g. Romer 2001, Kocsis et al., 2010), therefore a method is needed for distinguishing altered versus unaltered material. The main challenge is the difficulty in determining how much trace element modification occurs during fossilisation compared to post-fossilisation alteration, and the extent to which fossils exhibit open system behaviour.

This study compares closely spaced *in situ* geochemical and geochronological analysis for several fossil teeth to explore the relationship between U-Pb dates and trace element composition. The main goal is to determine whether a geochemical screen might be used to identify regions of fossils that will

yield geologically meaningful bioapatite dates, and to then use this to further understanding on the

nature and timing of fossilisation and post-fossilisation processes.

The novel approach taken in this study is to acquire high-density analyses from multiple teeth

from each unit, with the hope of sampling teeth, and regions of teeth, whose fossilisation signatures

have been preserved. By comparing corresponding trace element concentrations and U-Pb isotopic

compositions, two important questions may be addressed: 1) How much trace element enrichment

occurred at the time of fossilisation, and how much occurred at a later time, 2) Is there a simple

geochemical indicator that can be used to identify regions of tooth that have not experienced post-

fossilisation alteration?

In this study, trace element concentrations and *in situ* U-Pb dates for fourteen fossil teeth,

collected from two units (the Arroyo Chijuillita Member, San Juan Basin, New Mexico and the Dinosaur

Park Formation, Alberta), where the depositional ages are reasonably well-known, were analyzed. These

teeth were then evaluated for their potential for the identification of discreet age regions, which could

then be used to elucidate the nature and timing of fossilisation and post-fossilisation alteration.

6.1 Cross-sectional Y profiles as a geochemical screen

Yttrium and the REE are the most sensitive elements in addressing the extent of post-

fossilisation alteration; they show a steeper cross-sectional concentration profile than Pb, U, and Sr

(Figure 6), suggesting that Y and the REE have a slower diffusivity in bioapatite than most other

elements (Kohn and Moses, 2013). The cross-sectional REE profiles are similar in shape to that of Y, but

at different concentrations; at similar or higher concentrations for the LREE, and at significantly lower

concentrations for the MREE and HREE (Y and La relative concentrations in Figure 6). The similarities in

profile suggest similar diffusivities, while the differences in concentration may be attributed to different

compatibilities with various sites in the fluoroapatite structure (Pan and Fleet, 2002) or concentrations

in the host sediment (Kohn and Moses, 2013). In any case, the similarity in behaviour between Y and the REE in bioapatite is well supported, while the lower cross-sectional compositional gradient of U, Pb, and Sr indicates more rapid diffusivities. For simplicity, the cross sectional profile of Y will be used to represent the behavior of this low-diffusivity group.

In this study, the most- and least-disturbed parts of the fossil teeth were determined based on the U-Pb dates and the Y profile. Based on the Y profiles of fourteen teeth from two sedimentary basins, four gradational patterns were identified (Figure 7). The Pattern 1 sample has a reverse U-shaped Y profile, with the fossilisation age preserved across much of the tooth. The Pattern 2 sample has a U-shaped Y profile, where the fossilisation age is preserved in the low-Y center. Pattern 3 samples are transitional between Pattern 1 or 2 and Pattern 4 in terms of Y profile, and the fossilisation-age signature is altered to varying degrees over the entire sample. Pattern 4 samples are the most abundant and have low Y gradients with variable amounts of scatter, and largely preserve younger secondary or meaningless dates.

Least-disturbed samples or portions of samples could not be independently identified using the generally-flat cross-sectional compositional profiles of U, Pb or Sr. While consistently high Pb concentrations (Pb > 100 ppm) in the Arroyo Chijuillita Member and low Pb concentrations (Pb < 1 ppm) in the Dinosaur Park Formation fossils are correlated with samples that preserve a U-Pb signature approaching the $^{207}Pb/^{206}Pb$ value for common Pb ($^{238}U/^{206}Pb$ ratios less than 2), the Pb profile or concentration of a sample does not correlate with the preservation of a fossilisation date. The Y profile can thus be used to distinguish regions most affected by post-fossilisation element diffusion from those least affected; the generally flat profiles of Sr, U and Pb give no such indication.

Yttrium concentrations and profiles, viewed in the context of the variation present in fossils from the unit in question, thus provide the best geochemical indicator of the degree of alteration a

sample has experienced. While all teeth analyzed in this study have been altered to some degree,

samples with high Y gradients (Pattern 1 and 2) represent the least altered material. Flattening of the Y

profile occurs during alteration, at which time open system behaviour also alters the U-Pb isotopic

composition. A fossil tooth's cross-sectional Y profile can thus be used to screen teeth for the ones most

likely to preserve the age of fossilisation.

6.2 Physical features and age preservation

It would be logical to assume that teeth samples that best preserve the fine concentric zonation

and radial patterns present in unfossilised teeth would be the least likely to have experienced post-

fossilisation alteration, and would thus be most likely to preserve a fossilisation age. For the teeth

analyzed in this study, this was not found to be the case. As would be expected, analyses sampling sand

lodged in the center of the L-4546 Arroyo Chijuillita teeth (indicated by asterisks on the sample ID in

Table 7) do not retain the age of diagenesis, although neither do analyses from the rest of those teeth.

In the Dinosaur Park Formation, T408-C alone preserves the age of fossilisation; while it

preserves concentric zoning through most of the sample, it also has large dark patches. The region of

T408-C that appears disturbed is cross-cut by two significant cracks; these cracks would act as a

preferential channel for fluid flow, allowing post-diagenetic fluid access into the tooth despite this

sample's well-preserved enamel. The disturbed area can be broadly characterized as occurring between

and around these two significant cracks, representing about 70% of the analyzed cross-section.

The samples with features most closely matching that of unfossilised teeth are the four Pattern

4 C269 samples, which preserve only secondary dates. In the Arroyo Chijuillita Member, both AL-C,

which preserves the age of fossilisation, and the Pattern 4 samples with meaningless dates are

dominantly black in colour. These Pattern 4 samples however, are heavily cracked and infilled. Samples

AL-A and AL-B preserve fine concentric zoning and radial patterns, but neither preserve the age of

fossilisation. It can thus be surmised that the preservation of pristine textural features is a poor indicator of whether a tooth sample will retain a fossilisation-age U-Pb signature.

Despite numerous attempts at direct dating of fossils (e.g. Sano and Terada, 1999; Romer, 2001), there is significant disagreement on which portions of the teeth are the most promising for preserving accurate fossilisation dates; it has been suggested that the compact enamel might be more resistant to post-fossilisation overprinting (e.g. Ayliffe et al., 1994; Kocsis et al., 2010). Alternatively, it has been suggested that the enamel's placement at the outer surface would make it more likely to experience post-fossilisation overprinting and that internal boundaries might be most promising (e.g. Kohn, 2008). Evidence has also been presented that enamel and dentine may be just as prone to overprinting, at least in the Lu-Hf system (Herwartz et al., 2011).

In the case of the Arroyo Chijuillita Member samples, the enamel was not found to preserve a fossilisation-age signature, and in the Pattern 2 sample indeed represented the most altered material. The Dinosaur Park Formation samples also did not preserve the fossilisation age in the enamel, although for Pattern 1 sample T408-C, elevated Pb contents tripping the instrument's sensors meant that the enamel could not be analyzed using the analytical protocol used. Physical features thus do not appear to be good indicators of the state of chemical preservation, although the effect of proximity to the point of the tooth was not explored in this study.

6.3 Fossilisation-age geochemical signatures

Some parts of teeth examined in this study yield U-Pb dates that overlap within analytical uncertainty the known depositional age for the Nacimiento (~65.7 Ma) and Dinosaur Park (~76 Ma) formations, suggesting that meaningful fossilisation U-Pb dates are preserved in some cases. The U-Pb systematics of these two suites of teeth are very different: in the Arroyo Chijuillita Member, the analyses that preserve the fossilisation age have among the highest $^{238}U/^{206}Pb$ ratios (Figure 9), while in

the Dinosaur Park Formation, these analyses define the low $^{238}U/^{206}Pb$ portion of the array (Figure 10). If, as discussed above, Y indeed diffuses more slowly into bioapatite than Pb and U, post-diagenetic trace element alteration of Y and the REE could not occur without some disruption to the U-Pb system. Thus, if the U-Pb fossilisation age has not been disturbed in some regions of a tooth, the Y (and REE) concentration present in those regions has also likely been preserved from the time of fossilisation.

6.3.1 Arroyo Chijuillita Member

In Pattern 2 sample AL-C, the lowest-Y concentration analyses produce the fossilisation age of the sample; inclusion of a single adjacent point of higher concentration increases the precision slightly (Figure 8b). The least disturbed portion of the sample produces a U-Pb date of 64.2±3.7 Ma (n=7; MSWD = 1.7). The analyses that produce this date have some of the highest $^{238}U/^{206}Pb$ ratios, reflecting U-enrichment during fossilisation; the disturbed analyses from all teeth show considerable scatter towards lower $^{238}U/^{206}Pb$ ratios (Figure 9). If Y diffuses more slowly than U and Pb in bioapatite, the low-Y region of AL-C which preserves a fossilisation age can be considered the only remaining pristine portion of the fossil tooth.

Within the least disturbed, low-Y region, the highest Y concentration is at the center and the lowest Y concentration is at the edges (Figure 11). No evidence of depletion is apparent in any of the altered teeth from this unit, suggesting later-stage depletion is not an important process in the Arroyo Chijuillita Member; it is thus most likely that this profile reflects enrichment from the center of the tooth outward. It has been suggested that infiltration of diagenetic fluids is more likely to occur through the central tubule than through the enamel, because at the time of fossilisation an open central tubule will be easier to infiltrate than the compact enamel (e.g. Kohn, 2008); this appears to be the case for this tooth.

It thus appears likely that Pattern 2 sample AL-C experienced a low-level Y-enrichment (10 to 30 ppm) from the center of the tooth outwards at the time of fossilisation. Later, as the central tubule was

28

cemented, post-diagenetic fluid could most effectively infiltrate the tooth from the edges inward,

producing the dramatic elevated Y concentrations at the edges of the tooth, decreasing gradually

towards the least-disturbed center. Only this center-most portion of the tooth thus remains undisturbed

post-fossilisation.

6.3.2 Dinosaur Park Formation

For Pattern 1 sample T408-C, a portion of the sample (n=8) preserves a meaningful U-Pb

fossilisation date of 75±14 (n=7; MSWD=1.2; Figure 8a). The analyses that produce this date define the

low-^{238}U/^{206}Pb end of the array not just of this sample, but of the entire Dinosaur Park Formation (Figure

10), with disturbed analyses identified by a skew towards higher ^{238}U/^{206}Pb and lower ^{207}Pb/^{206}Pb ratios,

or at values approaching common Pb.

The Y profile of T408-C is symmetrical and displays little scatter (Figure 8a); the disturbed region

is continuous in terms of Y concentration with the undisturbed regions on either side. The altered

section appears to have experienced no change in Y, suggesting that this sample has experienced

relatively restricted levels of alteration. If the Y profile preserved in T408-C can be considered

representative of its fossilisation-age enrichment pattern, some inferences can be made about how the

tooth was fossilised.

The presence of elevated Y concentrations at the center of T408-C and low concentrations at

the edges may suggest that fossilisation-age enrichment occurred from the center of this tooth outward,

as suggested by Kohn (2008). The presence of pristine enamel may have also protected this sample from

the extensive post-fossilisation overprinting experienced by other teeth in the Dinosaur Park Formation,

although the enamel itself could not be analyzed due to elevated Pb content tripping the LA-ICP-MS'

sensors.

In the preserved least-disturbed portions of both Pattern 1 sample T408-C from the Dinosaur

Park Formation and Pattern 2 sample AL-C from the Arroyo Chijuillita Member, the Y concentration is

elevated at the center and low at the edges. These profiles are opposite to the predicted fossilisation

enrichment situation, where the concentration of trace elements would be highest at the edges; this

finding is in agreement with the uptake mechanism proposed by Kohn (2008).

6.4 Post-fossilisation alteration

Dating attempts reported as unsuccessful generally give dates younger than the host unit (e.g.

Romer, 2001; Herwartz et al., 2011); the results from this study are in general agreement with this

finding. Most of the teeth analyzed preserve dates younger than the host unit, usually by tens of millions

of years. However, these dates may still be useful in determining the age of overprinting events.

The geochemical characteristics of fossil teeth from the Arroyo Chijuillita Member and the

Dinosaur Park Formation vary substantially; the age of fossilisation in the Dinosaur Park Formation is

preserved in the low-^{238}U/^{206}Pb end of the U-Pb array, with disturbed analyses having higher ^{238}U/^{206}Pb

ratios or extremely low ^{238}U/^{206}Pb ratios, clustering about the common Pb composition (Figure 10). In

the Arroyo Chijuillita Member, the opposite trend is observed: the analyses that record the age of

fossilisation represent the high-^{238}U/^{206}Pb section of the U-Pb array, with disturbed analyses skewed

towards lower ^{238}U/^{206}Pb values approaching a common Pb composition (Figure 9). It is thus apparent

that post-fossilisation alteration can have markedly different characters depending on whether U-

enrichment during diagenesis occurred.

6.4.3 Nature of alteration in the Arroyo Chijuillita Member

The center of Pattern 2 sample AL-C preserves the age of fossilisation, while the rest of that

sample and all other teeth from the Arroyo Chijuillita Member experienced post-fossilisation alteration

that variably disturbed the fossilisation-age U-Pb signature. One sample, Pattern 4 sample AL-B, records

a secondary date of 25.7±2.1 Ma (n = 25, MSWD = 5.3; Figure 9), when two outlier analyses are

excluded. Pattern 4 sample AL-B is enriched in Y by about 100x from the preserved least-disturbed center of AL-C, while the U and Pb concentrations are similar. If the elevated Y concentration, flat Y profile, and younger dates indicate that Pattern 4 sample AL-B experienced a pervasive alteration event or alteration period, it is likely that other samples from the same unit have been affected as well.

The outer 7%-19% of Pattern 2 sample AL-C has a U-Pb isotopic composition similar to that of Pattern 4 sample AL-B, suggesting that the alteration event that affected AL-B also affected AL-C (Figure 11). In between the thoroughly-overprinted edges and the central region that preserves the fossilisation age, the isotopic composition and Y concentration, can best be described as transitional. The spots closer to the least-disturbed center tend to have isotopic signatures that are more similar to the center; with increased proximity to the edges, $^{238}U/^{206}Pb$ values generally decrease and $^{207}Pb/^{206}Pb$ values increase, approaching the isotopic composition of the edges (Figure 11). Similarly, the U-Pb isotopic composition of Pattern 3 sample AL-A overlaps with that of Pattern 4 sample AL-B at the outer 5% and 16% edges of the tooth. In the rest of the tooth, the isotopic composition overlaps with that of the transitional portion of Pattern 2 sample AL-C. This indicates that the alteration recorded in Pattern 4 sample AL-B is also recorded to varying extents at the edges of other teeth, and that mixing between the fossilisation signature and the alteration signature produced the intermediate U-Pb isotopic compositions (Figure 9, 11).

Some samples preserve compositions with very low $^{238}U/^{206}Pb$ ratios, and $^{207}Pb/^{206}Pb$ ratios of 0.82 – 0.84 (Table 7), approaching a common Pb value. These teeth were categorized as Pattern 4, because they have flat cross-sectional Y profiles at very elevated concentrations (Y= 5 000 ppm to 8 000 ppm), as well as more elevated U and Pb elemental concentrations. These teeth have likely experienced more alteration than other teeth from this unit, a process which progressively increases the common Pb component until the $^{238}U/^{206}Pb$ values became too low to generate a meaningful date.

Post-fossilisation disturbance in $^{238}U/^{206}Pb$ values can be explained by a decrease in U/Pb values

through alteration (Figure 12). Both U and Pb concentrations increase in teeth from this unit with

increased disturbance from the fossilisation-age signature, but Pb increases more quickly, producing

lower U/Pb ratios with progressive alteration. The least-disturbed center of Pattern 2 sample AL-C has a

U/Pb ratio of ~12. Alteration, identified by increase in Y concentrations and flattening of the Y profile,

progressively decreases U/Pb and $^{238}U/^{206}Pb$ through the Pattern 2, Pattern 3, and then Pattern 4

samples (Figure 12).

All U-Pb analyses from samples in this unit can be explained as variable mixing of the

fossilisation-age signature (64.2±3.7 Ma), the alteration-age signature (25.7±2.1 Ma), and the common

Pb value ($^{238}U/^{206}Pb < 6$, $^{207}Pb/^{206}Pb$ of 0.82 – 0.84), as illustrated in Figure 9. If this is true, there may be

some geological significance to the 25.7 Ma secondary date.

6.4.4 Constraints on the alteration event in the Arroyo Chijuillita Member

If 25.7 Ma is accepted as either the age of an alteration event or the age of the end of alteration

in the Arroyo Chijuillita Member of the Nacimiento Formation, the alteration event in question may be

related to important regional tectonic, mineralization, or volcanic events. It is known from studies of ore

deposits that regional groundwater systems can transport fluids over hundreds of kilometers to

paleotopographic lows (Ingebritsen & Appold, 2012). Fluids and thermal energy from magmatic systems

also promote fluid flow over vast areas (Ingebritsen & Appold, 2012).

Uplift associated with the Laramide and Sevier orogenies are too old (ending at about 50 Ma) to

explain a 25.7±2.1 Ma alteration event. The bulk of mineralization of the Colorado Mineral Belt is

thought to have ended at about 37 Ma, however a molybdenum-rich intrusive system of leucocratic

alkali-feldspar granite and granite porphyry was emplaced between 33 and 24 Ma at Climax, Arizona,

about 600 km from the field area (Wallace and Booksrom, 1993; Chapin, 2012).

Magmatism in the region in the middle Cenozoic is thought to be caused by rollback of part of the Farallon plate and inception of the Rio Grande Rift (Chapin et al., 2004). Activity in the Southern Rocky Mountain volcanic field began at 38 Ma and ended at 23 Ma. The Questa-Latir volcanic locus is about 200 km NE from the field area and was active between 28 and 25 Ma (Lipman et al., 1986), with the Amalia Tuff dated at ~25.1 Ma (Lipman et al., 2007). Much of the volcanic activity in the Mogollon-Datil volcanic field predates the 25.7±2.1 Ma date, with only two major ignimbrite units whose activities extend to 24.3 Ma (McIntosh et al., 1992).

The secondary date derived from Pattern 4 sample AL-B appears to be synchronous with the end of wide-spread volcanic activity in the region. Because the bulk of the volcanic activity in both the Southern Rocky Mountain volcanic field and the Mogollon-Datil volcanic field ended at or before 25.7±2.1 Ma, it is unknown whether these teeth experienced only one overprinting event, or whether the U-Pb system has been disturbed continuously or by multiple discreet events, with the ~25.7 Ma secondary date representing the age of last disturbance. At this stage, it is unknown whether it was a magmatic fluid, hydrothermal activity related to coeval magmatism, the influence of an ignimbrite on the groundwater, regional groundwater flow in the San Juan Basin, or a thermal perturbation that caused this alteration event and resulting secondary date. However, the significant enrichment in trace elements (Y concentration increases by two orders of magnitude) suggests an enriched fluid source.

The trace element compositions and U-Pb dates of all the samples from the Arroyo Chijuillita Member presented in this study can be explained by the variable influence of post-fossilisation trace element uptake occurring at 25.7±2.1 Ma, associated with the end of major magmatic activity in the region.

6.4.1 Nature of alteration in the Dinosaur Park Formation

About 30% of Pattern 1 sample T408-C preserves a date within uncertainty of the age of the Dinosaur Park Formation; all other samples analysed from this unit experienced post-fossilisation

alteration that disturbed to varying degrees that fossilisation-age signature. Disturbed fossil analyses from this unit can be identified by a skew towards higher ^{238}U/^{206}Pb ratios, or values approaching common Pb (Figure 10). Several teeth preserve secondary dates across most or all of the analysed cross-section; two Pattern 4 teeth (T808-A and C269-D) give dates of ~49 Ma, and two Pattern 4 teeth (T408-D and C269-C) and the Pattern 3 tooth produce dates of ~33 Ma. The remaining two Pattern 4 teeth (C269-A and C269-B) have low-^{238}U/^{206}Pb (< 3) ratios reflecting the dominance of a common Pb component. All altered teeth have Y concentrations that are significantly lower than the least-disturbed Pattern 1 sample, with flatter Y profiles. Each date is preserved in teeth from microsites kilometers apart; this strongly suggests that the secondary dates measured represent significant alteration events in this unit.

A notable feature of the teeth in this unit is that they can be separated into two categories: high-Sr (Patterns 1 and 3 teeth; Figure 13a) and low-Sr (Pattern 4 teeth; Figure 13b). The low-Sr Pattern 4 samples from the Dinosaur Park Formation have low Y concentrations, and Sr concentrations that are not just lower than those measured in the other teeth (from both the Dinosaur Park Formation and the Nacimiento Formation), but lower than the concentration measured in modern, unfossilised teeth (Table 3). There are two possible explanations for these very low Sr concentrations: these teeth had less than expected Sr concentrations *in vivo*, and experienced little to no enrichment post-fossilisation, or that these teeth experienced a Sr-depletion event sometime after fossilisation.

The *in vivo* Sr concentration of fossil teeth cannot be known, and variability in *in vivo* concentrations should be expected. However, Y concentrations in the low-Sr teeth are higher than are reasonable to expect *in vivo* (Y = 2 – 50 ppm), indicating that Y enrichment has occurred in these samples. Because Sr diffuses more quickly, is more compatible in bioapatite, and can be expected to be present in larger concentrations in the sediment, enrichment in Y could not have occurred during fossilisation without enrichment in Sr. This is observed in all other teeth analysed in this study; it is

34

unlikely that an unusually low *in vivo* Sr concentration was preserved while Y concentration increased by as much as four orders of magnitude. In addition, among the high-Sr samples, the Pattern 3 sample preserving a ~33 Ma date is depleted in Sr compared to the least-disturbed Pattern 1 sample (Figure 13a). The favoured explanation is that trace element enrichment occurred in the low-Sr Pattern 4 teeth at some time, which was followed by later depletion.

Two Pattern 4 teeth from this unit preserve relatively precise dates of ~49 Ma (Figure 13b); T408-A records a date of 48.0±6.3 Ma (n=11, MSWD=1.4) when one outlier is excluded, and C269-D records a date of 49.5±6.3 Ma (n=12, MSWD=4.4), also with one outlier excluded. These samples are interpreted as having been depleted in trace elements at ~49 Ma. The Sr concentrations of T408-A and C269-D do not overlap, and show no correlation with other, more slowly-diffusing trace elements such as U, Pb and Y. There is, however, compositional overlap between the two ~49 Ma samples for U, Pb, and Y, and they preserve distinct trends in Y-U and Y-Pb plots (Figure 13b). This suggests that Sr was extensively leached during this event, while more slowly diffusing elements were variably affected. Depletion at ~49 Ma variably lowered concentrations of Y, Pb and U, producing correlations between these elements that are likely controlled by the relative rates of diffusion (Figure 13b).

A ~33 Ma date is recorded in several Dinosaur Park Formation teeth: Pattern 3 sample T408-B produces a date of ~34.4 Ma when all analyses are considered together, and ~31 Ma when the two ends of the tooth are calculated separately (Figure 13a). The altered sections of Pattern 1 sample T408-C have similar U-Pb isotopic compositions to the lower $^{238}U/^{206}Pb$ portions of T408-B, and produce dates between ~30 and ~35 Ma. Analyses from the ~33 Ma T408-B have lower Sr, Pb, U and Y concentrations than analyses from the least-disturbed T408-C, indicating again that depletion has occurred (Figure 13a).

Pattern 4 samples T408-D and C269-C preserve dates of 33.8±5.2 (n=7, MSWD=8.5) and 33.4±6.2 Ma (n=13, MSWD=4.8), respectively. When analyses from both teeth are calculated together,

the date produced is 33.4±3.3 Ma (n=20, MSWD=5.4; Figure 13b). These teeth have overlapping, although on average lower Sr, U, and Y concentrations than the teeth disturbed at ~49 Ma; however, Y concentrations are still higher than would be reasonable to expect in unfossilised teeth (Y > 2 ppm). This suggests again that enrichment occurred (likely during fossilisation), and was later followed by a depletion event at ~33 Ma.

A significant proportion of analyses acquired along the cross-sections of ~33 Ma Pattern 4 samples have very low ^{238}U/^{206}Pb ratios (< 3), similar to those measured along the entire cross-sections of Pattern 4 teeth C269-A and C269-B. These low-^{238}U/^{206}Pb teeth preserve no meaningful age information because of a very high common Pb component. The teeth disturbed at ~33 Ma and the low-^{238}U/^{206}Pb teeth have overlapping U, Pb and Y concentrations, with analyses from the low-^{238}U/^{206}Pb teeth trending to higher U, Pb, and Y concentrations (Figure 13b). This overlap in the trace element concentration and U-Pb isotopic composition between the teeth disturbed at ~33 Ma and the low-^{238}U/^{206}Pb teeth strongly suggests a shared alteration history.

There are two possible mechanisms by which the teeth disturbed at ~33 Ma and the low-^{238}U/^{206}Pb teeth may be connected: depletion or enrichment. If the trend in Y-Pb space defined by the low-^{238}U/^{206}Pb samples (Figure 13b) represents depletion, the ^{238}U/^{206}Pb values in these samples would be expected to increase; a secondary date would likely have been preserved. Depletion is thus not considered likely.

In the Arroyo Chijuillita Member, low ^{238}U/^{206}Pb values were shown to be caused by enrichment in Pb compared to U (Figure 12); a similar process is likely to have occurred in these samples. The overlap in the trace element concentration and U-Pb isotopic composition between the teeth disturbed at ~33 Ma and the low-^{238}U/^{206}Pb teeth strongly suggests that a late enrichment produced the low ^{238}U/^{206}Pb values in both sets of teeth at or after ~33 Ma.

36

The extent to which the teeth disturbed at ~33 Ma might have been affected by the ~49 Ma depletion event is poorly resolved. No selection of analyses produce the age of fossilisation, or the older ~49 Ma alteration age; available U-Pb isotopic data thus cannot discern an older event from the teeth disturbed at ~33 Ma. However, several outlier analyses from the Pattern 4 teeth disturbed at ~33 Ma overlap compositionally with the teeth disturbed at ~49 Ma in terms of Y and U, which may suggest that these samples were subject to the ~49 Ma depletion event.

Both the ~49 Ma and the ~33 Ma secondary dates are thus preserved in multiple teeth from both fossil sites. Strontium concentrations in some of these fossil teeth are lower than in unfossilised teeth, despite Y concentrations orders of magnitude greater than in unfossilised teeth; this suggests that depletion has occurred. Yttrium, U, and Pb concentrations, as well as the U-Pb isotopic compositions of these teeth, are consistent with depletion of trace elements, including Pb loss. The presence of two distinct ages, preserved in multiple teeth from both fossil sites, suggests that this Pb loss might have occurred as two distinct events at ~49 Ma and ~33 Ma. If that is the case, there may be some broader geological significance to these dates.

6.4.2 Constraints on alteration events in the Dinosaur Park Formation

If ~49 Ma and ~33 Ma U-Pb dates obtained in some teeth are assumed to represent the ages of alteration events that affected the Dinosaur Park Formation, the alteration events in question may be related to known regional tectonic or magmatic events. Volcanic rocks in nearby Montana are known to have ages in the range 54 – 50 Ma (Hearn et al., 1978; Figure 1e); this time also represents a period of fault displacement along the McConnell fault and the final stage of mountain building in the Rocky Mountains (Pană et al., 2015; Figure 1e). Of the two ~50 Ma events, fluid flow resulting from renewed tectonic activity appears to be most likely (Oliver, 1989; Ge and Garvin, 1992). Magmatic fluids would be more likely to cause an enrichment in trace elements, as seen in the Arroyo Chijuillita Member, instead of the depletion measured. The depletion of trace elements in the Dinosaur Park Formation samples,

including the Pb loss which disturbed the U-Pb system, was most likely caused by interaction with a meteoric, trace element-poor groundwater system. Such a system would likely be affected by orogenic activity.

The nature of the ~33 Ma alteration event is less clear; like the ~49 Ma event, the alteration appears to be characterized by trace element (including Pb) loss, suggesting the influence of a trace element-poor groundwater system. However, there is evidence for a late re-enrichment event, which produces low ^{238}U/^{206}Pb values (Figure 13b). The cause of this disturbance, however, is not currently well understood. Post-orogenic lithospheric rebound occurs after ~50 Ma, with rebound occurring first in southern British Columbia at this time, in Idaho and Montana by 39 Ma, and in Nevada and Utah by 28 Ma (Mix et al., 2011); there does not seem at the moment to be evidence of significant lithospheric rebound in the area at ~33 Ma.

Significant climatic changes were also occurring in Eocene-Oligocene time, with global cooling and growth of the Antarctic ice sheet resulting in a eustatic drop in sea level of ~100 meters at 35 Ma (Gradstein et al., 2012). It is not clear whether changes in paleotopography or climate might have instigated the fluid flow that produced the ~33 Ma alteration. However, secondary dates at ~49 Ma in the Dinosaur Park Formation and ~25 Ma in the Nacimiento Formation can both be tied to the major geological events in the region, suggesting that an event affecting fluid flow also produced the ~33 Ma secondary date.

7. Conclusion

A major conclusion of this study is that U-Pb analyses can be coupled with certain geochemical proxies (e.g., Y concentration profiles) of unaltered fossil teeth to deconvolve their fossilisation and post-fossilisation history. Applying such geochemical screens allow for a more targeted approach to

successfully dating fossil teeth. What follows is a summary of the fossilisation and post-fossilisation process, as recorded in samples analyzed in this study:

1. During fossilisation, the structure and composition of bioapatite change and trace element uptake occurs. The results of this study support a fossilisation process that occurs from the center of the tooth outward (as suggested by Kohn, 2008), but other uptake patterns may occur.

2. Post-fossilisation alteration is very common in fossils, and occurs through the interaction of fluids related to magmatic, tectonic, and possibly climatic events. Interaction with magmatic fluids may be responsible for the trace element enrichment measured in the San Juan Basin samples, while depletion may be the result of interaction with meteoric-fed groundwater during a period of tectonic uplift. Trace element enrichment and depletion was detected in certain fossil teeth in this study and both indicate open system behaviour, where the U-Pb system is reset and the possibility of retaining meaningful secondary dates exists. The effects of alteration are gradational, progressing through the following stages with distinct cross-sectional Y profiles:

   a. Pattern 1: Minor or short-lived disruption of the U-Pb system from the edge of the tooth towards the center, or along significant cracks, may occur without apparent change in Y concentration, but some changes in U and Pb concentration. In this case, disturbed analyses can only be identified based on displacement from a clear fossilisation-age signature.

   b. Pattern 2: More pervasive trace element modification, occurring from the edges inward or along significant cracks will produce a change in the Y concentration and profile. Meaningful fossilisation U-Pb dates may still be preserved if the Y profile can be used to discard disturbed regions of the tooth, which may themselves record alteration-age U-Pb isotopic compositions.

c. Pattern 3: The entire sample experiences post-fossilisation diffusion, leading to pervasive overprinting. This is apparent by a flattening of the Y profile towards more elevated concentrations when enrichment occurs (Y > 3000 ppm in the Arroyo Chijuillita Member) and low concentrations when depletion occurs (Y < 100 ppm in the Dinosaur Park Formation). In these samples, low-precision fossilisation or secondary dates may be preserved.

d. Pattern 4: If enrichment is pervasive and thorough, the progressive uptake of trace elements will produce a flat Y profile at elevated concentrations compared to Pattern 1-2 samples. Greater scatter indicates a more heterogeneous uptake process. Both U and Pb uptake will occur, and the U/Pb ratios will decline, resulting in a skew towards low ^{238}U/^{206}Pb values. Secondary dates may be preserved, but the decrease in U/Pb will eventually lead to U-Pb isotopic compositions dominated by the common Pb component in most altered samples.

e. Pattern 4: In some units, fluid-assisted depletion, not uptake, may occur pervasively. In these cases, the ^{238}U/^{206}Pb values will tend to increase and secondary dates are likely to be preserved.

The range of Y profiles and concentrations observed reflect the range of geochemical alteration experienced by two suites of fossil teeth examined. When viewed in context, the shape of the cross-sectional Y profile can be used to determine which samples are the most disturbed and which potentially preserve the age of fossilisation. In the two units targeted in this investigation, a small number (n=2) of samples preserve high-gradient Y concentration profiles (Patterns 1 and 2). These produced accurate fossilisation dates, with precision on these dates limited by the amount of spread in the U-Pb data. The remaining 12 teeth experienced post-fossilisation overprinting which compromised or obliterated the original U-Pb systematics, which may be associated with volcanic activity in the Four

Corners region and uplift of the Rocky Mountains. A third secondary date (~33 Ma in the Dinosaur Park Formation) remains enigmatic, but it is considered likely that ~33 Ma represents the timing of a meaningful regional alteration event, possibly due to the significant climatic changes occurring at this time.

It appears that despite the tendency of fossils to experience post-fossilisation U-Pb disturbance, and the high uncertainties compared to dates derived from $^{40}Ar/^{39}Ar$ dating of sanidine from interbedded bentonite horizons, U-Pb dating of fossils may be an alternative method of providing useful stratigraphic age constraints once the U-Pb systematics are understood. In the absence of bentonite beds, direct dating of fossils may indeed be the only available way of determining the depositional age of the fossil's host unit. This study shows that preserved fossilisation-age U-Pb signatures can be discerned in fossil teeth; additional, high-density U-Pb analyses of these identified regions may significantly increase the precision on the dates.

In addition to the application of this technique to providing age constraints on stratigraphic units and correlation between fossil localities, the resolution of meaningful secondary dates raises the possibility of describing the nature and timing of basin fluid flow events. Currently, there are few constraints on the timing of fluid flow within sedimentary basins. The results presented here suggest that fluid flow events may be preserved in the post-fossilisation trace element signatures of fossil teeth.

8. Figures
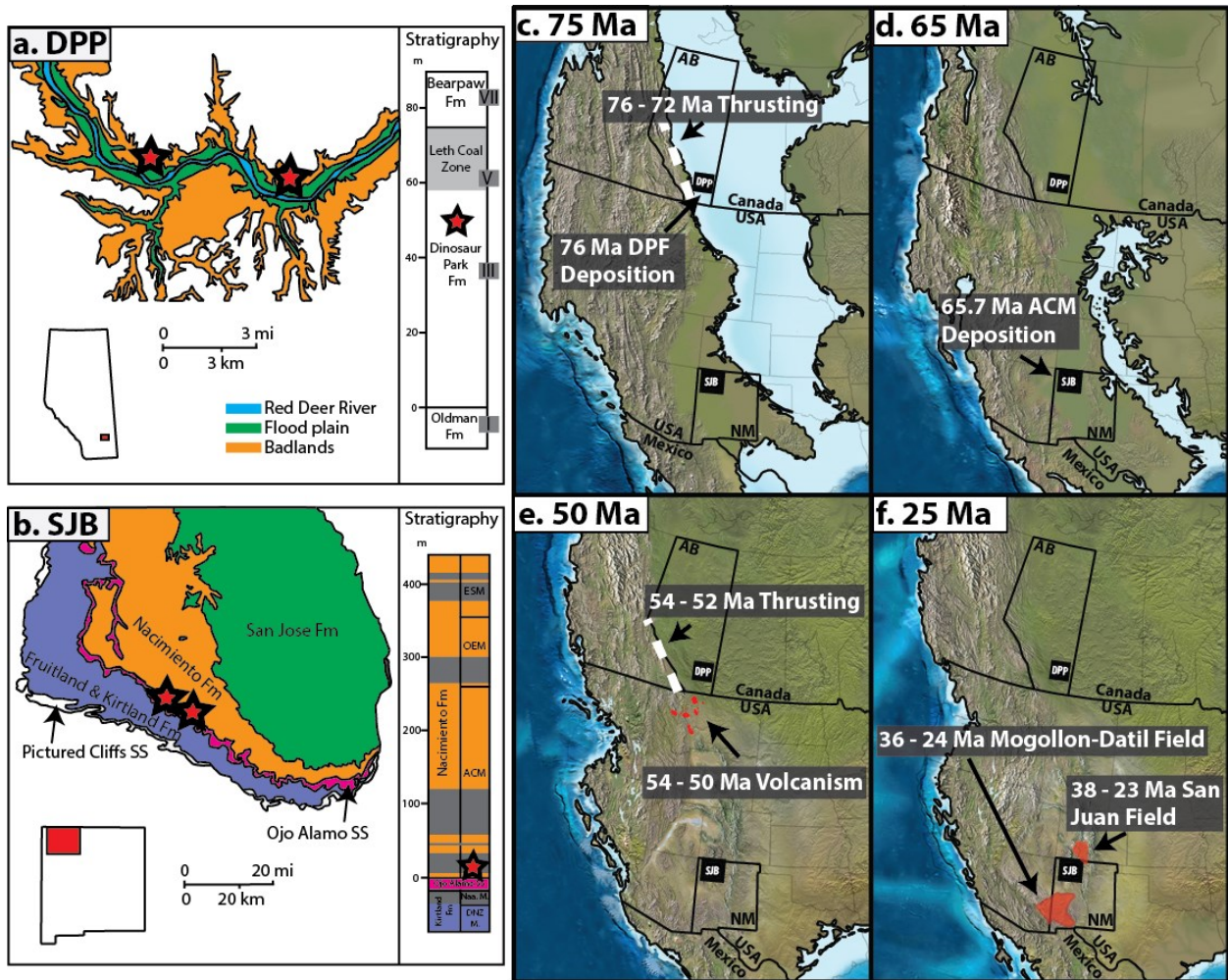
Figure 1: a. Map and stratigraphy of Dinosaur Provincial Park, Alberta; b. Geological map and stratigraphy of the San Juan Basin, New Mexico; Summary of major geological events at: c. 75 Ma, d. 65 Ma, e. 50 Ma, and f. 25 Ma. Stars indicate sample locality and stratigraphic position. Dinosaur Provincial Park map modified from Eberth et al. (2013), San Juan Basin map modified from Williamson et al. (2008), and paleogeographic reconstructions copyright of Ron Blakey and Colorado Plateau Geosystems Inc.
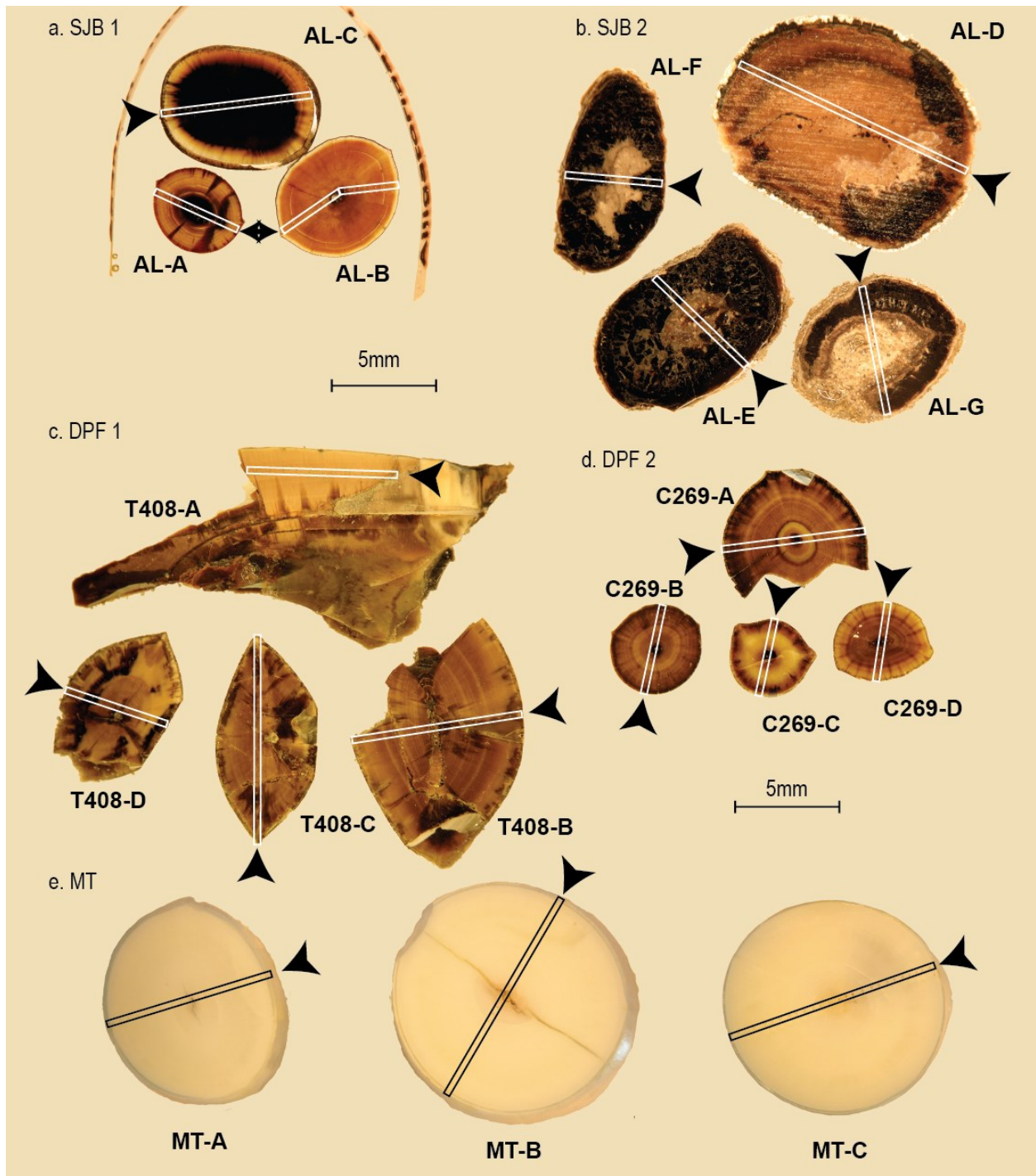
Figure 2: Photographs of the epoxy mounts of the teeth analyzed and discussed in this study, separated by analytical session. Black and white bars indicate transects along which analyses were acquired, with arrows indicating the start.
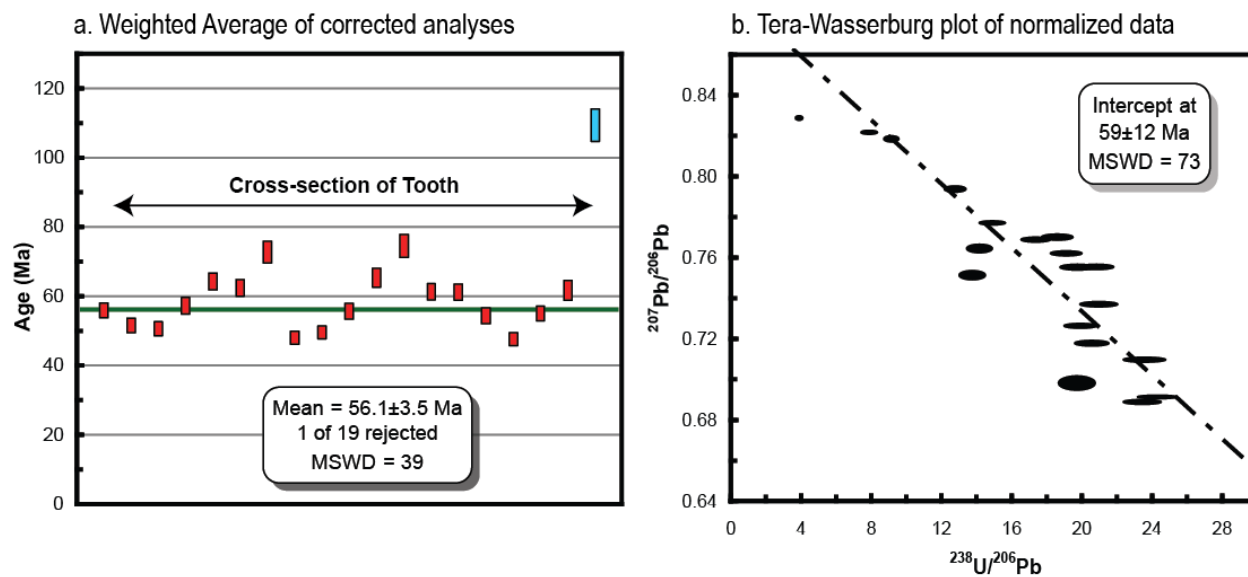
Figure 3: a. The weighted average of sample AL-A analyses normalized to Durango and corrected for common Pb. The blue box is the rejected analysis, and b. Tera-Wasserburg plot of sample data normalized to Durango apatite.
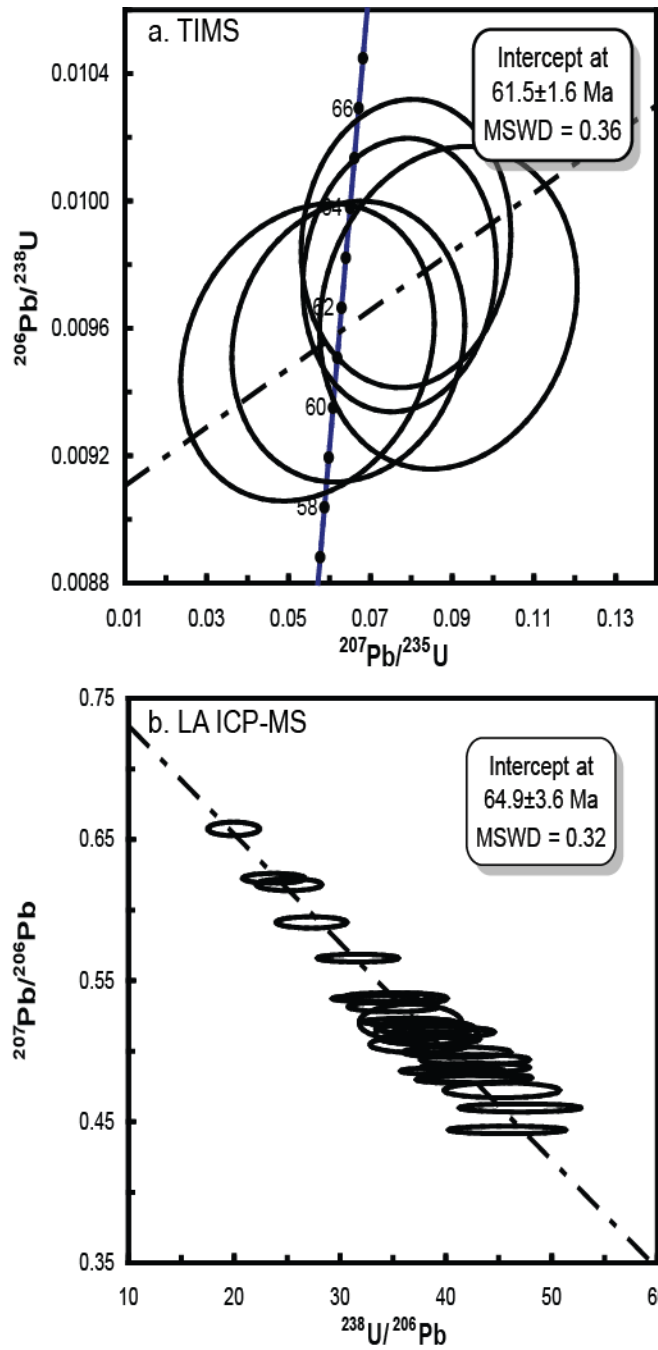
Figure 4 a. U-Pb concordia plot of the five TIMS analyses acquired on a chip removed from sample AL-D.
b. Tera-Wasserburg plot of laser ablation ICP-MS analyses acquired around the circumference of the pit.
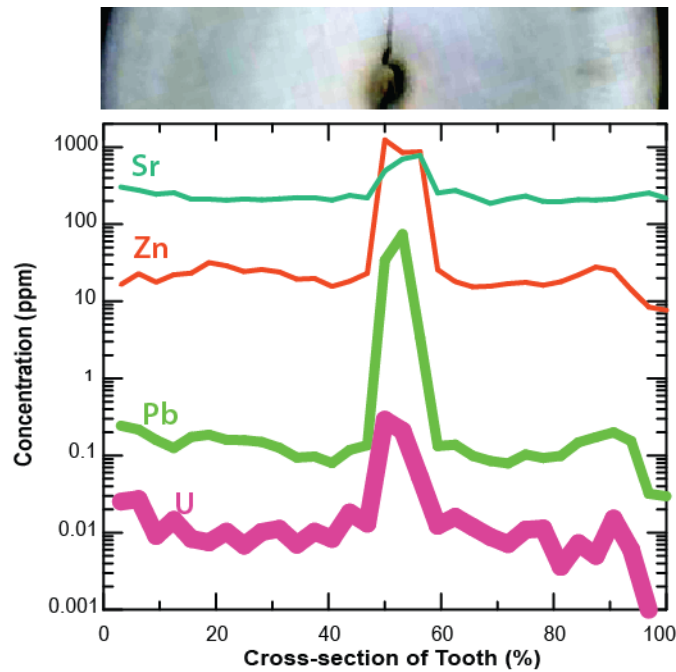
Figure 5 Trace element profiles for select elements along the cross-section of an unfossilised American Alligator tooth. Photo of the analyzed cross-section is digitally enhanced to increase contrast. Uncertainties on measurements are less than the thickness of the line for most analyses.
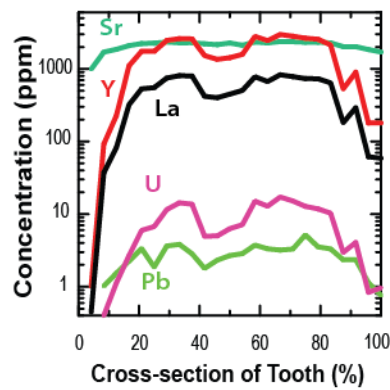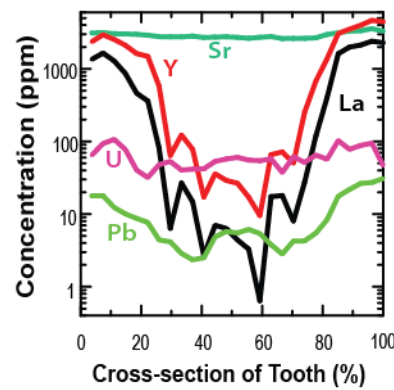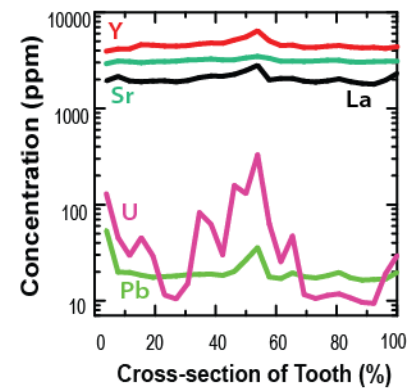
Figure 6 Cross-sectional trace element profiles of select elements for samples a. T408-C; b. AL-C; and c. AL-B. Uncertainties are less than the thickness of the line for most measurements.

46
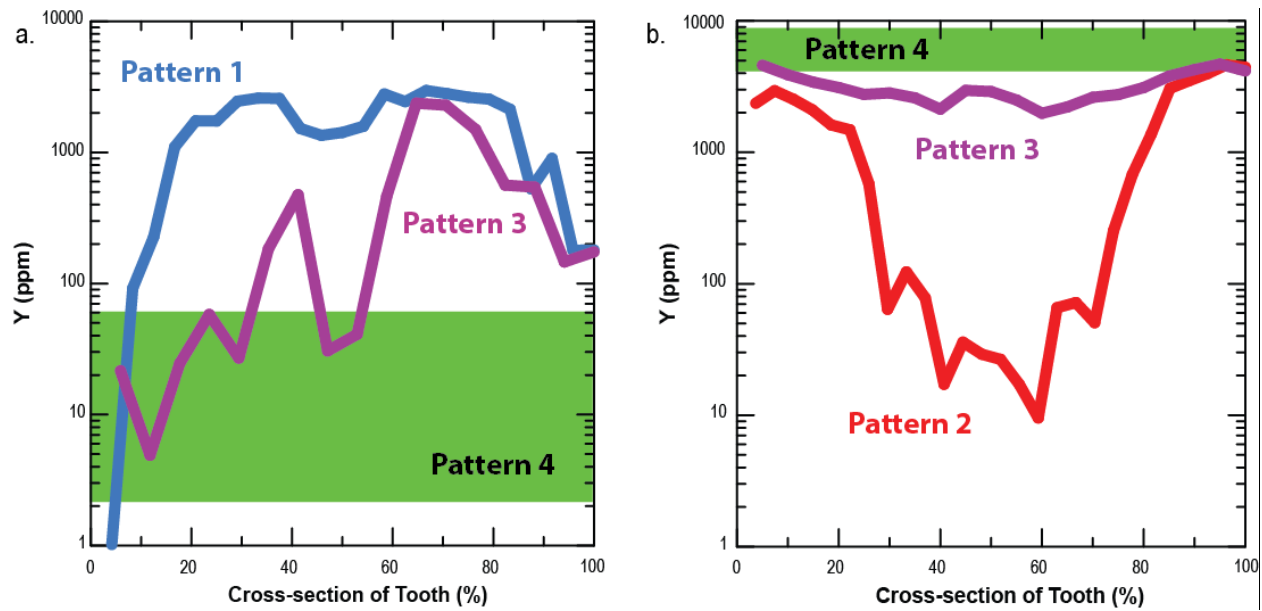
Figure 7: The degree of enrichment and the Y profile are used to distinguish the following 4 patterns in a. Dinosaur Park Formation, Alberta, b. the Arroyo Chijuillita Member, New Mexico. Green fields represent the range of concentrations found in Pattern 4 teeth.
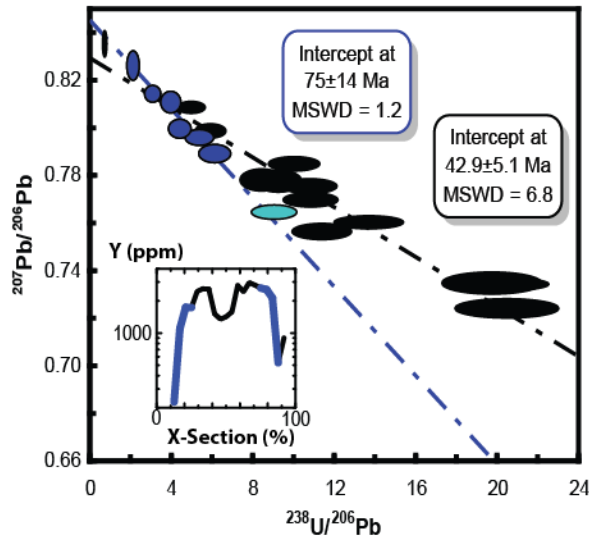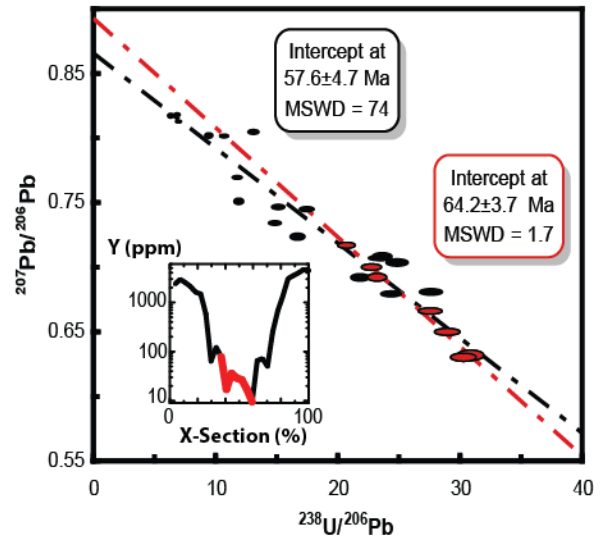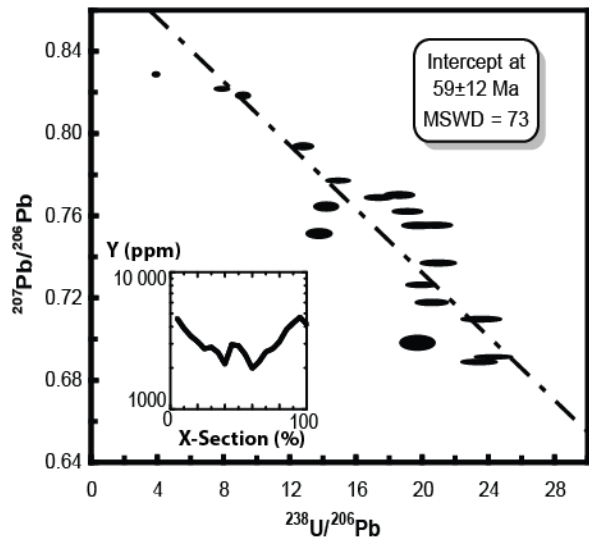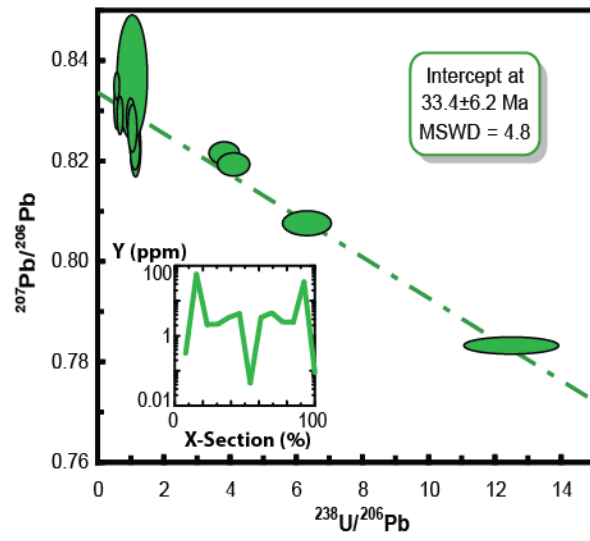
Figure 8: Tera-Wasserburg plots and associated Y profiles for a. Pattern 1 tooth T408-C, where the pale blue analysis, when calculated with the ~75 Ma selection, produces a date of 71.8±9.4 Ma (n=7, MSWD = 1.06), b. Pattern 2 tooth AL-C, c. Pattern 3 tooth AL-A, d. Pattern 4 tooth C269-C. Uncertainties on Y are less than the thickness of the line for most analyses. Error ellipses are 2σ.
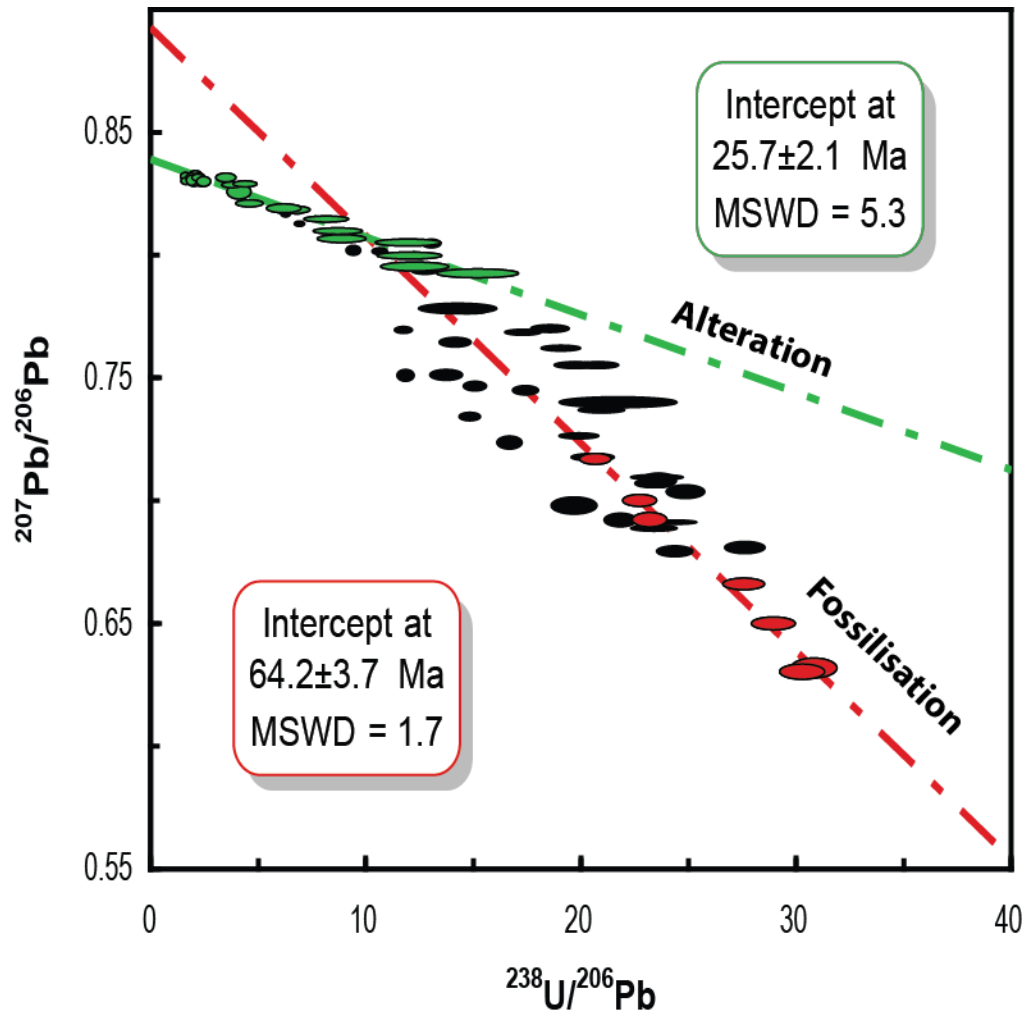
Figure 9: A Tera-Wasserburg plot containing all the U-Pb data acquired from three of the teeth analyzed from the Arroyo Chijuillita Member of the Nacimiento Formation, in the San Juan Basin of New Mexico. In red, the analyses from the center of Pattern 2 sample A L-C, which preserved an accurate fossilisation age. In green, Pattern 4 sample AL-B, which preserved a precise secondary date. Error ellipses are 2σ.
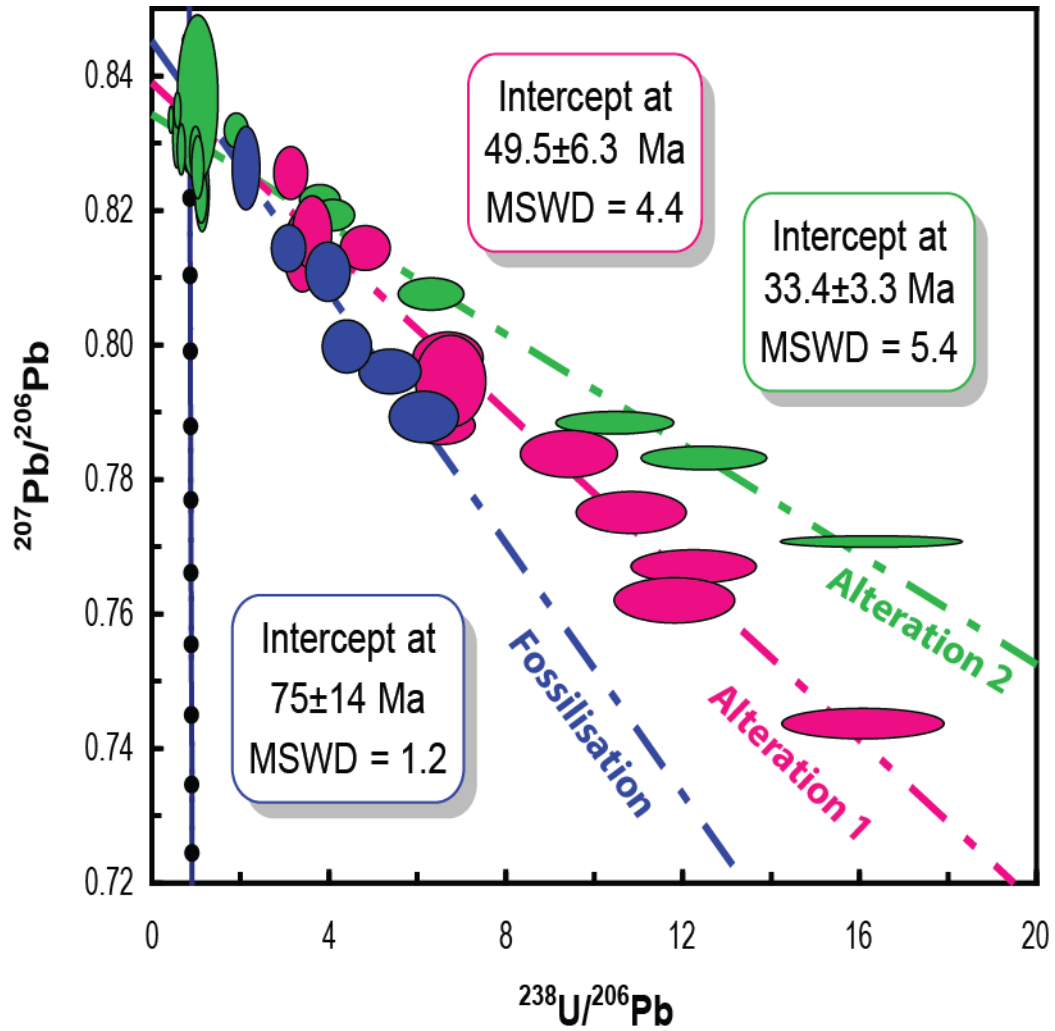
Figure 10: Tera-Wasserburg plot of U-Pb analyses acquired on fossil teeth from the Dinosaur Park Formation. The fossilisation age is derived from analyses defining the low $^{238}U/^{206}Pb$ end of the array. Disturbed analyses are skewed to higher $^{238}U/^{206}Pb$ ratios, possibly related to Eocene-Oligocene disturbances. Error ellipses are 2σ.
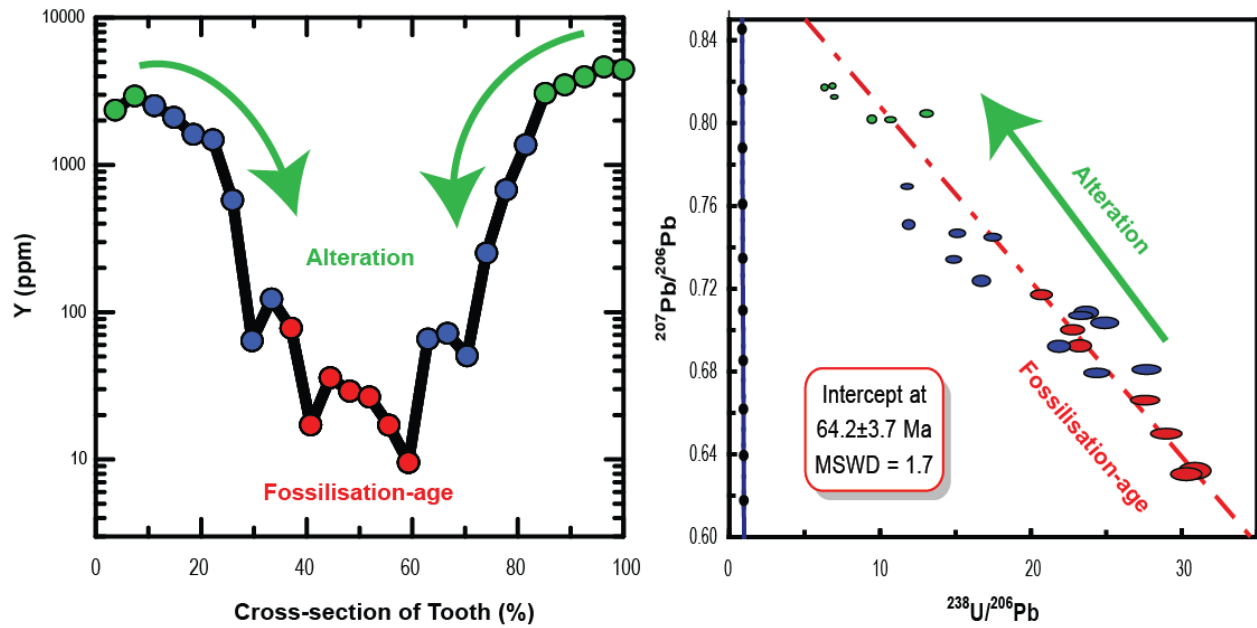
Figure 11: The Y profile for Pattern 2 sample AL-C is segregated into three age regions: the alteration-age edge (green), the least-disturbed center (red), and the transitional region (purple) using the corresponding Tera-Wasserburg plot. Uncertainties are less than the thickness of the line; error ellipses are 2σ.
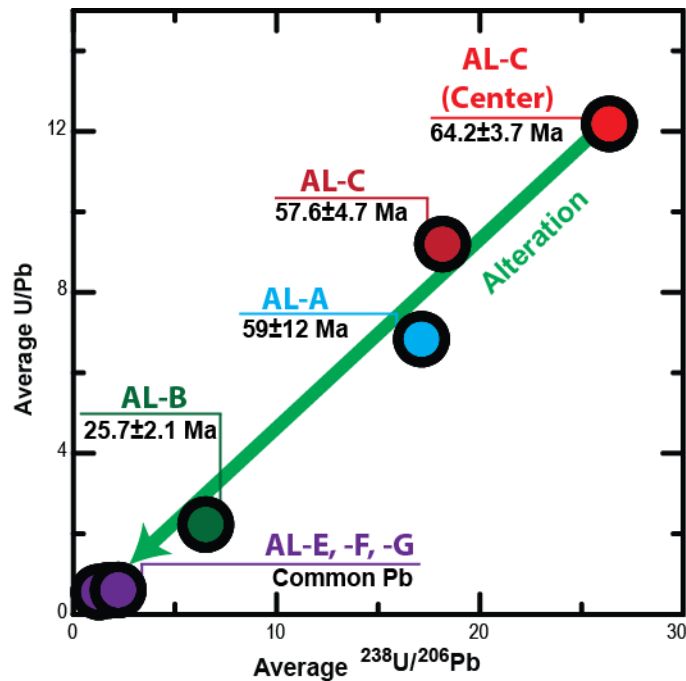
Figure 12: Average elemental U/Pb ratios compared to average $^{238}U/^{206}Pb$ ratios for each tooth analysed from the Arroyo Chijuillita Member of the Nacimiento Formation. A decrease in both ratios is associated with progressively younger dates, and can thus be attributed to the action of post-fossilisation alteration.
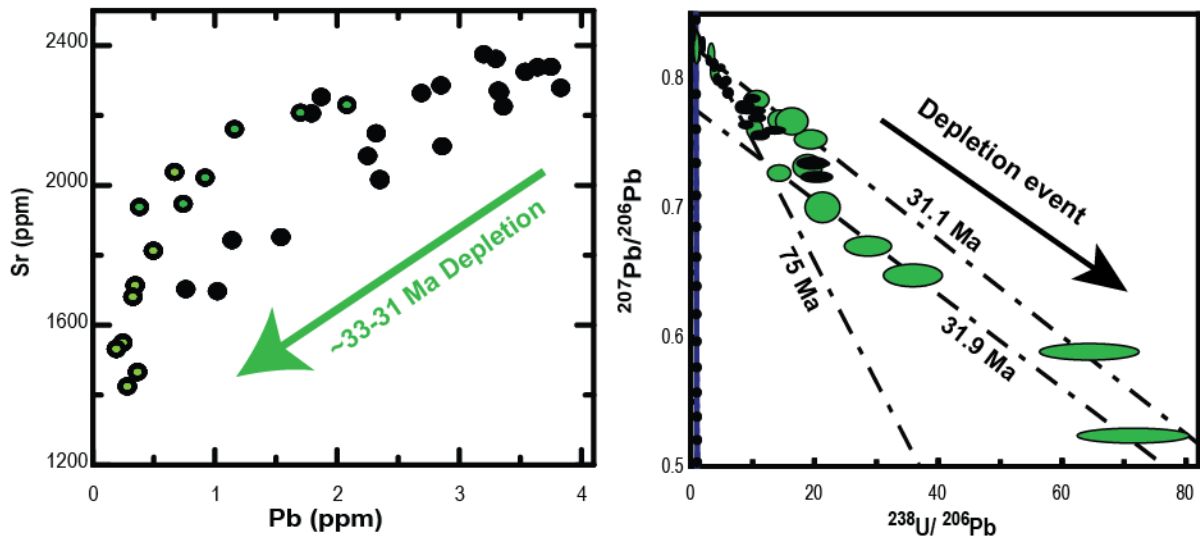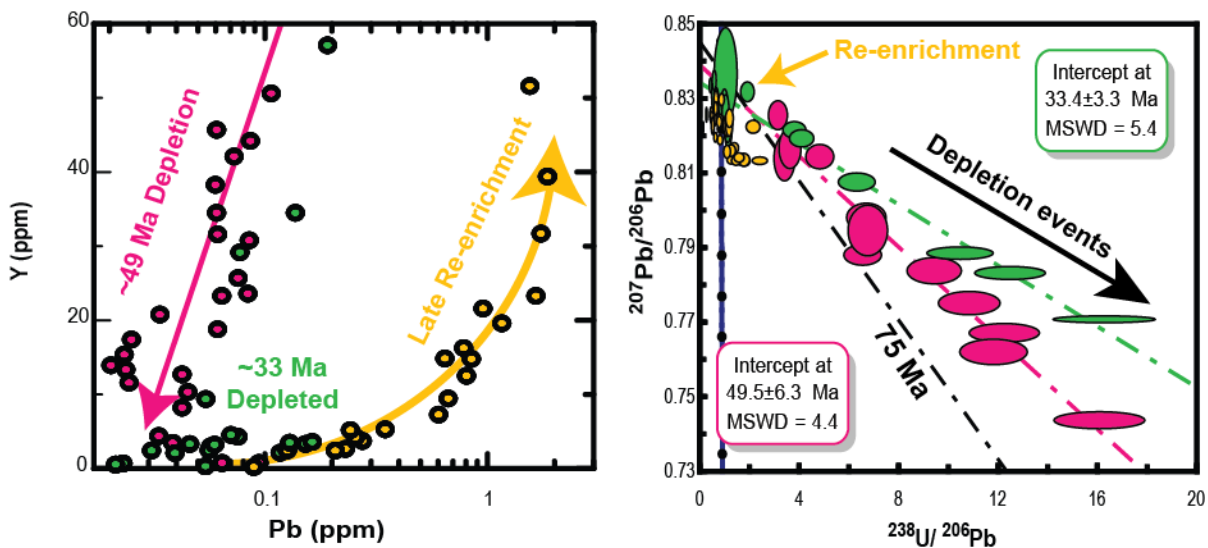
Figure 13 a. Variation in Sr with Pb and corresponding Tera-Wasserburg plot for high-Sr teeth from the Dinosaur Park Formation, demonstrating that altered analyses are depleted in trace elements and skewed to higher $^{238}U/^{206}Pb$ values compared to the fossilisation-age signature. Dates represent reference lines produced using a selection of T408-C or T408-B analyses; b. Variation in Y with Pb and corresponding Tera-Wasserburg plot for low-Sr teeth from the Dinosaur Park Formation, showing ~49 Ma and ~33 Ma depletion events. A late re-enrichment skews U-Pb analyses towards a common Pb composition. Error ellipses are 2σ.

9. Tables

Table 1
Isotopic and age data acquired using IDTIMS on material extracted from AL-D. '1s' represents 1 sigma.

	Weight (mg)	U (ppm)	Pb (ppm)	Model Th (ppm)	Model Th/U	$^{207}Pb/^{235}U$ Ratio	%err (1s)	$^{206}Pb/^{238}U$ Ratio	%err (1s)	rho	$^{207}Pb/^{206}Pb$ Ratio	%err (1s)	$^{238}U/^{204}Pb$	1s	$^{206}Pb/^{204}Pb$	1s	$^{206}Pb/^{238}U$ (Ma)	Error (1s)	Disc. (%)
AL-D-1	0.1163	56.76	3.30	8.87	0.156	0.07715	12.53	0.00977	1.80	0.082	0.0573	12.51	1308.6	14.48	31.389	0.084	62.7	1.12	87.96
AL-D-2	0.0292	60.93	3.68	2.81	0.046	0.05464	23.17	0.00952	2.00	0.191	0.0416	22.87	1232.4	24.47	30.349	0.245	61.1	1.22	124.99
AL-D-3	0.0146	62.48	3.72	9.08	0.145	0.06463	18.00	0.00956	1.88	0.117	0.0490	17.87	1260.7	44.05	30.660	0.431	61.3	1.15	59.32
AL-D-4	0.1360	47.63	3.00	9.70	0.204	0.07874	13.30	0.00987	1.87	0.058	0.0579	13.32	1193.1	12.61	30.380	0.065	63.3	1.18	88.37
AL-D-5	0.0259	51.65	3.52	12.62	0.244	0.08908	14.44	0.00966	2.14	0.140	0.0669	14.30	1087.5	24.14	29.120	0.236	62.0	1.32	92.99

Table 2a
U-Pb laser ablation ICP-MS results for AL-D, an alligatoroid crocodilian from the De-na-zin Member, San Juan Basin, and the Durango apatite standard acquired during this session.

Sample ID	^{206}Pb (cps)	^{204}Pb (cps)	$\dfrac{^{238}U}{^{206}Pb}$ meas.	1 SE	$\dfrac{^{207}Pb}{^{206}Pb}$ meas.	1 SE	f_{206}	$1\text{-}f_{206}$	$\dfrac{^{206}Pb}{^{238}U}$ corr.	$\dfrac{^{206}Pb}{^{238}U}$ age (Ma)	1 SE
AL-D-1	73878	3656	34.28	0.33	0.486	0.0011	0.584	0.416	0.0121	77.7	1.77
AL-D-2	70312	3672	26.72	0.22	0.566	0.0011	0.691	0.309	0.0116	74.1	1.93
AL-D-3	96458	4703	21.23	0.25	0.618	0.0018	0.760	0.240	0.0113	72.4	3.53
AL-D-4	96535	4813	16.82	0.20	0.658	0.0020	0.813	0.187	0.0111	71.3	4.41
AL-D-5	93286	4484	20.03	0.28	0.623	0.0014	0.766	0.234	0.0117	74.8	4.37
AL-D-6	79960	3697	23.02	0.26	0.591	0.0016	0.725	0.275	0.0120	76.6	3.09
AL-D-7	66470	2971	28.77	0.30	0.538	0.0013	0.654	0.346	0.0120	77.1	2.28
AL-D-8	62716	2876	28.05	0.24	0.537	0.0009	0.653	0.347	0.0124	79.3	1.90
AL-D-9	82267	3121	38.19	0.31	0.472	0.0022	0.566	0.434	0.0114	72.8	1.34
AL-D-10	81910	3100	36.19	0.30	0.481	0.0014	0.578	0.422	0.0117	74.7	1.48
AL-D-11	77977	3144	32.49	0.33	0.509	0.0016	0.615	0.385	0.0119	76.0	1.97
AL-D-12	78781	3175	31.90	0.27	0.516	0.0012	0.625	0.375	0.0118	75.4	1.70
AL-D-13	73672	3011	30.69	0.17	0.521	0.0009	0.631	0.369	0.0120	77.0	1.18
AL-D-14	67554	2775	34.61	0.49	0.499	0.0016	0.602	0.398	0.0115	73.7	2.60
AL-D-15	59375	2668	29.87	0.33	0.538	0.0010	0.654	0.346	0.0116	74.2	2.37
AL-D-16	57290	2605	30.14	0.36	0.537	0.0016	0.653	0.347	0.0115	73.8	2.50
AL-D-17	59220	2662	29.21	0.24	0.538	0.0012	0.654	0.346	0.0118	75.8	1.76
AL-D-18	56775	2432	33.46	0.29	0.513	0.0009	0.620	0.380	0.0114	72.8	1.67
AL-D-19	60707	2622	30.92	0.30	0.521	0.0016	0.630	0.370	0.0120	76.6	2.01
AL-D-20	67520	2777	32.06	0.35	0.517	0.0021	0.625	0.375	0.0117	74.9	2.15
AL-D-21	75602	3018	31.60	0.45	0.505	0.0024	0.609	0.391	0.0124	79.2	2.88
AL-D-22	76722	3162	29.53	0.28	0.531	0.0014	0.645	0.355	0.0120	77.0	2.06
AL-D-23	73080	2948	33.55	0.27	0.514	0.0015	0.621	0.379	0.0113	72.4	1.52
AL-D-24	70903	2825	36.05	0.27	0.488	0.0013	0.588	0.412	0.0114	73.3	1.32
AL-D-25	81363	2972	38.61	0.34	0.444	0.0011	0.529	0.471	0.0122	78.2	1.46
AL-D-26	80738	2896	39.64	0.45	0.460	0.0012	0.550	0.450	0.0114	72.8	1.81
AL-D-27	92293	3685	30.90	0.74	0.520	0.0053	0.630	0.370	0.0120	76.7	4.93
AL-D-28	79772	2933	35.67	0.29	0.480	0.0011	0.576	0.424	0.0119	76.1	1.44
AL-D-29	84557	3343	32.16	0.62	0.512	0.0032	0.619	0.381	0.0118	75.8	3.85
AL-D-30	101125	3686	36.04	0.29	0.494	0.0015	0.595	0.405	0.0112	72.0	1.43
Durango-1	6570	372	123.71	1.38	0.236	0.0035	0.240	0.760	0.0061	39.5	0.58
Durango-2	6687	443	122.20	2.01	0.252	0.0075	0.260	0.740	0.0061	38.9	0.86
Durango-3	6840	420	121.39	2.43	0.245	0.0067	0.250	0.750	0.0062	39.7	1.06
Durango-4	4150	532	103.95	1.58	0.340	0.0082	0.371	0.629	0.0061	38.9	0.94
Durango-5	3966	509	102.53	2.05	0.334	0.0077	0.364	0.636	0.0062	39.9	1.25
Durango-6	4052	516	102.64	2.57	0.332	0.0113	0.360	0.640	0.0062	40.0	1.56
Durango-7	3708	327	109.14	2.63	0.312	0.0108	0.335	0.665	0.0061	39.2	1.41
Durango-8	3562	304	109.21	2.07	0.318	0.0055	0.343	0.657	0.0060	38.7	1.11
Durango-9	3540	311	107.44	1.66	0.330	0.0053	0.359	0.641	0.0060	38.4	0.92

Table 2b
U-Pb laser ablation ICP-MS results reported in Table 2a for AL-D,
normalized using Durango apatite.

Sample ID	$\frac{^{238}U}{^{206}Pb}$ norm.	1 SE	$\frac{^{207}Pb}{^{206}Pb}$ meas.	1 SE	$\frac{^{206}Pb}{^{238}U}$ norm.	$\frac{^{206}Pb}{^{238}U}$ age (Ma)	1 SE
AL-D-1	41.86	0.94	0.4859	0.0011	0.0102	65.6	2.22
AL-D-2	32.63	0.71	0.5660	0.0011	0.0098	62.6	2.31
AL-D-3	25.93	0.61	0.6180	0.0018	0.0095	61.1	3.74
AL-D-4	20.54	0.48	0.6575	0.0020	0.0094	60.2	4.58
AL-D-5	24.45	0.60	0.6225	0.0014	0.0098	63.1	4.56
AL-D-6	28.11	0.65	0.5913	0.0016	0.0101	64.7	3.37
AL-D-7	35.13	0.80	0.5381	0.0013	0.0101	65.1	2.64
AL-D-8	34.26	0.75	0.5373	0.0009	0.0104	66.9	2.34
AL-D-9	46.64	1.02	0.4723	0.0022	0.0096	61.4	1.83
AL-D-10	44.20	0.97	0.4812	0.0014	0.0098	63.1	1.96
AL-D-11	39.67	0.90	0.5086	0.0016	0.0100	64.2	2.36
AL-D-12	38.96	0.86	0.5161	0.0012	0.0099	63.7	2.14
AL-D-13	37.48	0.79	0.5210	0.0009	0.0101	65.0	1.77
AL-D-14	42.27	1.05	0.4993	0.0016	0.0097	62.2	2.90
AL-D-15	36.47	0.84	0.5385	0.0010	0.0098	62.6	2.69
AL-D-16	36.81	0.87	0.5374	0.0016	0.0097	62.3	2.80
AL-D-17	35.68	0.78	0.5384	0.0012	0.0100	64.0	2.19
AL-D-18	40.87	0.90	0.5125	0.0009	0.0096	61.5	2.09
AL-D-19	37.76	0.85	0.5205	0.0016	0.0101	64.6	2.41
AL-D-20	39.15	0.90	0.5167	0.0021	0.0099	63.2	2.51
AL-D-21	38.58	0.96	0.5047	0.0024	0.0104	66.9	3.19
AL-D-22	36.07	0.81	0.5315	0.0014	0.0101	65.0	2.45
AL-D-23	40.97	0.90	0.5136	0.0015	0.0095	61.1	1.97
AL-D-24	44.02	0.95	0.4884	0.0013	0.0096	61.9	1.82
AL-D-25	47.15	1.05	0.4442	0.0011	0.0103	66.0	1.99
AL-D-26	48.40	1.12	0.4598	0.0012	0.0096	61.5	2.20
AL-D-27	37.74	1.18	0.5203	0.0053	0.0101	64.7	5.11
AL-D-28	43.56	0.95	0.4799	0.0011	0.0100	64.2	1.95
AL-D-29	39.28	1.10	0.5122	0.0032	0.0100	64.0	4.07
AL-D-30	44.01	0.96	0.4941	0.0015	0.0095	60.8	1.89

Table 3
Trace element concentrations in ppm measured by laser ablation ICP-MS along the cross-sections of unfossilised American Alligator teeth from the Toronto Zoo.

Sample ID	Cr	Mn	Fe	Cu	Zn	Rb	Sr	Pb	U
MT-A-1	0.13	2.37	218.1	3.77	16.5	0.751	303	0.244	0.0253
MT-A-2	0.63	8.02	212.2	3.81	22.8	0.793	276.2	0.217	0.0271
MT-A-3	1.01	1.54	211.1	1.33	17.7	0.792	245	0.159	0.0091
MT-A-4	1.16	1.31	208	1.93	22.1	0.828	256	0.125	0.0146
MT-A-5	1.12	2.47	200.1	0.88	23.2	0.924	211	0.174	0.0083
MT-A-6	1.33	2.57	205.3	0.867	31.8	1.113	211.4	0.186	0.0075
MT-A-7	1.08	2.7	199.1	0.744	28.9	1.133	205.1	0.16	0.0103
MT-A-8	1.42	3.019	199.9	0.85	24.3	1.186	212.5	0.158	0.0068
MT-A-9	1.47	7.8	202.4	0.693	25.9	1.277	206.8	0.15	0.0102
MT-A-10	2.01	6.7	195.5	0.692	24	1.65	213.1	0.126	0.0112
MT-A-11	1.31	3.9	186.5	0.95	19.37	1.518	221.2	0.094	0.007
MT-A-12	1.44	3.19	192.5	0.92	19.8	1.326	220.4	0.097	0.0103
MT-A-13	1.79	4.88	187.8	0.89	15.62	1.131	205.4	0.08	0.0083
MT-A-14	1.41	3.64	183.7	1.08	18.16	0.801	236.5	0.118	0.0182
MT-A-15	1.48	2.87	186.1	1.071	23.1	0.72	219.5	0.136	0.0131
MT-A-16	261	93	1230	760	1240	5.3	492	34	0.29
MT-A-17	144	70	1250	630	850	5.3	700	74	0.21
MT-A-18	119	37.4	570	350	870	4.2	780	3.42	0.052
MT-A-19	1.47	2.9	182.6	1.18	25.7	0.776	254	0.133	0.0123
MT-A-20	1.82	3.49	183.1	1.19	18	0.729	274	0.138	0.016
MT-A-21	1.3	4.4	174.6	1.11	15.4	0.847	227.2	0.099	0.0118
MT-A-22	1.69	4.07	175.3	1.34	15.71	0.985	185.9	0.085	0.0088
MT-A-23	1.69	2.93	175.3	1.068	16.95	0.97	212.4	0.079	0.0071
MT-A-24	1.3	3.8	179.8	1.027	17.6	0.983	232.1	0.103	0.0109
MT-A-25	1.46	6.29	169.8	0.94	16.2	1.018	197.4	0.093	0.0113
MT-A-26	1.53	7.72	174.4	0.818	17.9	0.914	196.1	0.099	0.0036
MT-A-27	1.32	3.33	171.1	0.744	22	0.678	208.2	0.148	0.0073
MT-A-28	1.77	2.86	171.4	0.763	27.8	0.609	205.9	0.173	0.005
MT-A-29	2.26	2.23	172.5	0.73	25.2	0.432	212.9	0.2	0.0152
MT-A-30	2.64	1.13	176.4	0.7	14.2	0.413	234	0.154	0.006
MT-A-31	1.08	1.88	171.8	0.43	8.41	0.545	254.5	0.032	0.001
MT-A-32	0.87	0.316	174	1.49	7.66	0.497	217.3	0.0297	0.00047
MT-B-1	0.37	3.61	173.3	1.45	11.76	0.517	211.2	0.206	-
MT-B-2	1.17	5.24	177	0.493	21.6	0.435	209.8	0.1386	-
MT-B-3	1.11	6.92	172.9	0.53	20.18	0.567	211.9	0.104	-
MT-B-4	1.06	5.37	168.2	0.622	15.3	0.706	210.9	0.063	-
MT-B-5	1.12	7.79	170.5	0.66	15.15	0.75	242.6	0.0817	-
MT-B-6	1.25	6.36	171.9	0.91	14.26	0.854	216.3	0.091	-

Table 3 (*continued*)

Sample ID	Cr	Mn	Fe	Cu	Zn	Rb	Sr	Pb	U
MT-B-7	1.23	8.62	170.6	0.657	22.8	0.9	237.7	0.097	-
MT-B-8	1.53	8.68	172.2	0.71	24.8	0.9	239.2	0.054	-
MT-B-9	1.43	5.15	172.1	0.92	29.5	0.758	253.7	0.061	-
MT-B-10	1.44	6.33	173.7	0.849	36.7	0.572	262	0.116	-
MT-B-11	1.74	7.35	173.7	0.932	28	0.39	245	0.091	-
MT-B-12	1.61	12.55	171	1	29.7	0.616	264.3	0.098	-
MT-B-13	1.54	14.16	173.6	0.87	28.3	0.612	245.2	0.094	-
MT-B-14	1.15	8.21	174.6	0.572	55.7	0.33	235.3	0.225	-
MT-B-15	1.59	8.44	173.9	0.67	54.2	0.332	263.7	0.274	-
MT-B-16	20.6	5.4	215.7	93	152	0.88	1195	0.275	-
MT-B-17	1.24	6.18	178.1	0.91	25.2	0.644	252.6	0.131	-
MT-B-18	1.62	12.62	175.8	0.892	31.7	1.007	243	0.095	-
MT-B-19	1.7	8.65	176.3	1.04	25.6	1.31	251.7	0.106	-
MT-B-20	1.74	8.01	177.9	1.09	35.4	1.58	261.6	0.095	-
MT-B-21	1.01	6.6	173.6	0.908	35.3	1.626	272	0.125	-
MT-B-22	1.21	7.21	180.9	0.9	25.7	1.45	245.3	0.064	-
MT-B-23	1.63	9.56	178.4	0.78	25.2	1.37	234.7	0.063	-
MT-B-24	1.28	7.87	178.2	0.67	16.76	1.275	238	0.037	-
MT-B-25	1.6	5.59	183.3	0.58	16.07	1.168	250.6	0.07	-
MT-B-26	1.22	5.64	178.4	0.4	20.27	1.024	223.4	0.086	-
MT-B-27	1.5	4.6	184.2	0.505	20.3	1.03	192.7	0.095	-
MT-B-28	1.1	2.99	185	0.77	10.23	0.777	212	0.057	-
MT-C-1	-	0.637	183.2	-	7.07	1.183	298	0.028	-
MT-C-2	-	1.111	191.3	-	8.02	1.473	277	0.034	-
MT-C-3	1.28	1.88	189.4	0.47	20.7	1.551	267.1	0.108	-
MT-C-4	1.02	4.24	190.9	0.44	30.3	1.983	301	0.131	-
MT-C-5	1.25	6.72	191	0.59	30.6	2.99	278	0.165	-
MT-C-6	1.33	10.73	196.5	0.732	24.8	3.05	253	0.149	-
MT-C-7	0.86	8.35	198.3	0.76	21.7	3.79	210.3	0.082	-
MT-C-8	1.32	14.44	197.5	0.81	21.7	3.72	225.2	0.163	-
MT-C-9	1.38	12.58	194.2	0.85	24.1	3.57	215.1	0.171	-
MT-C-10	1.3	8.74	194.1	0.97	22.3	3.22	222.9	0.112	-
MT-C-11	1.57	5.65	196.9	1.01	22.6	3.43	241.8	0.118	-
MT-C-12	2.27	11.11	204.3	2.18	31.9	2.89	251.1	0.231	-
MT-C-13	1.39	5.86	204.4	0.91	21.93	3.72	239.2	0.118	-
MT-C-14	1.09	10.79	206.3	0.99	22.8	4.35	222.3	0.14	-
MT-C-15	1.04	13.7	210.3	0.93	21.7	5.53	223.1	0.197	-
MT-C-16	-	7.35	211	0.913	17.5	6.43	202.1	0.105	-
MT-C-17	1.38	8.47	218.5	0.752	21.8	6.77	220.4	0.101	-
MT-C-18	0.89	10.85	215.3	0.94	26.4	6.64	264.9	0.162	-

Table 3 (*continued*)

Sample ID	Cr	Mn	Fe	Cu	Zn	Rb	Sr	Pb	U
MT-C-19	0.84	5.89	218.9	1.18	29.5	5.47	276.2	0.162	-
MT-C-20	1.05	2.5	219.6	0.544	31.3	3.77	284.2	0.177	-
MT-C-21	1.13	1.14	224.9	0.68	15.4	2.93	267.4	0.09	-
MT-C-22	-	0.651	226.7	0.57	8.57	1.732	279.5	0.048	-

Table 4

Trace element concentrations in ppm measured by high resolution laser ablation coupled with sector field ICP-MS along the cross-section of unfossilised American Alligator tooth MT-B.

Sample ID	La	Ce	Pr	Nd	Sm	Eu	Gd	Tb	Dy	Ho	Er	Tm	Yb	Lu
MT-B-1	0.0016	-	-	-	-	-	-	0.00126	-	-	-	-	-	0.00137
MT-B-2	-	-	-	0.0017	-	-	-	0.00065	-	-	-	-	-	0.00089
MT-B-3	0.00102	0.00022	-	-	-	-	-	0.00067	-	-	-	-	-	-
MT-B-4	-	-	-	-	-	-	-	0.00086	-	-	-	-	-	0.00098
MT-B-5	0.00062	0.00024	0.000086	-	-	-	-	0.00075	-	-	-	-	-	-
MT-B-6	-	-	-	-	-	-	-	0.00065	-	-	-	-	-	-
MT-B-7	-	-	-	-	-	-	-	0.00086	-	-	-	-	-	-
MT-B-8	-	-	-	-	-	-	0.0131	0.00091	-	-	-	-	-	0.00125
MT-B-9	0.00131	0.00028	-	-	-	-	-	0.0009	-	-	-	-	-	-
MT-B-10	0.00112	-	-	-	-	-	-	0.00119	-	-	-	-	-	0.00125
MT-B-11	-	-	-	-	-	-	-	0.00107	-	-	-	-	-	0.00107
MT-B-12	-	-	-	-	-	-	-	0.00112	-	-	-	-	-	-
MT-B-13	0.00094	-	0.000098	-	-	-	0.0156	0.00131	-	-	-	-	-	0.00161
MT-B-14	0.0038	0.00158	0.000222	0.00096	-	-	-	-	-	-	-	-	-	-
MT-B-15	0.00092	0.00103	0.000094	0.00039	-	-	-	-	-	-	-	-	-	-
MT-B-16	0.00057	0.00055	-	-	-	-	0.0126	0.00126	-	-	-	-	-	0.00151
MT-B-17	0.00062	0.00019	-	-	-	-	-	0.00098	-	-	-	-	-	-
MT-B-18	0.0024	0.000177	-	-	-	-	-	0.00151	-	-	-	-	-	0.00116
MT-B-19	0.0004	0.000135	-	-	-	-	-	0.00081	-	-	-	-	-	-
MT-B-20	0.00038	0.00018	-	-	-	-	-	0.00117	-	-	-	-	-	-
MT-B-21	0.00072	0.00026	0.000085	-	-	-	-	0.00111	-	0.00006	-	-	-	0.00127
MT-B-22	0.002	0.00031	-	-	-	-	-	0.00101	-	-	-	-	-	0.00121
MT-B-23	0.0004	0.0003	-	-	-	-	0.0114	0.00127	-	-	-	-	-	0.00152
MT-B-24	0.00053	-	-	-	-	-	-	0.00079	-	-	-	-	-	-
MT-B-25	0.00022	-	-	-	-	-	-	0.00088	-	-	-	-	-	-
MT-B-26	0.00039	0.000063	-	-	-	-	-	0.00093	-	-	-	-	-	-
MT-B-27	0.00021	-	-	-	-	-	-	-	-	-	-	-	-	-

59

Table 5
Trace element concentrations in ppm measured by laser ablation ICP-MS along the cross-section of fossil tooth samples.

Sample ID	Ti	V	Cr	Mn	Fe	Ni	Cu	Zn	Rb	Sr	Zr
Arroyo Chijuillita Member, Nacimiento Fm											
AL-A-1	233	85.2	2.53	4817	457	1.48	13.7	46.1	0.177	3124	6.86
AL-A-2	234	158	2.06	6281	518	1.54	13.3	48.9	0.129	2988	4.13
AL-A-3	234	164	1.99	7480	533	1.42	15.7	53.1	0.138	2835	4.18
AL-A-4	235	195	2.03	9650	602	1.58	17.7	48.4	-	2788	4.45
AL-A-5	234	154	1.92	10520	643	1.42	15.5	44.7	0.141	2803	3.83
AL-A-6	233	150	1.45	10391	642	1.45	13.5	39.5	-	2749	3.49
AL-A-7	231	130	1.79	10710	663	1.57	16.6	39.8	-	2806	3.13
AL-A-8	237	126	2.18	9212	772	1.91	18.8	35.1	-	2603	1.44
AL-A-9	232	88.3	2.80	6080	1027	1.63	28.9	48.5	-	2776	1.91
AL-A-10	235	146	1.81	6450	882	2.14	23.1	56.9	-	2754	1.87
AL-A-11	235	138	2.30	7730	777	1.70	25.8	43.4	-	2709	1.77
AL-A-12	236	152	2.81	9130	1003	2.08	21.5	40.3	-	2579	1.41
AL-A-13	232	153	2.72	11290	790	1.96	21.1	32.6	-	2820	2.53
AL-A-14	237	141	1.33	10770	668	1.35	14.7	37.9	-	2791	3.55
AL-A-15	231	187	1.82	10210	640	1.69	14.3	40.2	-	2819	3.66
AL-A-16	234	219	1.60	9300	613	1.50	12.3	41.9	0.113	2790	3.58
AL-A-17	234	128	1.58	8270	590	1.45	12.5	47.4	0.138	2889	4.40
AL-A-18	230	44.8	2.28	6790	545	1.63	13.3	43.8	0.146	2973	5.42
AL-A-19	234	19.6	1.71	5222	454	1.24	13.6	42.9	0.151	3150	9.75
AL-A-20	236	32.0	2.09	4413	419	3.04	47.9	37.1	0.191	3013	25.5
AL-B-1	237	123	3.00	6500	1963	5.84	70.4	44.5	3.20	2922	18.7
AL-B-2	226	137	-	4420	506	1.18	31.3	22.8	0.227	3110	6.27
AL-B-3	235	137	-	5693	547	1.38	26.2	25.9	0.255	3064	5.08
AL-B-4	234	98.3	1.73	6310	576	1.38	19.7	23.6	0.163	2991	6.07
AL-B-5	230	90.4	-	6510	571	1.79	25.4	23.0	-	3059	5.17
AL-B-6	232	90.1	-	6256	556	1.66	29.2	24.6	-	3072	4.88
AL-B-7	235	84.8	0.910	6148	541	2.07	30.5	25.2	0.186	3100	4.54
AL-B-8	234	80.3	-	6230	568	2.16	33.5	28.1	0.190	3184	4.69
AL-B-9	233	100	-	5920	586	1.78	35.8	24.5	0.173	3213	6.19
AL-B-10	232	91.6	-	5625	543	1.74	42.6	26.1	0.150	3268	6.65
AL-B-11	235	64.5	-	6290	532	1.91	39.6	25.1	0.177	3191	5.44
AL-B-12	231	93.9	1.28	6732	627	1.38	24.4	27.4	0.193	3206	6.24
AL-B-13	242	159	2.90	6240	792	1.85	12.1	29.0	1.460	3360	11.5
AL-B-14	246	120	1.88	5990	1000	2.02	22.6	36.2	1.730	3476	17.1
AL-B-15	235	69.7	-	6002	541	1.20	19.9	25.6	0.212	3322	5.89
AL-B-16	233	60.3	1.14	6970	598	1.81	27.3	23.2	0.157	3097	4.99
AL-B-17	237	72.4	-	7470	698	1.99	35.2	25.2	0.182	3109	5.70
AL-B-18	234	73.0	-	7140	636	2.06	31.2	26.3	0.149	3082	4.49
AL-B-19	235	89.2	-	7100	618	1.57	28.1	24.7	0.192	3118	3.87
AL-B-20	234	69.5	-	6759	601	1.76	28.2	26.2	-	3165	4.33
AL-B-21	234	73.6	-	6311	564	1.60	29.9	27.4	0.170	3164	4.80
AL-B-22	236	71.8	-	6480	568	1.26	28.4	24.2	0.154	3047	4.58
AL-B-23	230	63.2	-	6688	575	1.32	25.3	24.5	-	3027	4.25
AL-B-24	235	62.0	-	6979	623	1.63	19.6	25.7	0.114	3068	4.19
AL-B-25	231	79.4	-	5953	574	1.46	23.9	25.5	-	3085	4.81
AL-B-26	235	79.2	1.21	4542	513	0.84	12.2	24.3	0.137	3101	5.90

Table 5 (continued)

Sample ID	Y	La	Ce	Pr	Nd	Sm	Eu	Gd	Tb	Dy	Ho
Arroyo Chijuillita Member, Nacimiento Fm											
AL-A-1	4600	2143	5860	877	4160	1022	183	1065	150	804	128
AL-A-2	3894	1771	4814	704	3459	861	151	913	128	678	109
AL-A-3	3418	1559	4522	644	3098	770	138	796	112	601	92.7
AL-A-4	3113	1377	3911	575	2684	675	121	724	100	555	86.5
AL-A-5	2759	1250	3541	517	2437	615	108	650	92.6	491	77.7
AL-A-6	2833	1297	3540	531	2490	653	115	692	97.3	521	80.6
AL-A-7	2597	1216	3357	492	2230	613	115	648	91.2	492	74.6
AL-A-8	2131	444	743	75.7	325	98.2	33.6	181	32.9	233	42.5
AL-A-9	2961	1211	2757	357	1558	436	102	560	84.0	481	76.9
AL-A-10	2901	1176	2648	326	1510	425	95.4	546	79.7	469	75.3
AL-A-11	2499	923	1949	234	1079	302	73.5	422	63.1	380	63.0
AL-A-12	1984	400	650	64.8	282	83.3	30.8	162	29.4	207	39.8
AL-A-13	2214	967	2614	345	1539	449	89.8	497	72.9	403	61.6
AL-A-14	2623	1203	3398	501	2358	612	114	657	93.0	500	75.5
AL-A-15	2752	1262	3524	520	2535	643	117	670	96.3	512	77.5
AL-A-16	3108	1332	3699	552	2640	672	121	714	102	546	85.3
AL-A-17	3800	1612	4360	659	3190	792	148	863	121	649	103
AL-A-18	4256	1831	5030	734	3580	890	159	949	131	709	115
AL-A-19	4690	2192	5970	883	4191	1034	188	1082	148	793	130
AL-A-20	4160	2240	6300	871	4020	929	177	953	130	709	116
AL-B-1	3940	1937	4980	726	3230	811	161	855	124	691	117
AL-B-2	4152	2152	5570	809	3700	918	183	991	143	777	124
AL-B-3	4160	1927	5070	714	3330	841	169	936	138	769	122
AL-B-4	4610	1897	4690	661	3120	839	161	955	138	783	131
AL-B-5	4554	1927	4927	687	3266	865	170	972	144	799	131
AL-B-6	4461	1937	4869	686	3418	873	179	983	145	804	130
AL-B-7	4445	1891	4869	679	3343	881	177	981	145	801	128
AL-B-8	4502	1950	5045	698	3371	904	182	998	146	801	130
AL-B-9	4684	2096	5302	749	3560	934	183	1061	154	849	138
AL-B-10	4790	2172	5566	782	3797	986	193	1097	160	875	138
AL-B-11	4749	2162	5450	775	3698	969	197	1105	160	873	139
AL-B-12	5145	2257	5698	800	3856	989	194	1132	167	919	149
AL-B-13	5530	2480	6230	917	4410	1111	213	1222	178	1001	164
AL-B-14	6420	2805	6770	953	4490	1166	230	1319	189	1074	178
AL-B-15	5037	1979	5000	704	3401	914	194	1062	158	880	144
AL-B-16	4507	2052	5290	744	3559	935	194	1046	156	849	134
AL-B-17	4555	2049	5103	739	3504	915	182	1033	151	819	133
AL-B-18	4298	1920	4913	693	3311	888	183	989	146	800	126
AL-B-19	4314	1882	4676	669	3210	854	172	957	141	774	123
AL-B-20	4433	1934	4990	686	3290	876	178	974	143	793	127
AL-B-21	4511	2027	5169	726	3488	933	191	1027	152	828	131
AL-B-22	4347	1895	4879	695	3307	865	174	974	144	789	126
AL-B-23	4270	1816	4610	657	3141	831	169	936	134	756	120
AL-B-24	4305	1785	4520	629	3041	808	163	923	134	753	122
AL-B-25	4207	1962	4950	702	3319	853	172	966	141	772	123
AL-B-26	4381	2310	5929	848	3983	1002	196	1065	154	841	133

Table 5 (*continued*)

Sample ID	Er	Tm	Yb	Lu	Pb	Th	U
Arroyo Chijuillita Member, Nacimiento Fm							
AL-A-1	269.6	28.2	139	18.32	23.22	18.7	90.5
AL-A-2	224.5	22.61	107.4	13.96	21.6	7.23	133.7
AL-A-3	191.1	19.15	88.7	11.43	23.19	6.92	141.1
AL-A-4	173.9	17.58	83.2	11.08	23.4	3.31	235.8
AL-A-5	157	15.27	70.1	8.77	20.91	1.928	126.8
AL-A-6	158.9	15.04	67.5	8.11	17.45	1.436	150.8
AL-A-7	143.7	13.46	56.5	6.34	17.21	0.383	135.6
AL-A-8	95.1	9.8	45.4	4.89	19.6	0.032	169.7
AL-A-9	151.9	13.78	57.3	6.22	43.9	0.0045	258
AL-A-10	148	13.85	58.5	6.51	41.4	0.0053	210.8
AL-A-11	126.8	12.02	50.28	5.46	32.8	0.0179	203.4
AL-A-12	89.6	9.44	44.65	4.77	38.3	0.022	201.4
AL-A-13	118.9	11.12	47.6	5.076	19.5	0.093	301
AL-A-14	144.4	13.8	58.5	6.67	17.18	0.596	152.4
AL-A-15	150.3	14.46	64	7.53	17.76	0.709	147
AL-A-16	172.1	17.04	78.1	10.15	18.7	1.241	151.7
AL-A-17	214.9	22.5	108.9	14.51	20.11	3.16	143.7
AL-A-18	246.6	26.4	126.7	17.45	20.47	6.56	91.6
AL-A-19	271	29	140.9	18.97	21.12	13.12	57.4
AL-A-20	257	28.6	151	21	33.7	90.4	59.1
AL-B-1	265	31.5	178	25.3	54.1	25.8	129
AL-B-2	268	29.8	161	21.8	19.8	12.7	45.4
AL-B-3	265	29.4	152	20.8	19.7	5.91	29.5
AL-B-4	284	31.5	164	23.8	18.4	2.86	45.4
AL-B-5	280	30.6	163	21.9	17.6	3.28	29.3
AL-B-6	279	30.4	156	21.7	17.8	2.99	11.5
AL-B-7	275	29.3	152	21.1	18.1	2.63	10.5
AL-B-8	274	29.6	151	20.2	18.7	3.72	15.2
AL-B-9	295	32.6	166	22.9	18.8	5.90	82.6
AL-B-10	295	32.5	168	23.0	18.9	5.99	62.4
AL-B-11	295	31.4	161	21.3	18.4	4.24	30.0
AL-B-12	318	34.3	175	23.1	20.2	3.70	158
AL-B-13	364	39.4	209	28.9	26.6	9.50	130
AL-B-14	396	45.6	239	33.0	35.8	8.90	329
AL-B-15	312	33.7	180	24.8	17.7	0.43	63.1
AL-B-16	280	29.5	151	19.9	17.0	1.86	25.3
AL-B-17	283	30.5	155	21.2	19.5	8.76	47.1
AL-B-18	268	28.2	144	19.0	17.8	3.36	11.6
AL-B-19	258	27.7	140	19.1	17.3	2.91	10.6
AL-B-20	269	29.8	150	19.9	18.2	4.30	11.4
AL-B-21	280	30.2	153	20.6	19.7	5.23	11.8
AL-B-22	268	29.3	149	20.3	17.3	3.96	10.7
AL-B-23	258	27.9	144	19.5	16.4	3.88	9.63
AL-B-24	262	28.8	147	20.5	16.6	3.09	9.40
AL-B-25	268	29.2	151	20.7	16.8	5.31	19.1
AL-B-26	284	31.5	169	22.9	19.7	14.9	29.6

Table 5 (*continued*)

Sample ID	Ti	V	Cr	Mn	Fe	Ni	Cu	Zn	Rb	Sr	Zr
Arroyo Chijuillita Member, Nacimiento Fm											
AL-C-1	232	50.3	-	6540	705	1.12	11.0	32.8	-	3120	3.53
AL-C-2	230	80.2	-	6532	704	1.11	8.87	31.9	-	3143	2.54
AL-C-3	232	89.3	1.59	7580	772	1.29	16.8	30.7	-	3043	1.97
AL-C-4	234	122	1.57	7350	795	1.24	18.8	27.9	-	3021	1.16
AL-C-5	234	32.9	-	7390	854	1.19	20.3	31.9	-	2978	0.733
AL-C-6	237	29.7	-	7201	815	1.14	22.2	31.5	-	2899	0.530
AL-C-7	233	32.5	-	7270	767	2.01	15.3	35.1	-	2773	0.457
AL-C-8	233	31.9	-	7950	782	2.58	8.56	31.7	-	2757	0.302
AL-C-9	221	31.3	-	7769	739	2.23	10.9	31.1	-	2750	0.276
AL-C-10	225	34.6	-	8020	763	2.18	8.24	29.5	-	2814	0.233
AL-C-11	225	30.8	-	7990	778	2.24	5.23	27.2	-	2692	0.190
AL-C-12	207	72.5	-	8020	764	3.05	5.45	30.1	-	2730	0.187
AL-C-13	185	60.3	-	7980	789	2.55	5.07	29.7	-	2759	0.173
AL-C-14	211	64.1	1.51	8000	1144	3.40	5.01	31.4	-	2704	0.203
AL-C-15	228	58.6	1.46	8220	1155	3.08	4.87	31.3	-	2633	0.185
AL-C-16	235	77.5	1.29	8570	1175	2.70	4.64	30.8	-	2715	0.193
AL-C-17	233	81.4	1.44	8367	1227	2.57	9.22	30.8	-	2781	0.252
AL-C-18	229	48.6	-	8260	1187	2.42	8.03	28.6	-	2602	0.233
AL-C-19	229	61.2	0.880	8480	1256	2.22	6.16	29.0	-	2620	0.239
AL-C-20	236	51.7	1.75	8190	1224	2.11	9.53	31.5	-	2626	0.280
AL-C-21	233	42.2	2.00	7730	1253	1.52	14.2	31.7	-	2672	0.400
AL-C-22	224	39.3	2.25	7710	1485	1.89	19.0	35.3	-	2970	0.790
AL-C-23	230	87.0	1.71	7540	1380	1.26	9.43	34.4	-	3137	2.66
AL-C-24	230	94.1	2.18	6890	1565	1.02	9.48	36.0	-	3290	3.08
AL-C-25	233	102	1.81	7413	1678	1.27	11.8	34.7	-	3341	3.90
AL-C-26	235	122	1.66	8181	1996	1.38	13.3	37.8	-	3565	6.98
AL-C-27	237	27.5	1.32	8640	2059	1.23	17.0	37.7	-	3308	13.1
De-na-zin Member											
AL-D-1	190	15.9	6.50	4277	1040	8.130	19.6	32.3	2.40	2240	46.2
AL-D-2	178	30.5	9.28	4362	765	2.330	16.7	28.5	0.118	1829	58.3
AL-D-3	179	12.0	4.43	4498	733	2.470	14.3	25.9	0.070	1811	51.6
AL-D-4	179	15.4	3.14	4480	752	1.810	16.9	42.0	0.218	1858	45.9
AL-D-5	176	11.3	1.98	4641	729	2.030	24.6	31.8	0.184	1921	55.3
AL-D-6	179	8.97	1.86	4950	743	2.450	14.6	20.5	0.048	1849	44.8
AL-D-7	180	9.33	4.13	4910	730	2.720	14.7	22.7	0.048	1781	47.6
AL-D-8	179	8.12	1.95	5310	763	2.140	16.8	29.5	0.094	1854	46.2
AL-D-9	178	8.35	2.62	5067	770	2.030	17.5	26.9	0.184	1806	42.0
AL-D-10	173	8.10	3.20	5010	770	2.620	19.7	23.6	0.169	1809	38.6
AL-D-11	176	8.90	2.10	5450	819	5.000	22.3	42.1	0.020	2050	29.5
AL-D-12	174	7.85	2.78	5041	775	2.440	14.1	27.3	0.157	1834	31.8
AL-D-13	178	9.00	3.90	5060	808	5.520	14.0	27.3	0.044	1831	27.1
AL-D-14	173	9.29	2.58	4910	802	3.370	15.9	26.3	0.088	1891	32.8
AL-D-15	175	10.7	3.60	4700	754	2.040	12.6	20.5	0.130	1808	36.8
AL-D-16	179	11.2	4.77	4780	765	2.980	14.0	23.5	0.131	1794	74.1
AL-D-17	175	11.3	3.30	4490	757	2.870	15.0	28.7	0.158	1778	68.3
AL-D-18	180	11.8	2.68	4223	756	3.740	15.2	32.0	0.168	1864	70.6
AL-D-19	174	3.40	2.76	2760	641	1.950	14.8	26.1	0.115	1200	9.50

Table 5 (*continued*)

Sample ID	Y	La	Ce	Pr	Nd	Sm	Eu	Gd	Tb	Dy	Ho
Arroyo Chijuillita Member, Nacimiento Fm											
AL-C-1	2361	1348	3452	453	2005	504	101	550	75.7	419	64.2
AL-C-2	2940	1650	4360	618	2740	656	129	730	98.1	524	82.1
AL-C-3	2533	1280	2980	362	1601	436	95.2	504	73.9	425	67.3
AL-C-4	2106	860	1850	208	913	245	62.2	318	49.7	298	49.8
AL-C-5	1617	461	981	107	457	125	34.6	177	30.1	198	33.7
AL-C-6	1484	361	673	73.3	308	86.6	25.5	133	23.8	163	28.7
AL-C-7	578	81.2	101	11.0	46.3	13.0	4.65	27.2	5.66	46.5	10.0
AL-C-8	64.0	6.39	12.0	1.67	6.76	1.79	0.524	2.59	0.456	3.67	0.780
AL-C-9	123	26.8	54.1	6.62	27.8	8.09	2.14	10.9	1.99	13.5	2.42
AL-C-10	78.0	14.8	29.1	3.58	14.9	4.56	1.07	5.74	1.10	7.65	1.49
AL-C-11	17.2	2.67	5.29	0.671	3.02	0.730	0.195	1.12	0.204	1.45	0.284
AL-C-12	35.9	7.02	14.3	1.78	8.10	2.12	0.518	3.43	0.540	3.29	0.584
AL-C-13	29.1	6.35	13.3	1.77	7.20	2.12	0.550	2.83	0.500	3.41	0.603
AL-C-14	26.6	4.41	8.17	0.969	4.54	1.10	0.393	2.00	0.337	2.41	0.466
AL-C-15	17.1	3.30	6.59	0.793	3.56	0.810	0.270	1.55	0.255	1.80	0.309
AL-C-16	9.54	0.65	0.980	0.126	0.510	0.112	0.065	0.222	0.039	0.523	0.105
AL-C-17	65.8	17.4	35.5	4.54	19.5	5.15	1.39	6.63	1.16	8.15	1.43
AL-C-18	71.9	18.0	37.1	4.82	20.58	5.60	1.50	7.43	1.30	8.70	1.55
AL-C-19	50.6	7.96	15.9	2.09	8.98	2.55	0.634	3.39	0.548	3.76	0.768
AL-C-20	253	27.6	42.6	4.86	21.4	5.86	1.85	10.3	2.03	16.7	3.75
AL-C-21	679	119	190	23.0	99.0	27.5	8.16	44.7	8.36	63.6	12.3
AL-C-22	1373	401	808	86.1	371	103	28.8	153	25.6	169	29.5
AL-C-23	3066	1613	4280	598	2670	672	133	724	99.9	556	88.2
AL-C-24	3502	1990	5397	772	3656	855	162	904	124	656	101
AL-C-25	3975	2120	5730	806	3844	895	171	987	132	715	116
AL-C-26	4640	2398	6130	861	4090	961	180	1031	138	754	123
AL-C-27	4448	2281	5710	796	3809	873	175	976	130	727	124
De-na-zin Member											
AL-D-1	1605	855	1852	263	1192	324	64.6	348	48.3	271	47.4
AL-D-2	1100	545	1174	171	793	222	47.1	248	34.4	182	29.0
AL-D-3	1003	480	1013	146	678	192	41.1	220	30.6	162	26.2
AL-D-4	1398	885	1924	286	1390	375	73.2	415	53.4	268	41.8
AL-D-5	1448	864	1850	275	1328	360	70.7	407	52.7	268	42.0
AL-D-6	940	449	926	133	634	181	39.5	215	30.3	161	25.3
AL-D-7	971	431	881	125	595	167	36.7	202	28.9	157	25.7
AL-D-8	964	461	955	136	646	183	39.0	216	30.2	163	26.0
AL-D-9	944	438	898	128	604	169	36.5	203	28.3	154	25.4
AL-D-10	865	409	835	118	549	154	33.9	186	26.5	140	22.7
AL-D-11	771	362	759	106	491	133	29.9	166	24.2	132	19.3
AL-D-12	789	382	801	113	529	147	32.3	181	25.4	135	20.4
AL-D-13	788	411	896	127	596	166	36.8	199	28.1	145	20.8
AL-D-14	861	473	1026	149	675	191	41.8	226	31.1	160	23.6
AL-D-15	812	405	886	128	593	167	36.6	193	27.9	142	21.7
AL-D-16	1222	473	940	131	618	173	36.2	208	29.5	173	32.3
AL-D-17	1170	532	1113	164	768	209	43.8	242	34.1	183	31.7
AL-D-18	1403	711	1468	213	989	272	56.4	308	42.5	232	39.9
AL-D-19	470	280	540	77.0	420	93.0	17.6	99.0	15.2	67.0	11.5

Table 5 (*continued*)

Sample ID	Er	Tm	Yb	Lu	Pb	Th	U
Arroyo Chijuillita Member, Nacimiento Fm							
AL-C-1	131	12.6	55.7	6.30	17.8	-	64.8
AL-C-2	164	15.6	69.9	7.89	17.9	-	93.6
AL-C-3	136	13.0	57.1	6.31	12.3	-	107
AL-C-4	107	10.7	48.8	5.33	10.1	-	77.3
AL-C-5	77.7	8.30	40.0	4.40	8.74	-	40.2
AL-C-6	67.6	7.63	36.7	4.05	7.67	-	31.9
AL-C-7	26.9	3.40	17.8	2.14	4.42	-	47.9
AL-C-8	2.37	0.40	3.24	0.45	4.16	-	53.2
AL-C-9	5.78	0.71	4.05	0.45	2.88	-	40.4
AL-C-10	3.68	0.47	2.93	0.34	2.35	-	41.6
AL-C-11	0.77	0.11	0.69	0.10	2.51	-	42.0
AL-C-12	1.65	0.22	1.43	0.18	4.86	-	53.1
AL-C-13	1.44	0.18	1.27	0.16	5.77	-	57.4
AL-C-14	1.19	0.17	1.10	0.14	5.51	-	60.3
AL-C-15	0.845	0.11	0.80	0.10	6.16	-	55.4
AL-C-16	0.350	0.06	0.50	0.07	5.41	-	54.4
AL-C-17	3.26	0.39	2.33	0.25	3.80	-	57.6
AL-C-18	3.73	0.44	2.58	0.33	2.82	-	37.5
AL-C-19	2.23	0.33	2.45	0.34	4.25	-	61.6
AL-C-20	10.9	1.52	9.36	1.16	4.29	-	51.4
AL-C-21	32.1	3.96	20.1	2.36	5.47	-	65.2
AL-C-22	66.8	7.41	34.1	3.70	8.36	-	56.9
AL-C-23	180	17.3	77.0	9.31	17.6	-	103
AL-C-24	207	19.8	87.6	10.4	21.8	-	77.9
AL-C-25	240	23.5	107	13.8	26.5	-	88.2
AL-C-26	272	28.4	140	18.8	27.2	-	94.7
AL-C-27	281	31.0	159	21.8	30.9	-	46.8
De-na-zin Member							
AL-D-1	127	16.9	107	17.2	14.6	0.809	51.2
AL-D-2	71.2	9.02	55.8	9.03	4.65	0.230	91.5
AL-D-3	64.4	8.07	51.1	8.12	3.85	0.102	67.1
AL-D-4	97.1	11.8	69.5	10.6	5.95	0.469	88.8
AL-D-5	100	12.3	73.6	11.4	4.56	0.529	99.1
AL-D-6	58.2	7.10	41.5	6.54	2.93	0.062	68.0
AL-D-7	63.0	7.84	47.7	7.75	3.05	0.073	66.6
AL-D-8	58.8	7.02	41.4	6.32	3.71	0.085	94.1
AL-D-9	59.2	7.31	43.7	6.66	3.36	0.118	54.8
AL-D-10	52.1	6.52	38.3	5.81	3.26	0.112	57.1
AL-D-11	42.8	4.98	27.8	4.11	7.40	0.058	58.4
AL-D-12	46.4	5.44	31.0	4.51	3.20	0.066	82.3
AL-D-13	44.1	4.95	27.6	3.87	5.85	0.082	47.0
AL-D-14	50.5	5.78	33.0	4.82	5.96	0.111	52.1
AL-D-15	49.1	5.86	34.3	5.29	3.35	0.106	70.4
AL-D-16	92.7	12.4	82.2	13.6	5.96	0.139	64.9
AL-D-17	83.2	10.9	68.4	11.7	6.73	0.223	73.5
AL-D-18	104	13.5	85.0	13.8	8.44	0.278	72.3
AL-D-19	29.0	3.80	24.0	3.70	6.20	0.180	14.5

Table 5 (*continued*)

Sample ID	Ti	V	Cr	Mn	Fe	Ni	Cu	Zn	Rb	Sr	Zr
Arroyo Chijuillita Member, Nacimiento Fm											
AL-E-1	179	37.4	1.45	2983	884	1.18	33.2	45.6	0.351	2673	101
AL-E-2	179	25.2	2.48	5700	839	1.44	49.0	29.2	0.196	2458	179
AL-E-3	225	12.5	4.44	6300	1047	1.28	174	22.6	6.23	1992	104
AL-E-4	178	34.9	2.19	3624	1479	2.25	54.9	46.6	0.99	2788	128
AL-E-5	250	15.7	7.60	3910	1780	2.80	62.2	27.5	74.0	2470	83.2
AL-E-6	288	144	15.6	3660	18200	2.84	52.0	27.1	15.8	1716	58.2
AL-E-7	318	21.6	6.00	3770	2030	2.03	7.50	18.2	18.3	1679	49.3
AL-E-8	462	36.8	11.3	3710	11700	14.0	31.4	104	48.1	1830	162
AL-E-9	191	26.8	3.80	4670	5900	6.90	510	71.8	10.7	2606	148
AL-E-10	204	17.4	2.29	5670	3980	4.23	231	42.6	9.82	2127	160
AL-E-11	178	19.7	2.13	5149	819	1.50	35.6	31.7	0.198	2575	178
AL-E-12	177	18.6	2.00	4020	477	1.26	17.8	30.6	0.241	1972	128
AL-F-1	178	51.3	1.08	3036	774	1.15	14.1	47.5	0.399	2463	146
AL-F-2	180	73.9	2.26	4860	638	1.42	48.2	23.9	0.218	2321	232
AL-F-3	179	91.4	2.75	4650	593	1.41	47.2	23.3	0.231	2398	227
AL-F-4	190	59.2	4.40	4089	2000	2.94	524	42.9	7.60	2522	161
AL-F-5	372	41.5	15.1	2460	2670	4.80	319	64.0	149	1499	127
AL-F-6	366	29.4	15.7	2389	2230	3.59	153	27.1	62.2	1381	126
AL-F-7	362	46.2	16.2	2590	6110	7.60	195	58.5	66.6	2250	146
AL-F-8	193	73.3	3.70	5150	7600	10.5	149	102	5.46	2270	206
AL-F-9	180	90.0	2.77	4839	686	1.08	47.4	26.0	0.189	2344	231
AL-F-10	178	72.5	2.72	4689	625	1.42	33.4	23.7	0.203	2403	225
AL-F-11	174	59.9	2.10	3580	680	1.28	53.8	32.5	0.361	2557	165
AL-G-1	177	29.6	2.77	3290	1820	3.39	63.0	82.2	4.20	2721	165
AL-G-2	175	26.8	2.20	4050	682	2.62	80.2	79.0	0.400	2816	203
AL-G-3	175	28.9	1.50	3946	3640	5.59	115	123	4.80	2780	198
AL-G-4	740	32.9	10.1	1726	3590	5.42	23.5	37.2	73.0	1289	180
AL-G-5	390	33.8	14.6	1365	3910	5.28	43.0	40.1	42.7	1095	115
AL-G-6	505	59.6	23.2	1268	6650	10.3	248	87.0	78.0	1116	140
AL-G-7	396	45.6	14.8	1502	4620	6.40	36.2	50.6	80.0	1108	120
AL-G-8	198	40.5	2.60	3845	2300	3.40	127	122	7.14	2483	182
AL-G-9	177	27.1	1.60	3890	687	2.28	83.8	71.8	0.448	2845	203
AL-G-10	177	28.1	2.00	3520	687	2.32	65.3	76.5	0.372	2895	169
Dinosaur Park Formation											
T408-A-1	4.75	0.074	0.062	132	81.5	-	-	1.36	-	59.1	0.282
T408-A-2	4.63	0.073	0.078	129	80.6	-	-	1.11	-	59.8	0.271
T408-A-3	4.74	0.083	0.069	128	78.6	-	-	1.24	-	60.0	0.345
T408-A-4	4.79	0.100	0.089	129	80.9	-	-	1.17	-	59.6	0.386
T408-A-5	4.71	0.089	0.059	127	78.5	-	-	0.960	-	57.2	0.394
T408-A-6	4.70	0.099	0.064	123	76.4	-	-	1.07	-	56.8	0.505
T408-A-7	4.73	0.094	0.072	119	74.8	-	-	1.15	-	57.2	0.585
T408-A-8	4.76	0.101	0.082	116	73.8	-	-	1.42	-	59.4	0.696
T408-A-9	4.69	0.104	0.104	120	76.3	-	-	1.32	-	58.4	0.693
T408-A-10	4.81	0.106	0.113	114	71.8	-	-	1.59	-	60.9	1.50
T408-A-11	4.87	0.103	0.117	115	72.8	-	-	1.45	-	59.5	1.48
T408-A-12	4.76	0.126	0.700	129	76.6	-	0.280	0.830	-	57.8	1.22

Table 5 (*continued*)

Sample ID	Y	La	Ce	Pr	Nd	Sm	Eu	Gd	Tb	Dy	Ho
Arroyo Chijuillita Member, Nacimiento Fm											
AL-E-1	6410	1967	4520	621	3074	868	257	1086	167	1078	208
AL-E-2	4490	1180	1672	205	950	226	98.1	336	52.9	416	103
AL-E-3	5026	1465	2185	249	1113	253	130	391	59.9	451	112
AL-E-4	6655	2068	4036	501	2362	597	217	862	134	925	193
AL-E-5	6800	2240	4350	548	2450	592	300	800	124	893	195
AL-E-6	6650	1975	3956	483	2116	478	274	687	106	804	190
AL-E-7	6818	2109	4117	511	2210	505	300	707	110	836	200
AL-E-8	6840	2044	4330	545	2524	618	307	829	129	921	206
AL-E-9	6640	2037	3950	504	2376	625	229	854	132	895	189
AL-E-10	5934	1674	2935	356	1631	388	194	551	86.3	655	154
AL-E-11	5144	1234	1999	255	1195	295	114	439	69.3	520	127
AL-E-12	4790	1290	2410	298	1330	318	149	431	69.0	545	133
AL-F-1	7790	2406	5210	688	3290	865	299	1135	176	1193	247
AL-F-2	4922	1267	1915	239	1083	256	106	378	58.4	465	119
AL-F-3	5665	1465	2231	271	1237	281	122	425	65.4	518	137
AL-F-4	8430	2686	5880	773	3708	1016	336	1283	195	1296	259
AL-F-5	7590	2320	5740	806	3960	1090	432	1315	198	1336	269
AL-F-6	7390	2165	5480	761	3776	1012	421	1234	193	1285	268
AL-F-7	7270	2147	5470	756	3730	1023	414	1241	193	1284	264
AL-F-8	6520	1880	3440	428	1980	495	192	682	106	772	176
AL-F-9	4370	1155	1849	238	1085	256	103	372	57.4	445	112
AL-F-10	5150	1304	1973	247	1137	263	111	390	60.4	486	129
AL-F-11	8270	2515	5570	748	3590	978	319	1224	189	1274	260
AL-G-1	7710	2570	6050	794	3870	1043	348	1302	200	1296	257
AL-G-2	8320	2378	5260	681	3331	907	299	1206	186	1230	251
AL-G-3	8330	2492	5340	685	3349	891	306	1204	185	1224	249
AL-G-4	6960	2041	5352	738	3678	1021	394	1251	192	1275	252
AL-G-5	6990	2046	5630	787	3985	1173	417	1388	212	1320	253
AL-G-6	6910	2090	5950	831	4220	1198	426	1430	216	1347	254
AL-G-7	6820	2076	5360	762	3850	1107	414	1309	203	1316	253
AL-G-8	7830	2467	5770	754	3611	962	348	1219	186	1234	252
AL-G-9	8520	2582	5680	736	3620	981	330	1307	198	1307	268
AL-G-10	8250	2672	6100	814	3965	1100	359	1389	212	1373	270
Dinosaur Park Formation											
T408-A-1	12.7	6.12	12.1	1.45	5.91	1.40	0.349	1.71	0.262	1.82	0.378
T408-A-2	11.6	5.15	9.91	1.19	4.93	1.16	0.297	1.44	0.227	1.63	0.340
T408-A-3	13.4	5.61	10.8	1.30	5.37	1.30	0.333	1.62	0.265	1.82	0.394
T408-A-4	15.4	6.36	12.1	1.49	6.26	1.52	0.381	1.95	0.302	2.21	0.460
T408-A-5	13.9	5.38	9.83	1.20	5.06	1.25	0.312	1.62	0.268	1.91	0.399
T408-A-6	17.4	6.49	11.7	1.44	6.11	1.49	0.383	1.96	0.315	2.36	0.506
T408-A-7	20.8	7.57	13.6	1.70	7.36	1.77	0.451	2.33	0.378	2.77	0.589
T408-A-8	25.7	9.29	16.2	2.02	8.84	2.18	0.540	2.90	0.469	3.45	0.733
T408-A-9	23.6	8.18	14.2	1.74	7.72	1.88	0.467	2.61	0.418	3.13	0.671
T408-A-10	45.7	15.2	25.6	3.23	13.9	3.49	0.892	4.81	0.786	5.90	1.30
T408-A-11	42.1	13.1	21.5	2.68	11.8	2.99	0.738	4.15	0.687	5.31	1.19
T408-A-12	31.6	9.75	15.4	1.94	8.48	2.18	0.568	3.06	0.492	3.79	0.861

Table 5 (*continued*)

Sample ID	Er	Tm	Yb	Lu	Pb	Th	U
Arroyo Chijuillita Member, Nacimiento Fm							
AL-E-1	517	63.5	368	55.5	182	0.153	158
AL-E-2	343	48.9	325	56.0	675	0.047	587
AL-E-3	351	49.6	324	57.2	762	0.436	229
AL-E-4	522	64.8	376	58.3	296	0.279	321
AL-E-5	596	78.5	507	84.0	540	2.88	122
AL-E-6	582	82.5	537	90.9	373	2.33	83.2
AL-E-7	629	89.8	583	99.1	360	2.21	76.6
AL-E-8	606	83.5	541	87.5	360	5.00	148
AL-E-9	520	67.1	406	65.6	592	0.811	519
AL-E-10	495	70.4	470	80.5	696	0.461	676
AL-E-11	393	55.9	357	60.9	511	0.041	378
AL-E-12	443	64.0	428	73.3	503	1.58	165
AL-F-1	667	86.9	523	82.5	395	1.16	210
AL-F-2	395	57.2	383	67.0	634	0.03	471
AL-F-3	456	66.1	441	76.5	594	0.02	434
AL-F-4	701	89.9	548	86.9	528	3.05	268
AL-F-5	740	97.6	599	93.0	249	81.3	79.0
AL-F-6	759	101	648	102	223	6.51	54.5
AL-F-7	717	96.0	587	90.1	208	4.46	54.1
AL-F-8	531	72.4	465	78.6	756	0.55	419
AL-F-9	369	52.7	353	61.3	628	0.02	566
AL-F-10	429	62.9	423	74.0	579	0.04	455
AL-F-11	720	95.2	581	94.1	575	0.31	308
AL-G-1	677	86.6	526	81.1	560	1.84	154
AL-G-2	676	86.8	523	85.2	1000	0.177	187
AL-G-3	671	86.2	518	82.4	1020	0.358	211
AL-G-4	675	89.6	523	79.6	99.0	8.80	108
AL-G-5	647	80.7	459	66.1	69.9	8.54	89.5
AL-G-6	621	74.9	425	58.3	73.3	10.2	91.3
AL-G-7	669	83.4	496	72.5	94.0	3.92	101
AL-G-8	681	88.6	534	84.0	790	2.77	156
AL-G-9	709	93.6	560	89.9	739	0.275	180
AL-G-10	713	87.3	529	81.8	599	0.408	154
Dinosaur Park Formation							
T408-A-1	1.13	0.157	1.02	0.153	0.042	0.081	0.083
T408-A-2	1.02	0.149	0.942	0.139	0.025	0.039	0.061
T408-A-3	1.19	0.169	1.09	0.167	0.024	0.031	0.079
T408-A-4	1.39	0.193	1.29	0.184	0.023	0.027	0.102
T408-A-5	1.25	0.181	1.13	0.173	0.020	0.011	0.083
T408-A-6	1.54	0.221	1.39	0.212	0.025	0.012	0.100
T408-A-7	1.78	0.255	1.66	0.248	0.034	0.021	0.130
T408-A-8	2.25	0.314	2.04	0.301	0.076	0.027	0.165
T408-A-9	2.05	0.297	1.92	0.285	0.084	0.030	0.131
T408-A-10	3.94	0.574	3.65	0.566	0.061	0.017	0.285
T408-A-11	3.63	0.539	3.52	0.550	0.073	0.015	0.216
T408-A-12	2.76	0.398	2.74	0.402	0.061	0.024	0.153

Table 5 (*continued*)

Sample ID	Ti	V	Cr	Mn	Fe	Ni	Cu	Zn	Rb	Sr	Zr
Dinosaur Park Formation											
T408B-1	179	-	-	774	864	-	-	22.3	-	993	-
T408B-2	180	-	-	759	929	1.10	-	20.6	-	1010	0.250
T408B-3	177	-	-	4751	3559	-	-	26.7	-	1550	1.34
T408B-4	181	3.68	-	5800	4189	-	-	25.9	-	1466	3.59
T408B-5	181	-	-	5834	3889	1.02	-	19.8	-	1532	-
T408B-6	182	-	-	5114	3960	-	-	21.4	-	1714	6.00
T408B-7	183	1.93	-	5740	4119	2.25	1.85	27.3	-	1813	11.1
T408B-8	176	-	-	6280	4189	-	-	20.2	-	1425	-
T408B-9	177	1.06	-	5020	3730	-	-	18.1	-	1681	2.18
T408B-10	184	3.70	-	4670	3350	2.28	7.81	33.6	-	2038	16.3
T408B-11	191	2.82	5.00	3772	2888	5.40	3.58	61.2	-	2230	141
T408B-12	191	2.97	6.50	3620	2774	3.92	2.81	55.4	-	2208	139
T408B-13	193	4.45	7.24	3900	2946	3.50	2.13	47.7	-	2161	93.2
T408B-14	184	4.87	-	4413	3353	4.50	-	37.7	-	2022	24.8
T408B-15	186	7.07	4.18	4115	3126	2.12	-	45.5	-	1947	27.6
T408B-16	179	-	-	4360	3334	1.47	-	29.8	-	1938	-
T408B-17	189	1.76	-	971	1194	3.05	17.8	48.6	2.3	1132	5.77
T408C-1	183	-	-	751	822	-	-	24.6	-	988	-
T408C-2	184	0.720	1.28	5070	3580	1.03	3.14	32.2	-	1697	1.53
T408C-3	182	2.63	1.85	4847	3220	1.67	0.970	35.8	-	1852	4.11
T408C-4	192	4.30	4.22	4568	3054	1.80	1.59	35.3	-	2084	50.6
T408C-5	192	4.11	5.10	4329	2915	1.79	2.01	38.4	-	2226	76.3
T408C-6	193	4.14	5.54	4297	2943	2.25	2.03	36.6	-	2253	71.9
T408C-7	197	2.16	5.30	4000	2804	2.38	2.72	68.0	-	2338	103
T408C-8	196	2.00	4.88	3990	2712	2.34	3.71	77.0	-	2279	105
T408C-9	195	2.24	5.47	3886	2739	1.91	4.93	61.2	-	2286	99.4
T408C-10	191	4.49	5.27	4184	2881	1.43	1.88	46.3	-	2206	70.2
T408C-11	196	4.92	4.55	4305	2987	1.12	3.21	46.5	-	2149	60.3
T408C-12	188	4.79	3.96	4320	2968	1.63	1.93	55.8	-	2264	54.0
T408C-13	193	4.00	3.92	4439	3049	1.59	1.45	50.0	-	2112	61.4
T408C-14	195	2.30	4.90	3932	2814	2.62	4.00	68.5	-	2339	109
T408C-15	191	2.65	4.78	4000	2854	2.78	2.93	68.9	-	2267	91.1
T408C-16	194	2.00	5.90	3830	2784	2.23	3.71	75.1	-	2375	122
T408C-17	194	2.30	4.91	3975	2771	2.33	4.13	73.7	-	2362	110
T408C-18	193	2.06	5.86	3928	2799	1.95	2.54	59.7	-	2321	109
T408C-19	194	2.33	5.57	4107	2875	1.48	2.37	41.6	-	2325	105
T408C-20	191	3.13	5.05	4300	2983	1.72	2.25	41.1	-	2271	85.2
T408C-21	185	4.30	2.21	4724	3174	1.53	3.36	37.7	-	2018	11.1
T408C-22	184	4.31	3.41	4738	3142	2.24	3.31	39.8	-	2015	29.3
T408C-23	179	1.61	1.48	4802	3174	1.09	1.21	37.1	-	1843	2.79
T408C-24	183	0.340	1.22	4806	3191	-	-	27.9	-	1703	-
T408-D-1	4.69	0.019	-	95.6	53.7	-	-	0.764	-	43.8	0.081
T408-D-2	4.67	-	-	117.6	56.1	-	-	0.707	-	42.1	0.018
T408-D-3	4.75	-	-	121.1	62.0	-	-	0.606	-	38.3	0.023
T408-D-4	4.72	-	-	119.2	69.2	-	-	0.689	-	45.3	0.008
T408-D-5	5.03	0.164	0.184	132.8	65.9	0.065	0.072	1.15	-	53.5	1.35
T408-D-6	5.05	0.105	0.163	118.6	61.4	0.060	0.073	1.35	-	55.1	5.75

Table 5 (*continued*)

Sample ID	Y	La	Ce	Pr	Nd	Sm	Eu	Gd	Tb	Dy	Ho
Dinosaur Park Formation											
T408B-1	21.6	14.0	29.6	3.60	15.5	3.70	0.97	3.90	0.55	3.50	0.70
T408B-2	4.90	2.60	4.60	0.59	3.10	0.48	0.18	0.70	0.12	0.63	0.14
T408B-3	24.5	3.22	4.04	0.54	2.49	0.74	0.53	1.42	0.30	2.51	0.61
T408B-4	58.0	17.0	23.0	2.65	12.7	2.83	0.89	4.20	0.68	5.70	1.34
T408B-5	27.0	8.20	13.3	1.62	7.40	1.80	0.67	2.30	0.42	3.10	0.74
T408B-6	184	67.0	128	14.9	67.0	15.2	4.04	19.9	3.40	24.0	5.60
T408B-7	475	190	372	46.4	213	51.1	13.0	60.0	9.70	68.2	14.3
T408B-8	30.6	13.2	24.1	3.1	13.8	3.60	1.14	4.50	0.62	4.20	0.94
T408B-9	41.0	8.50	12.0	1.81	7.50	1.90	0.72	2.90	0.47	3.70	1.03
T408B-10	463	138	250	31.4	146	37.8	9.66	48.3	8.23	60.9	13.5
T408B-11	2373	527	835	111	517	131	32.6	191	33.6	277	65.3
T408B-12	2292	500	784	104	487	126	31.9	184	32.6	258	62.8
T408B-13	1494	285	427	54.7	257	65.5	15.9	101	18.0	151	37.7
T408B-14	563	126	210	26.9	124	31.9	8.50	44.4	8.00	62.1	14.7
T408B-15	543	112	177	23.5	109	27.5	7.89	39.5	7.22	56.9	13.5
T408B-16	146	37.7	66.6	8.64	41.0	10.3	3.23	14.5	2.43	18.9	4.04
T408B-17	174	116	247	30.5	132	31.1	7.30	32.6	4.84	30.5	5.93
T408C-1	-	-	-	-	-	-	-	-	-	-	-
T408C-2	92.0	37.0	70.0	8.70	40.0	9.90	2.84	10.3	1.87	12.9	2.73
T408C-3	227	82.4	149	18.5	81.7	21.4	5.52	26.3	4.18	30.3	6.65
T408C-4	1100	320	520	66.9	302	76.6	18.5	102	17.0	128	29.6
T408C-5	1740	530	878	112	509	127	29.2	167	28.1	209	47.9
T408C-6	1735	551	904	117	525	133	31.6	174	29.1	215	50.1
T408C-7	2457	747	1210	156	705	181	41.6	241	40.1	308	71.2
T408C-8	2598	804	1321	175	786	200	47	269	44.2	330	75.8
T408C-9	2577	796	1296	169	769	198	46	259	42.9	321	74.3
T408C-10	1520	418	681	84.7	381	97.2	22.9	134	23.1	173	41.3
T408C-11	1349	400	674	81.7	376	93.7	22.2	126	21.1	158	37.4
T408C-12	1420	448	745	93	429	107	25.1	139	23.9	178	40.7
T408C-13	1582	504	841	109	479	120	27.5	159	26.2	199	45.5
T408C-14	2788	777	1266	166	753	193	46.6	263	45.3	341	79.0
T408C-15	2440	668	1084	141	642	167	40.3	229	39.6	297	70.3
T408C-16	2964	828	1337	175	806	207	49.9	284	47.8	371	85.0
T408C-17	2807	780	1261	165	762	195	46.5	267	45.1	344	81.7
T408C-18	2638	733	1195	156	705	178	43.2	249	41.8	324	75.9
T408C-19	2548	729	1182	153	701	179	42.6	241	40.6	316	73.0
T408C-20	2130	640	1010	135	619	157	37.4	217	36.1	270	62.4
T408C-21	528	181	326	41.9	188	47.7	12.4	59.9	9.43	71.0	15.6
T408C-22	900	291	498	64.6	299	73.7	18.7	96.0	15.9	114	25.8
T408C-23	179	61.6	112	14.4	64.7	16.4	4.3	20.6	3.32	23.6	5.02
T408C-24	180	58.7	111	14.5	67.8	18.2	4.7	22.8	3.50	25.2	5.48
T408-D-1	3.23	1.61	3.33	0.39	1.61	0.39	0.10	0.54	0.07	0.48	0.10
T408-D-2	0.72	0.34	0.71	0.08	0.34	0.09	0.03	0.21	0.02	0.10	0.02
T408-D-3	0.56	0.18	0.42	0.05	0.21	0.05	0.02	0.18	0.01	0.07	0.01
T408-D-4	-	-	-	-	-	-	-	-	-	-	-
T408-D-5	9.39	2.12	4.53	0.54	2.23	0.56	0.17	0.79	0.13	0.98	0.22
T408-D-6	29.2	4.26	7.77	0.94	3.83	1.01	0.31	1.60	0.28	2.45	0.63

Table 5 (*continued*)

Sample ID	Er	Tm	Yb	Lu	Pb	Th	U
Dinosaur Park Formation							
T408B-1	1.97	0.25	1.65	0.20	-	-	-
T408B-2	0.35	0.06	0.33	0.05	1.31	0.50	0.13
T408B-3	1.90	0.27	1.53	0.24	0.25	-	0.05
T408B-4	4.60	0.69	4.60	0.77	0.37	0.02	0.13
T408B-5	2.04	0.38	1.96	0.31	0.19	0.04	0.11
T408B-6	17.3	2.49	15.1	2.57	-	0.80	1.08
T408B-7	41.8	5.74	36.8	5.21	0.50	4.85	3.52
T408B-8	2.53	0.37	2.17	0.33	0.28	-	-
T408B-9	3.30	0.48	3.40	0.63	0.33	-	0.17
T408B-10	41.8	5.94	36.5	5.59	0.67	0.63	5.11
T408B-11	222	32.2	217	33.2	2.08	0.78	18.2
T408B-12	210	31.0	208	32.4	1.70	1.33	11.2
T408B-13	127	19.7	138	21.6	1.16	0.77	5.45
T408B-14	48.4	7.32	47.9	7.43	0.92	0.53	3.59
T408B-15	45.6	6.70	45.7	7.06	0.74	0.31	2.66
T408B-16	12.7	1.85	12.0	1.78	0.38	0.12	1.01
T408B-17	15.9	2.11	12.0	1.83	5.21	30.20	5.18
T408C-1	-	-	-	-	-	-	-
T408C-2	7.80	1.09	6.80	1.05	1.02	1.49	0.40
T408C-3	18.9	2.72	17.6	2.65	1.54	1.18	1.13
T408C-4	92.8	14.5	92.8	15.0	2.25	2.77	2.68
T408C-5	155	23.1	152	24.3	3.36	3.22	5.97
T408C-6	154	22.9	151	23.4	1.87	4.22	6.74
T408C-7	225	32.5	213	33.4	3.64	3.13	11.6
T408C-8	232	34.2	222	34.4	3.83	3.62	14.3
T408C-9	231	34.2	222	34.2	2.85	3.42	13.7
T408C-10	133	20.2	136	21.5	1.79	1.36	4.98
T408C-11	117	17.4	118	18.3	2.32	1.89	5.00
T408C-12	129	18.8	124	19.0	2.69	1.78	6.31
T408C-13	143	20.9	139	21.4	2.86	2.19	7.15
T408C-14	251	36.7	244	37.4	3.75	1.83	15.1
T408C-15	216	32.1	214	32.8	3.33	2.52	12.9
T408C-16	266	39.3	257	39.0	3.20	2.82	17.2
T408C-17	255	36.9	244	37.4	3.30	3.38	15.2
T408C-18	240	35.3	237	35.4	5.18	3.38	12.8
T408C-19	235	34.1	225	35.3	3.54	2.94	11.8
T408C-20	203	29.3	196	29.8	3.32	2.96	10.3
T408C-21	45.4	6.33	40.4	5.85	2.35	1.56	2.97
T408C-22	79.0	11.2	72.0	11.1	2.35	2.74	4.07
T408C-23	15.2	2.09	13.7	2.08	1.14	0.85	0.84
T408C-24	15.5	2.07	12.6	1.83	0.76	0.98	0.97
T408-D-1	0.284	0.041	0.257	0.035	0.059	0.045	0.017
T408-D-2	0.059	0.008	0.051	0.008	0.023	0.018	0.004
T408-D-3	0.041	0.006	0.040	0.006	0.021	0.014	0.003
T408-D-4	-	-	-	-	-	-	-
T408-D-5	0.712	0.108	0.728	0.111	0.054	0.030	0.034
T408-D-6	2.21	0.344	2.47	0.404	0.077	0.026	0.050

Table 5 (*continued*)

Sample ID	Ti	V	Cr	Mn	Fe	Ni	Cu	Zn	Rb	Sr	Zr
Dinosaur Park Formation											
T408-D-7	4.91	0.092	0.113	98.5	55.1	0.153	0.219	2.50	-	55.2	4.80
T408-D-8	4.84	0.092	0.144	93.5	54.7	0.221	0.359	2.18	0.006	55.6	4.55
T408-D-9	4.96	0.093	0.148	115	62.5	-	0.061	1.12	-	52.7	3.51
T408-D-10	4.56	-	-	125	69.0	0.057	0.057	0.917	-	47.4	0.086
T408-D-11	4.74	-	-	114	70.4	0.061	0.055	0.900	-	45.5	0.086
T408-D-12	4.68	0.088	-	165	165	1.45	0.215	1.11	-	63.4	0.314
T408-D-13	4.86	0.254	0.093	171	172	0.610	0.305	2.78	-	64.6	0.648
C269-A-1	4.48	-	0.930	17.8	27.5	-	0.540	0.810	0.009	19.2	-
C269-A-2	4.75	0.137	-	85.4	91.1	0.068	-	0.527	0.001	48.1	0.139
C269-A-3	4.81	0.185	-	84	86.0	-	-	0.477	0.001	49.7	1.09
C269-A-4	4.79	0.118	-	71.7	78.7	0.068	0.078	0.454	0.003	49.9	1.86
C269-A-5	4.80	0.207	-	76.1	79.4	0.057	0.063	0.363	0.002	45.5	0.441
C269-A-6	4.88	0.144	-	74.7	78.3	0.059	0.058	0.470	0.002	44.9	0.668
C269-A-7	4.76	0.140	-	73.6	77.6	0.055	0.052	0.407	0.003	45.0	0.860
C269-A-8	4.83	0.143	0.121	73.3	76.4	0.065	0.076	0.433	0.003	46.0	1.11
C269-A-9	4.66	0.147	-	74.4	77.4	-	-	0.329	0.001	44.9	0.497
C269-A-10	4.72	-	-	71.9	79.3	-	-	0.489	0.001	43.2	0.041
C269-A-11	4.65	-	-	74.6	79.2	-	-	0.367	0.003	43.4	0.086
C269-A-12	4.71	0.077	-	75.9	81.6	-	-	0.301	0.002	44.5	0.059
C269-A-13	4.70	-	-	78.3	83.8	-	-	0.332	0.001	44.3	0.065
C269-A-14	4.57	0.058	-	72.9	77.9	-	-	0.364	0.002	43.1	0.093
C269-A-15	4.68	0.086	-	75	81.1	-	-	0.224	0.001	45.0	0.146
C269-A-16	4.69	0.150	0.117	70.6	74.9	0.078	0.095	0.448	0.002	44.2	1.27
C269-A-17	4.69	0.155	-	74.5	81.1	0.053	0.052	0.365	0.001	44.0	0.543
C269-A-18	4.69	0.165	0.101	73.2	79.6	0.061	0.067	0.413	-	44.2	0.711
C269-A-19	4.73	0.108	-	73.2	81.3	0.057	-	0.419	0.002	44.1	0.380
C269-A-20	4.73	0.138	-	73.36	83.7	0.066	-	0.422	0.001	45.4	0.283
C269-A-21	4.65	0.099	-	75.1	87.9	0.063	-	0.489	0.001	45.2	0.223
C269-A-22	4.91	0.267	0.141	82.8	125	0.515	0.074	0.621	0.002	49.8	1.17
C269-B-1	4.98	0.146	0.147	140	140	1.32	0.469	1.03	-	54.0	2.35
C269-B-2	5.10	0.189	0.158	152	114	0.112	0.148	0.730	-	55.1	2.42
C269-B-3	4.93	0.216	0.120	143	108	0.104	0.190	0.739	-	51.4	0.780
C269-B-4	4.67	0.138	-	135	92.7	0.082	0.067	0.348	-	48.6	0.279
C269-B-5	4.65	0.131	-	132	90.9	0.051	0.079	0.486	-	46.3	0.241
C269-B-6	4.70	0.167	-	136	105	0.081	0.110	0.560	-	47.4	0.279
C269-B-7	4.80	0.150	0.159	128	81.7	-	0.084	0.305	-	48.5	1.41
C269-B-8	4.86	0.171	0.140	130	108	0.370	0.085	0.489	-	50.6	1.42
C269-B-9	5.19	0.131	0.161	103	91.2	1.48	0.063	0.260	-	56.8	4.07
C269-B-10	4.66	0.095	0.084	125	101	-	0.075	0.367	-	46.7	0.143
C269-B-11	4.64	0.134	0.100	133	98.2	-	-	0.298	-	47.0	0.237
C269-B-12	4.72	0.108	-	131	117	0.071	0.096	0.536	-	48.0	0.205
C269-B-13	4.73	0.128	-	134	118	0.115	0.108	0.470	-	48.7	0.247
C269-B-14	5.02	0.119	0.135	126	127	0.151	0.375	1.21	-	62.0	4.87
C269-B-15	5.09	0.092	0.126	131	109	0.268	0.439	1.18	0.006	66.2	4.92
C269-B-16	5.41	0.433	0.430	156	172	1.07	1.63	1.51	0.124	57.6	3.48

Table 5 (*continued*)

Sample ID	Y	La	Ce	Pr	Nd	Sm	Eu	Gd	Tb	Dy	Ho
Dinosaur Park Formation											
T408-D-7	61.6	17.6	33.6	4.24	18.1	4.74	1.19	6.37	1.10	8.30	1.81
T408-D-8	65.3	19.9	38.5	5.00	21.5	5.51	1.40	7.14	1.22	9.27	1.96
T408-D-9	22.4	4.00	7.30	0.903	3.87	1.02	0.285	1.50	0.250	2.07	0.493
T408-D-10	3.60	1.30	2.60	0.333	1.50	0.398	0.115	0.509	0.076	0.520	0.111
T408-D-11	3.50	1.37	2.74	0.360	1.57	0.410	0.119	0.538	0.076	0.522	0.099
T408-D-12	11.0	5.68	11.9	1.46	6.06	1.49	0.367	1.73	0.259	1.79	0.351
T408-D-13	20.1	10.0	20.4	2.49	10.5	2.55	0.605	2.97	0.461	3.16	0.634
C269-A-1	0.214	0.068	0.166	0.022	0.071	0.054	0.010	0.030	-	0.022	-
C269-A-2	5.30	1.88	3.48	0.434	1.94	0.48	0.125	0.670	0.098	0.700	0.152
C269-A-3	29.2	11.4	20.3	2.62	11.6	2.94	0.680	3.80	0.610	4.25	0.910
C269-A-4	51.6	21.8	41.8	5.60	24.7	6.19	1.41	7.93	1.21	8.41	1.70
C269-A-5	14.8	6.10	12.7	1.62	7.24	1.90	0.453	2.28	0.351	2.36	0.477
C269-A-6	19.6	7.85	15.4	2.07	9.17	2.31	0.547	2.89	0.444	3.05	0.625
C269-A-7	23.3	8.84	16.6	2.19	10.1	2.58	0.606	3.23	0.501	3.62	0.743
C269-A-8	31.7	13.1	25.1	3.43	15.3	3.90	0.909	4.91	0.756	5.10	1.06
C269-A-9	14.9	6.17	12.2	1.61	7.11	1.80	0.417	2.23	0.344	2.35	0.487
C269-A-10	2.66	1.02	2.15	0.281	1.19	0.318	0.080	0.405	0.061	0.415	0.083
C269-A-11	3.73	1.67	3.38	0.442	1.96	0.482	0.132	0.599	0.091	0.591	0.121
C269-A-12	2.43	1.01	2.08	0.271	1.17	0.283	0.077	0.423	0.058	0.377	0.077
C269-A-13	2.47	1.02	2.07	0.272	1.21	0.298	0.077	0.410	0.056	0.372	0.078
C269-A-14	4.23	1.69	3.52	0.464	2.03	0.507	0.139	0.648	0.095	0.674	0.133
C269-A-15	5.20	1.99	3.90	0.515	2.25	0.582	0.143	0.745	0.114	0.800	0.162
C269-A-16	39.4	15.4	30.6	4.13	19.0	4.83	1.14	5.94	0.925	6.32	1.27
C269-A-17	16.3	6.43	13.0	1.70	7.61	1.96	0.479	2.40	0.380	2.63	0.523
C269-A-18	21.6	8.21	16.0	2.17	9.56	2.46	0.602	3.10	0.481	3.38	0.676
C269-A-19	12.5	5.02	9.87	1.31	5.74	1.44	0.375	1.86	0.288	2.02	0.386
C269-A-20	9.46	3.84	7.56	1.00	4.43	1.11	0.285	1.37	0.218	1.49	0.300
C269-A-21	7.29	2.56	4.68	0.605	2.63	0.659	0.181	0.903	0.141	1.03	0.219
C269-A-22	23.4	8.17	13.1	1.56	7.00	1.66	0.383	2.20	0.346	2.49	0.572
C269-B-1	70.7	34.1	69.4	9.27	40.4	9.61	2.21	11.1	1.68	11.3	2.26
C269-B-2	57.3	23.1	41.7	5.32	23.1	5.61	1.29	6.76	1.05	7.36	1.58
C269-B-3	23.8	9.07	17.3	2.15	9.21	2.26	0.546	2.67	0.420	2.89	0.619
C269-B-4	9.91	3.97	8.08	1.04	4.39	1.06	0.278	1.22	0.189	1.31	0.266
C269-B-5	7.14	3.11	6.52	0.816	3.46	0.820	0.217	0.955	0.144	0.992	0.198
C269-B-6	6.94	2.82	5.83	0.729	3.11	0.748	0.196	0.893	0.136	0.930	0.186
C269-B-7	32.7	15.1	29.6	3.84	16.7	4.02	0.964	4.61	0.71	4.77	0.94
C269-B-8	29.6	13.8	27.4	3.52	15.2	3.66	0.869	4.15	0.64	4.38	0.88
C269-B-9	68.2	28.9	48.6	6.07	26.9	6.33	1.39	8.05	1.26	8.88	1.92
C269-B-10	3.52	1.70	3.46	0.438	1.86	0.440	0.120	0.521	0.080	0.532	0.105
C269-B-11	6.29	2.78	5.55	0.705	2.99	0.730	0.192	0.880	0.135	0.903	0.180
C269-B-12	4.16	2.03	4.16	0.518	2.18	0.543	0.139	0.647	0.097	0.632	0.126
C269-B-13	6.15	2.53	5.23	0.644	2.73	0.685	0.171	0.790	0.123	0.830	0.174
C269-B-14	99.2	49.4	103	13.7	59.1	14.8	3.35	16.0	2.46	16.3	3.25
C269-B-15	125	63.0	137	18.1	78.9	19.5	4.46	21.4	3.24	21.3	4.19
C269-B-16	98.6	53.5	114	14.5	63.9	15.7	3.55	16.7	2.52	16.5	3.25

Table 5 (*continued*)

Sample ID	Er	Tm	Yb	Lu	Pb	Th	U
Dinosaur Park Formation							
T408-D-7	5.49	0.767	4.96	0.728	0.305	0.071	0.819
T408-D-8	5.85	0.824	5.05	0.742	0.832	0.135	1.07
T408-D-9	1.71	0.264	1.86	0.300	0.455	0.043	0.046
T408-D-10	0.308	0.041	0.242	0.036	0.163	0.024	0.024
T408-D-11	0.291	0.038	0.237	0.033	0.129	0.023	0.023
T408-D-12	1.01	0.139	0.864	0.128	8.85	0.381	0.217
T408-D-13	1.86	0.262	1.65	0.245	12.3	0.812	0.273
C269-A-1	0.016	0.002	0.012	0.001	0.089	0.005	0.002
C269-A-2	0.44	0.059	0.389	0.056	0.347	0.011	0.057
C269-A-3	2.60	0.356	2.18	0.306	0.550	0.033	0.183
C269-A-4	4.71	0.621	3.67	0.500	1.55	0.086	0.696
C269-A-5	1.25	0.168	0.991	0.134	0.847	0.138	0.225
C269-A-6	1.71	0.231	1.34	0.183	1.16	0.133	0.303
C269-A-7	2.02	0.265	1.65	0.230	1.65	0.019	0.282
C269-A-8	2.88	0.370	2.19	0.307	1.74	0.041	0.545
C269-A-9	1.30	0.178	1.062	0.146	0.643	0.026	0.167
C269-A-10	0.227	0.032	0.185	0.027	0.230	0.008	0.025
C269-A-11	0.330	0.043	0.257	0.037	0.274	0.024	0.041
C269-A-12	0.205	0.027	0.161	0.023	0.207	0.001	0.024
C269-A-13	0.211	0.028	0.166	0.023	0.126	0.002	0.022
C269-A-14	0.370	0.047	0.288	0.040	0.255	0.034	0.041
C269-A-15	0.457	0.061	0.353	0.052	0.242	0.016	0.042
C269-A-16	3.55	0.453	2.630	0.376	1.86	0.046	0.745
C269-A-17	1.45	0.188	1.140	0.163	0.781	0.045	0.256
C269-A-18	1.91	0.243	1.455	0.202	0.955	0.063	0.328
C269-A-19	1.10	0.146	0.841	0.117	0.805	0.073	0.196
C269-A-20	0.834	0.106	0.643	0.090	0.666	0.090	0.140
C269-A-21	0.624	0.080	0.494	0.072	0.603	0.008	0.094
C269-A-22	1.66	0.238	1.410	0.215	4.26	0.002	0.113
C269-B-1	6.52	0.867	5.05	0.744	29.3	1.67	1.27
C269-B-2	4.87	0.666	4.12	0.655	3.87	0.046	0.191
C269-B-3	1.86	0.259	1.55	0.255	3.42	0.094	0.130
C269-B-4	0.788	0.104	0.652	0.102	1.16	0.032	0.082
C269-B-5	0.588	0.078	0.469	0.073	1.04	0.039	0.064
C269-B-6	0.555	0.078	0.472	0.073	1.28	0.033	0.050
C269-B-7	2.75	0.365	2.18	0.327	0.330	0.030	0.213
C269-B-8	2.55	0.339	2.00	0.297	3.00	0.031	0.203
C269-B-9	5.96	0.822	4.95	0.796	7.40	0.002	0.189
C269-B-10	0.304	0.039	0.247	0.036	0.667	0.017	0.030
C269-B-11	0.517	0.070	0.415	0.063	0.437	0.009	0.048
C269-B-12	0.360	0.049	0.291	0.045	1.27	0.018	0.042
C269-B-13	0.501	0.069	0.427	0.064	1.96	0.031	0.051
C269-B-14	9.25	1.21	7.09	1.05	10.1	0.500	1.72
C269-B-15	11.7	1.50	8.78	1.29	10.3	1.63	2.63
C269-B-16	9.19	1.20	6.97	0.991	10.1	5.60	1.86

Table 5 (*continued*)

Sample ID	Ti	V	Cr	Mn	Fe	Ni	Cu	Zn	Rb	Sr	Zr
Dinosaur Park Formation											
C269-C-1	4.49	-	2.40	15.5	30.7	0.122	0.900	0.610	-	20.2	0.026
C269-C-2	5.18	0.622	0.194	71.7	113	0.051	0.052	0.455	-	59.0	2.89
C269-C-3	4.68	-	-	69.8	118	-	-	0.232	-	50.0	0.036
C269-C-4	4.71	-	-	70.2	114	-	-	0.247	-	48.4	0.034
C269-C-5	4.66	-	-	69.0	108	0.052	-	0.341	-	47.4	0.061
C269-C-6	4.76	0.064	-	71.0	108	0.059	-	0.282	-	49.1	0.084
C269-C-7	4.58	-	-	64.7	120	-	-	0.400	-	43.0	0.012
C269-C-8	4.77	-	-	63.8	111	-	-	0.248	-	45.1	0.045
C269-C-9	4.73	-	0.107	67.6	103	0.064	0.051	0.277	-	46.8	0.086
C269-C-10	4.65	-	-	65.3	103	0.060	-	0.236	-	45.0	0.045
C269-C-11	4.64	-	-	67.4	107	0.056	-	0.233	-	47.1	0.049
C269-C-12	4.92	0.721	0.152	68.9	108	0.105	-	0.466	-	52.4	1.33
C269-C-13	4.67	-	-	11.4	25.0	-	0.061	0.385	-	19.0	-
C269-D-1	4.78	-	-	89.5	96.8	-	-	0.238	-	44.8	0.060
C269-D-2	4.82	0.280	-	84.3	81.1	-	-	0.314	-	42.6	0.238
C269-D-3	5.12	0.200	0.194	83.4	79.2	-	-	0.300	-	45.1	2.18
C269-D-4	5.08	0.293	0.174	82.4	77.7	-	-	0.334	-	44.4	1.85
C269-D-5	5.06	0.184	0.169	80.3	75.1	0.055	0.073	0.468	-	45.3	2.71
C269-D-6	5.20	0.223	0.212	81.5	77.6	-	-	0.349	-	45.4	2.59
C269-D-7	4.75	0.303	0.078	86.5	81.1	-	-	0.369	-	40.4	0.137
C269-D-8	5.08	0.402	0.190	82.5	77.6	-	-	0.358	-	43.6	1.26
C269-D-9	5.09	0.316	0.191	83.0	78.1	-	-	0.337	-	43.9	1.64
C269-D-10	4.99	0.436	0.200	84.3	78.3	-	-	0.290	-	43.1	0.982
C269-D-11	4.74	0.486	0.155	85.0	80.3	-	-	0.205	-	42.4	0.389
C269-D-12	4.76	0.079	0.092	81.5	82.6	-	-	0.354	-	43.0	0.072
C269-D-13	4.59	-	0.390	21.3	33.1	0.220	2.60	0.460	-	21.9	0.032

Table 5 (*continued*)

Sample ID	Y	La	Ce	Pr	Nd	Sm	Eu	Gd	Tb	Dy	Ho
Dinosaur Park Formation											
C269-C-1	0.318	0.214	0.650	0.046	0.165	0.055	0.015	0.060	0.008	0.042	0.015
C269-C-2	57.1	21.1	40.0	5.04	22.5	5.62	1.26	6.96	1.13	8.09	1.78
C269-C-3	2.09	0.830	1.63	0.198	0.879	0.228	0.061	0.303	0.044	0.308	0.062
C269-C-4	2.15	0.754	1.46	0.180	0.804	0.201	0.055	0.301	0.045	0.288	0.064
C269-C-5	3.33	1.57	3.01	0.379	1.64	0.416	0.108	0.522	0.076	0.507	0.107
C269-C-6	4.30	1.84	3.73	0.463	2.07	0.536	0.136	0.667	0.098	0.646	0.129
C269-C-7	-	-	-	-	-	-	-	-	-	-	-
C269-C-8	3.32	0.816	1.47	0.186	0.840	0.222	0.061	0.343	0.052	0.392	0.089
C269-C-9	4.55	2.08	3.96	0.493	2.25	0.557	0.142	0.654	0.102	0.686	0.142
C269-C-10	2.49	0.864	1.63	0.201	0.895	0.223	0.064	0.332	0.046	0.345	0.075
C269-C-11	2.44	0.938	1.77	0.222	1.01	0.264	0.073	0.335	0.051	0.340	0.071
C269-C-12	34.5	12.0	21.9	2.67	11.9	3.00	0.695	3.86	0.624	4.56	1.01
C269-C-13	0.089	0.042	0.087	0.012	0.044	0.012	0.004	0.019	0.002	0.016	0.004
C269-D-1	3.00	1.11	2.27	0.292	1.26	0.329	0.088	0.433	0.061	0.457	0.095
C269-D-2	8.23	2.99	5.73	0.721	3.20	0.826	0.206	1.02	0.163	1.13	0.245
C269-D-3	38.3	13.5	23.1	2.95	13.3	3.34	0.781	4.41	0.696	4.99	1.09
C269-D-4	34.5	12.1	21.0	2.73	12.3	3.11	0.730	4.08	0.660	4.66	1.01
C269-D-5	50.6	19.3	34.6	4.67	20.8	5.33	1.23	6.69	1.08	7.47	1.60
C269-D-6	44.2	15.7	26.7	3.54	16.0	4.03	0.938	5.36	0.854	6.04	1.32
C269-D-7	4.40	1.69	3.20	0.421	1.90	0.474	0.127	0.625	0.096	0.678	0.137
C269-D-8	23.3	7.83	13.6	1.76	8.10	2.04	0.494	2.66	0.416	2.95	0.649
C269-D-9	30.8	10.9	19.0	2.47	11.3	2.76	0.676	3.77	0.590	4.20	0.920
C269-D-10	18.8	6.41	10.9	1.40	6.22	1.61	0.386	2.09	0.326	2.38	0.519
C269-D-11	10.3	3.55	6.14	0.802	3.66	0.925	0.231	1.20	0.188	1.36	0.292
C269-D-12	3.48	1.28	2.38	0.308	1.38	0.353	0.096	0.446	0.073	0.504	0.106
C269-D-13	0.770	0.418	0.990	0.121	0.522	0.119	0.034	0.145	0.019	0.138	0.024

Table 5 (*continued*)

Sample ID	Er	Tm	Yb	Lu	Pb	Th	U
Dinosaur Park Formation							
C269-C-1	0.033	0.005	0.030	0.003	0.054	0.013	0.007
C269-C-2	5.37	0.764	4.72	0.711	0.191	0.205	0.530
C269-C-3	0.178	0.026	0.153	0.020	0.039	0.023	0.008
C269-C-4	0.183	0.024	0.151	0.021	0.117	0.005	0.008
C269-C-5	0.286	0.039	0.228	0.032	0.152	0.033	0.014
C269-C-6	0.366	0.051	0.303	0.043	0.076	0.145	0.015
C269-C-7	0.003	-	0.003	-	0.007	-	-
C269-C-8	0.275	0.038	0.227	0.034	0.046	0.002	0.006
C269-C-9	0.385	0.050	0.302	0.041	0.070	0.041	0.018
C269-C-10	0.213	0.029	0.180	0.025	0.056	0.009	0.008
C269-C-11	0.203	0.026	0.167	0.024	0.031	0.013	0.009
C269-C-12	3.07	0.435	2.79	0.411	0.137	0.049	0.094
C269-C-13	0.009	0.001	0.006	0.001	0.010	0.002	0.001
C269-D-1	0.266	0.036	0.222	0.029	0.057	0.037	0.023
C269-D-2	0.68	0.095	0.578	0.082	0.042	0.045	0.053
C269-D-3	3.19	0.441	2.72	0.385	0.060	0.065	0.167
C269-D-4	2.93	0.394	2.51	0.359	0.061	0.069	0.172
C269-D-5	4.49	0.601	3.72	0.520	0.107	0.173	0.450
C269-D-6	3.77	0.514	3.21	0.463	0.086	0.091	0.205
C269-D-7	0.386	0.053	0.313	0.044	0.033	0.035	0.038
C269-D-8	1.86	0.260	1.60	0.234	0.064	0.118	0.117
C269-D-9	2.62	0.354	2.26	0.323	0.085	0.082	0.200
C269-D-10	1.46	0.207	1.29	0.192	0.061	0.036	0.108
C269-D-11	0.848	0.114	0.734	0.101	0.045	0.025	0.064
C269-D-12	0.296	0.040	0.254	0.036	0.039	0.015	0.025
C269-D-13	0.065	0.009	0.050	0.007	0.094	0.083	0.019

Table 6
U-Pb laser ablation ICP-MS results for Durango apatite standard for each session.

Sample ID	^{206}Pb (cps)	^{204}Pb (cps)	$\frac{^{238}\text{U}}{^{206}\text{Pb}}$ meas.	1 SE	$\frac{^{207}\text{Pb}}{^{206}\text{Pb}}$ meas.	1 SE	f_{206}	$1-f_{206}$	$\frac{^{206}\text{Pb}}{^{238}\text{U}}$ corr.	$\frac{^{206}\text{Pb}}{^{238}\text{U}}$ age (Ma)	1 SE
Session 1 - ACM 1											
Durango-1	13342	640	157.79	0.99	0.227	0.0019	0.228	0.772	0.0049	31.5	0.20
Durango-2	13687	680	160.17	1.31	0.228	0.0028	0.229	0.771	0.0048	31.0	0.25
Durango-3	13900	670	162.15	1.32	0.226	0.0028	0.226	0.774	0.0048	30.7	0.25
Durango-4	3422	218	153.75	2.62	0.242	0.0075	0.246	0.754	0.0049	31.5	0.54
Durango-5	16150	1081	151.76	2.13	0.241	0.0038	0.246	0.754	0.0050	31.9	0.45
Durango-6	17620	1145	152.27	1.85	0.225	0.0052	0.225	0.775	0.0051	32.7	0.40
Durango-7	16295	989	154.45	1.08	0.212	0.0019	0.209	0.791	0.0051	32.9	0.23
Session 2 - ACM 2											
Durango-1	6241	2172	96.14	1.69	0.341	0.0103	0.372	0.628	0.0065	42.0	1.17
Durango-2	6221	2373	93.34	2.19	0.344	0.0126	0.376	0.624	0.0067	42.9	1.61
Durango-3	6272	2364	95.01	1.54	0.338	0.0085	0.369	0.631	0.0066	42.7	1.09
Durango-4	6052	2133	105.28	0.80	0.304	0.0054	0.325	0.675	0.0064	41.2	0.46
Durango-5	5464	922	110.54	1.05	0.252	0.0041	0.260	0.740	0.0067	43.0	0.55
Durango-6	5100	154	112.10	1.54	0.256	0.0063	0.264	0.736	0.0066	42.2	0.78
Durango-7	5148	352	111.34	1.65	0.267	0.0093	0.278	0.722	0.0065	41.6	0.85
Durango-8	5530	278	106.43	3.25	0.319	0.0187	0.345	0.655	0.0062	39.6	1.84
Durango-9	5315	61	109.52	2.86	0.285	0.0150	0.301	0.699	0.0064	41.0	1.53
Durango-10	4513	196	122.67	1.06	0.232	0.0058	0.235	0.765	0.0062	40.1	0.45
Durango-11	4967	0	110.57	3.13	0.285	0.0172	0.301	0.699	0.0063	40.6	1.64
Durango-12	4412	8	111.42	1.58	0.275	0.0090	0.289	0.711	0.0064	41.0	0.81
Session 3 - DPF 1											
Durango-1	6200	771	134.86	1.01	0.256	0.0044	0.265	0.735	0.0055	35.0	0.35
Durango-2	5534	678	144.70	1.76	0.201	0.0041	0.196	0.804	0.0056	35.7	0.54
Durango-3	5178	667	130.23	2.17	0.273	0.0079	0.286	0.714	0.0055	35.3	0.82
Durango-4	4740	571	120.86	2.51	0.307	0.0123	0.329	0.671	0.0056	35.7	1.10
Durango-5	5282	370	141.32	1.02	0.208	0.0058	0.205	0.795	0.0056	36.2	0.33
Durango-6	5320	553	138.22	1.27	0.205	0.0080	0.200	0.800	0.0058	37.2	0.43
Durango-7	5397	482	138.06	1.76	0.215	0.0070	0.213	0.787	0.0057	36.7	0.59
Durango-8	5538	260	139.28	1.01	0.209	0.0046	0.205	0.795	0.0057	36.7	0.33
Durango-9	5368	24	142.33	1.82	0.200	0.0051	0.194	0.806	0.0057	36.4	0.58
Session 4 - DPF 2											
Durango-1	5112	382	134.78	1.75	0.202	0.0049	0.197	0.803	0.0060	38.3	0.62
Durango-2	4680	378	127.86	1.05	0.211	0.0036	0.207	0.793	0.0062	39.8	0.41
Durango-3	5109	446	132.93	0.96	0.195	0.0044	0.188	0.812	0.0061	39.3	0.35
Durango-4	4935	333	136.27	0.64	0.184	0.0020	0.174	0.826	0.0061	39.0	0.22
Durango-5	4978	214	140.75	1.17	0.185	0.0051	0.175	0.825	0.0059	37.7	0.38
Durango-6	5077	349	141.20	0.93	0.184	0.0027	0.174	0.826	0.0059	37.6	0.30
Durango-7	4913	435	138.41	1.20	0.198	0.0025	0.190	0.810	0.0058	37.6	0.40
Durango-8	5016	416	133.60	1.13	0.201	0.0034	0.195	0.805	0.0060	38.7	0.40

Table 7

U-Pb laser ablation ICP-MS results for the cross-sections of fossil alligorid, tyrannosaur and crocodilian teeth from the Arroyo Chijuillita Member (ACM) and the Dinosaur Park Formation (DPF). Asterix indicates in-filling.

Sample ID	^{206}Pb (cps)	^{204}Pb (cps)	$\frac{^{238}U}{^{206}Pb}$ meas.	1 SE	$\frac{^{207}Pb}{^{206}Pb}$ meas.	1 SE	f_{206}	$1-f_{206}$	$\frac{^{206}Pb}{^{238}U}$ corr.	$\frac{^{206}Pb}{^{238}U}$ age (Ma)	1 SE
Session 1 - ACM 1											
AL-A-1	217269	11407	9.74	0.06	0.819	0.00061	0.920	0.080	0.0082	52.9	0.32
AL-A-2	207715	10203	18.38	0.13	0.769	0.00049	0.860	0.140	0.0076	48.8	0.35
AL-A-3	208750	10055	20.91	0.18	0.755	0.00057	0.844	0.156	0.0074	47.8	0.41
AL-A-4	225685	10140	24.94	0.26	0.709	0.00049	0.790	0.210	0.0084	54.2	0.56
AL-A-5	205957	8964	24.80	0.09	0.689	0.00049	0.765	0.235	0.0095	60.8	0.23
AL-A-6	169594	7669	21.79	0.14	0.718	0.00062	0.799	0.201	0.0092	59.1	0.37
AL-A-7	132449	5867	20.87	0.24	0.698	0.00145	0.776	0.224	0.0107	68.9	0.79
AL-A-8	239706	11526	22.04	0.12	0.755	0.00054	0.844	0.156	0.0071	45.4	0.25
AL-A-9	254824	12351	20.22	0.12	0.762	0.00051	0.852	0.148	0.0073	46.9	0.27
AL-A-10	325994	16140	15.80	0.14	0.777	0.00044	0.870	0.130	0.0082	52.7	0.48
AL-A-11	368735	17850	15.03	0.15	0.765	0.00083	0.855	0.145	0.0096	61.8	0.63
AL-A-12	329856	15754	14.59	0.19	0.751	0.00090	0.840	0.160	0.0110	70.5	0.90
AL-A-13	164390	7131	25.71	0.13	0.691	0.00038	0.768	0.232	0.0090	58.0	0.29
AL-A-14	180632	8299	21.10	0.11	0.726	0.00048	0.810	0.190	0.0090	57.9	0.29
AL-A-15	185788	8657	22.20	0.23	0.737	0.00052	0.822	0.178	0.0080	51.4	0.54
AL-A-16	192482	9425	19.69	0.15	0.770	0.00063	0.862	0.138	0.0070	45.1	0.34
AL-A-17	190304	9607	13.56	0.08	0.794	0.00062	0.890	0.110	0.0081	52.0	0.32
AL-A-18	192488	10033	8.40	0.12	0.822	0.00042	0.924	0.076	0.0091	58.3	0.82
AL-A-19	550537	29122	4.19	0.05	0.829	0.00044	0.932	0.068	0.0162	103.6	1.18
AL-B-1	86821	4876	4.33	0.08	0.826	0.00124	0.986	0.014	0.0032	20.8	0.41
AL-B-2	141367	7772	3.68	0.05	0.832	0.00074	0.993	0.007	0.0018	11.8	0.15
AL-B-3	155138	8275	9.03	0.15	0.810	0.00050	0.966	0.034	0.0038	24.4	0.39
AL-B-4	162500	8463	12.68	0.16	0.795	0.00073	0.947	0.053	0.0042	26.8	0.34
AL-B-5	163849	8849	6.81	0.09	0.819	0.00061	0.977	0.023	0.0034	22.0	0.29
AL-B-6	158986	8704	2.57	0.03	0.830	0.00045	0.990	0.010	0.0038	24.2	0.27
AL-B-7	172650	9409	2.26	0.04	0.833	0.00077	0.994	0.006	0.0025	16.2	0.26
AL-B-8	171076	9162	6.46	0.08	0.819	0.00068	0.977	0.023	0.0035	22.5	0.28
AL-B-9	186596	9932	8.47	0.10	0.815	0.00052	0.972	0.028	0.0033	21.5	0.25
AL-B-10	205027	10809	12.36	0.15	0.805	0.00061	0.960	0.040	0.0033	21.0	0.25
AL-B-11	194051	10036	15.65	0.12	0.793	0.00067	0.944	0.056	0.0036	23.2	0.18
AL-B-12	158992	8461	14.72	0.14	0.778	0.00084	0.926	0.074	0.0050	32.5	0.31
AL-B-13	151379	8247	9.22	0.04	0.807	0.00063	0.962	0.038	0.0042	26.8	0.13
AL-B-14	170209	9022	12.42	0.08	0.800	0.00056	0.953	0.047	0.0038	24.4	0.16
AL-B-15	214647	10877	22.36	0.21	0.740	0.00092	0.877	0.123	0.0055	35.3	0.33
AL-B-16	155713	8480	4.00	0.02	0.829	0.00054	0.990	0.010	0.0026	16.9	0.09
AL-B-17	149527	8210	2.39	0.03	0.832	0.00062	0.994	0.006	0.0027	17.4	0.21
AL-B-18	147748	8074	2.17	0.02	0.830	0.00070	0.991	0.009	0.0041	26.4	0.25
AL-B-19	144022	7930	1.78	0.01	0.832	0.00065	0.994	0.006	0.0034	22.0	0.17
AL-B-20	147273	8086	1.81	0.01	0.831	0.00057	0.992	0.008	0.0046	29.3	0.21

Table 7 (*continued*)

Sample ID	^{206}Pb (cps)	^{204}Pb (cps)	$\frac{^{238}U}{^{206}Pb}$ meas.	1 SE	$\frac{^{207}Pb}{^{206}Pb}$ meas.	1 SE	f_{206}	$1-f_{206}$	$\frac{^{206}Pb}{^{238}U}$ corr.	$\frac{^{206}Pb}{^{238}U}$ age (Ma)	1 SE
AL-B-21	153201	8411	2.04	0.02	0.832	0.00079	0.993	0.007	0.0034	21.7	0.22
AL-B-22	143175	7904	2.07	0.02	0.831	0.00082	0.992	0.008	0.0038	24.7	0.25
AL-B-23	146985	8069	2.36	0.02	0.832	0.00057	0.993	0.007	0.0029	18.6	0.19
AL-B-24	148128	8100	2.64	0.02	0.830	0.00080	0.991	0.009	0.0032	20.8	0.15
AL-B-25	162698	8809	4.82	0.11	0.821	0.00060	0.980	0.020	0.0042	26.8	0.61
AL-B-26	168293	9106	4.61	0.04	0.829	0.00048	0.990	0.010	0.0022	14.3	0.13
AL-C-1	195145	10983	0.06	0.01	0.853	0.00082	0.980	0.020	0.3231	1804	138
AL-C-2	165075	8585	9.58	0.08	0.802	0.00081	0.919	0.081	0.0085	54.5	0.43
AL-C-3	128505	6155	17.65	0.08	0.745	0.00072	0.849	0.151	0.0086	54.9	0.24
AL-C-4	108101	5107	15.03	0.08	0.734	0.00074	0.836	0.164	0.0109	70.0	0.36
AL-C-5	95230	4537	12.03	0.07	0.751	0.00099	0.856	0.144	0.0119	76.5	0.47
AL-C-6	78552	3867	11.93	0.07	0.770	0.00057	0.879	0.121	0.0101	65.1	0.36
AL-C-7	53991	2540	16.89	0.21	0.724	0.00108	0.823	0.177	0.0105	67.1	0.84
AL-C-8	41414	1713	24.59	0.18	0.679	0.00094	0.769	0.231	0.0094	60.3	0.45
AL-C-9	35955	1478	22.06	0.21	0.692	0.00115	0.785	0.215	0.0098	62.6	0.59
AL-C-10	27851	1029	31.14	0.24	0.632	0.00163	0.711	0.289	0.0093	59.5	0.45
AL-C-11	28785	1061	30.57	0.23	0.630	0.00130	0.709	0.291	0.0095	61.0	0.45
AL-C-12	37483	1481	29.23	0.41	0.650	0.00106	0.733	0.267	0.0091	58.6	0.81
AL-C-13	45122	1890	23.44	0.15	0.692	0.00118	0.785	0.215	0.0092	58.9	0.39
AL-C-14	58856	2624	20.91	0.17	0.717	0.00094	0.815	0.185	0.0088	56.8	0.47
AL-C-15	54570	2335	22.98	0.22	0.700	0.00102	0.794	0.206	0.0090	57.4	0.54
AL-C-16	48257	1976	27.82	0.28	0.666	0.00091	0.753	0.247	0.0089	57.0	0.58
AL-C-17	70211	2966	27.89	0.20	0.681	0.00096	0.771	0.229	0.0082	52.7	0.38
AL-C-18	71686	3144	23.87	0.11	0.708	0.00123	0.805	0.195	0.0082	52.6	0.25
AL-C-19	58773	2526	25.11	0.43	0.703	0.00114	0.799	0.201	0.0080	51.5	0.88
AL-C-20	66116	2918	23.54	0.21	0.707	0.00077	0.803	0.197	0.0084	53.7	0.47
AL-C-21	92321	4352	15.28	0.17	0.747	0.00080	0.851	0.149	0.0097	62.4	0.68
AL-C-22	166303	8450	13.24	0.09	0.805	0.00070	0.922	0.078	0.0059	37.9	0.24
AL-C-23	196048	10116	6.95	0.04	0.818	0.00058	0.938	0.062	0.0089	57.1	0.36
AL-C-24	206204	10714	6.43	0.09	0.818	0.00068	0.937	0.063	0.0097	62.5	0.86
AL-C-25	212258	10917	7.07	0.05	0.813	0.00040	0.932	0.068	0.0097	61.9	0.45
AL-C-26	221614	11217	10.82	0.06	0.802	0.00058	0.918	0.082	0.0076	48.5	0.28

Session 2 - SJB 2

Sample ID	^{206}Pb (cps)	^{204}Pb (cps)	$\frac{^{238}U}{^{206}Pb}$ meas.	1 SE	$\frac{^{207}Pb}{^{206}Pb}$ meas.	1 SE	f_{206}	$1-f_{206}$	$\frac{^{206}Pb}{^{238}U}$ corr.	$\frac{^{206}Pb}{^{238}U}$ age (Ma)	1 SE
AL-G-1	1114061	58742	1.63	0.02	0.830	0.00048	1.000	0.000	0.0000	-0.2	48.5
AL-G-2	2027139	106868	1.22	0.01	0.824	0.00032	0.993	0.007	0.0061	39.0	37.8
AL-G-3	2015295	106203	1.20	0.01	0.825	0.00041	0.994	0.006	0.0051	32.5	57.0
AL-G-4*	18688	564	-3.97	26.81	0.947	0.00423	1.150	-0.150	0.0377	238.7	6249
AL-G-5*	17171	273	3.97	0.12	0.834	0.00160	1.005	-0.005	-0.0013	-8.6	48.5
AL-G-6*	1209	6	213.49	3575.71	0.883	0.02530	1.068	-0.068	-0.0003	-2.1	487

Table 7 (*continued*)

Sample ID	^{206}Pb (cps)	^{204}Pb (cps)	$\frac{^{238}U}{^{206}Pb}$ meas.	1 SE	$\frac{^{207}Pb}{^{206}Pb}$ meas.	1 SE	f_{206}	$1-f_{206}$	$\frac{^{206}Pb}{^{238}U}$ corr.	$\frac{^{206}Pb}{^{238}U}$ age (Ma)	1 SE
AL-G-7*	42426	1872	4.95	0.19	0.828	0.00211	0.997	0.003	0.0006	4.0	48.9
AL-G-8	126471	6099	4.59	0.09	0.827	0.00130	0.996	0.004	0.0008	5.3	28.7
AL-G-9	602106	30957	2.84	0.05	0.822	0.00040	0.990	0.010	0.0036	23.1	42.4
AL-G-10	566883	29848	1.63	0.03	0.837	0.00059	1.009	-0.009	-0.0058	-37.3	83.9
AL-E-1	1174247	61235	2.90	0.03	0.824	0.00073	0.974	0.026	0.0091	58.4	22.3
AL-E-2	528604	28002	1.79	0.05	0.832	0.00064	0.983	0.017	0.0094	60.6	107
AL-E-3	296487	15188	2.48	0.06	0.828	0.00069	0.978	0.022	0.0087	55.9	57.5
AL-E-4	106687	4899	3.48	0.11	0.831	0.00128	0.982	0.018	0.0050	32.5	59.2
AL-E-5*	43	0	-232	275	0.199	0.32837	0.190	0.810	-0.0035	-22.5	33.0
AL-E-6*	13	0	-1346	10932	0.069	0.80079	0.027	0.973	-0.0007	-4.7	38.8
AL-E-7*	240855	12257	0.54	0.01	0.839	0.00063	0.993	0.007	0.0130	83.1	250
AL-E-8*	47245	1836	1.36	0.03	0.836	0.00120	0.988	0.012	0.0086	55.2	110
AL-E-9	573619	30043	2.18	0.04	0.834	0.00052	0.986	0.014	0.0066	42.2	55.8
AL-E-10	317971	16074	2.26	0.05	0.827	0.00047	0.977	0.023	0.0101	65.0	62.6
AL-E-11	171345	8354	2.16	0.03	0.833	0.00061	0.985	0.015	0.0067	43.3	43.0
AL-F-1	1373392	72940	1.64	0.03	0.850	0.01679	1.012	-0.012	-0.0075	-48.3	69.9
AL-F-2	220512	10712	0.22	0.01	0.828	0.00091	0.985	0.015	0.0668	417.1	633
AL-F-3*	27984	470	1.58	0.05	0.837	0.00182	0.996	0.004	0.0025	15.8	127
AL-F-4*	20395	200	1.99	0.08	0.839	0.00144	0.998	0.002	0.0008	5.5	131
AL-F-5*	50668	1696	1.24	0.04	0.841	0.00146	1.002	-0.002	-0.0013	-8.2	165
AL-F-6	404738	20678	2.51	0.10	0.836	0.00047	0.995	0.005	0.0019	12.2	96.7
AL-F-7	252934	12114	2.12	0.04	0.829	0.00124	0.986	0.014	0.0065	41.9	58.2
AL-F-8	375446	19159	1.30	0.02	0.839	0.00055	0.999	0.001	0.0006	3.8	66.6

Session 3 - DPF 1

Sample ID	^{206}Pb (cps)	^{204}Pb (cps)	$\frac{^{238}U}{^{206}Pb}$ meas.	1 SE	$\frac{^{207}Pb}{^{206}Pb}$ meas.	1 SE	f_{206}	$1-f_{206}$	$\frac{^{206}Pb}{^{238}U}$ corr.	$\frac{^{206}Pb}{^{238}U}$ age (Ma)	1 SE
C269-A-1	196081	10913	5.58	0.06	0.797	0.00067	0.968	0.032	0.0057	36.7	11.7
C269-A-2	253414	13957	2.00	0.03	0.822	0.00071	1.001	-0.001	-0.0005	-3.2	55.9
C269-A-3	199308	11088	1.31	0.01	0.817	0.00058	0.994	0.006	0.0048	30.9	44.8
C269-A-4	363129	19628	2.24	0.02	0.813	0.00043	0.989	0.011	0.0048	30.7	24.3
C269-A-5	376391	20255	1.69	0.01	0.813	0.00056	0.989	0.011	0.0065	41.6	19.6
C269-A-6	431874	23093	1.54	0.01	0.814	0.00055	0.989	0.011	0.0068	43.7	23.4
C269-A-7	352537	19186	1.17	0.01	0.815	0.00051	0.992	0.008	0.0071	45.5	32.9
C269-A-8	731234	38703	1.19	0.01	0.814	0.00046	0.990	0.010	0.0088	56.4	25.2
C269-A-9	269711	14898	1.19	0.02	0.816	0.00065	0.993	0.007	0.0061	39.1	73.7
C269-A-10	98057	5858	0.56	0.01	0.825	0.00075	1.004	-0.004	-0.0066	-42.7	175
C269-A-11	79457	4784	0.63	0.01	0.830	0.00108	1.010	-0.010	-0.0162	-105.5	100
C269-A-12	93589	5582	0.46	0.01	0.826	0.00083	1.005	-0.005	-0.0115	-74.8	204
C269-A-13	86304	5175	0.83	0.01	0.830	0.00067	1.011	-0.011	-0.0127	-82.7	51.2
C269-A-14	147918	8481	0.61	0.01	0.828	0.00073	1.008	-0.008	-0.0122	-79.4	123

Table 7 (*continued*)

Sample ID	^{206}Pb (cps)	^{204}Pb (cps)	$\frac{^{238}U}{^{206}Pb}$ meas.	1 SE	$\frac{^{207}Pb}{^{206}Pb}$ meas.	1 SE	f_{206}	$1-f_{206}$	$\frac{^{206}Pb}{^{238}U}$ corr.	$\frac{^{206}Pb}{^{238}U}$ age (Ma)	1 SE
C269-A-15	157241	8975	0.79	0.01	0.824	0.00066	1.003	-0.003	-0.0041	-26.7	91.8
C269-A-16	552632	29396	1.66	0.01	0.814	0.00069	0.990	0.010	0.0063	40.3	28.6
C269-A-17	328383	17776	1.38	0.01	0.813	0.00051	0.989	0.011	0.0078	50.0	26.7
C269-A-18	543577	28800	1.48	0.01	0.814	0.00054	0.990	0.010	0.0065	41.8	20.2
C269-A-19	331199	17865	1.04	0.01	0.816	0.00069	0.992	0.008	0.0074	47.2	49.6
C269-A-20	299180	16269	0.77	0.01	0.819	0.00053	0.997	0.003	0.0045	28.9	62.9
C269-A-21	227334	12434	1.02	0.02	0.822	0.00061	1.000	0.000	0.0002	1.3	98.3
C269-B-1	375039	20327	0.47	0.01	0.825	0.00069	0.981	0.019	0.0405	256.2	149
C269-B-2	324210	17559	0.59	0.00	0.820	0.00053	0.974	0.026	0.0431	271.8	71.7
C269-B-3	177132	9790	0.49	0.01	0.823	0.00097	0.978	0.022	0.0440	277.5	155
C269-B-4	85347	4966	0.72	0.01	0.824	0.00062	0.980	0.020	0.0282	179.5	133
C269-B-5	62686	3664	1.02	0.02	0.823	0.00121	0.978	0.022	0.0213	135.6	117
C269-B-6	43964	2791	1.08	0.01	0.823	0.00126	0.979	0.021	0.0197	126.1	52.6
C269-B-7	78833	4647	1.10	0.01	0.825	0.00100	0.981	0.019	0.0174	111.5	69.1
C269-B-8	494527	26705	0.08	0.00	0.827	0.00074	0.983	0.017	0.2126	1242.5	1114
C269-B-9	225905	12426	0.26	0.00	0.826	0.00080	0.982	0.018	0.0681	424.7	278
C269-B-10	420417	22565	0.15	0.00	0.822	0.00061	0.978	0.022	0.1463	880.3	704
C269-B-11	597855	33092	0.10	0.00	0.822	0.00045	0.977	0.023	0.2333	1351.6	1108
C269-D-1	11894	836	3.10	0.06	0.814	0.00247	0.968	0.032	0.0102	65.4	38.9
C269-D-2	15455	1102	2.87	0.04	0.826	0.00160	0.983	0.017	0.0059	37.7	28.0
C269-D-3	20720	1368	6.08	0.07	0.798	0.00156	0.948	0.052	0.0085	54.5	11.3
C269-D-4	29064	1800	8.54	0.08	0.784	0.00143	0.930	0.070	0.0082	52.4	6.7
C269-D-5	30527	1850	9.83	0.06	0.775	0.00128	0.919	0.081	0.0082	52.8	4.3
C269-D-6	24288	1553	5.94	0.05	0.788	0.00114	0.936	0.064	0.0108	69.5	9.8
C269-D-7	13721	917	6.14	0.06	0.795	0.00280	0.944	0.056	0.0091	58.6	11.0
C269-D-8	32676	1884	11.10	0.09	0.767	0.00102	0.909	0.091	0.0082	52.6	4.5
C269-D-9	40408	2178	17.23	0.12	0.745	0.00108	0.881	0.119	0.0069	44.3	2.5
C269-D-10	24404	1434	10.70	0.09	0.762	0.00139	0.903	0.097	0.0091	58.3	5.1
C269-D-11	27453	1516	14.55	0.09	0.744	0.00093	0.879	0.121	0.0083	53.2	2.7
C269-D-12	17564	1018	4.38	0.04	0.815	0.00135	0.969	0.031	0.0071	45.3	12.1
C269-D-13	11022	685	3.30	0.05	0.817	0.00225	0.972	0.028	0.0085	54.8	31.7
C269-C-1	87378	4428	5.73	0.07	0.808	0.00100	0.967	0.033	0.0058	37.1	12.9
C269-C-2	93119	4873	11.30	0.09	0.783	0.00070	0.936	0.064	0.0057	36.5	4.4
C269-C-3	13193	648	0.97	0.02	0.827	0.00193	0.991	0.009	0.0093	59.6	153
C269-C-4	24470	1250	0.54	0.02	0.835	0.00110	1.002	-0.002	-0.0033	-21.3	340
C269-C-5	28767	1542	0.63	0.02	0.829	0.00157	0.994	0.006	0.0090	58.0	288
C269-C-6	24682	1332	0.92	0.02	0.829	0.00155	0.994	0.006	0.0066	42.3	140
C269-C-7	3081	130	0.96	0.16	0.837	0.00510	1.004	-0.004	-0.0042	-26.9	1051

Table 7 (*continued*)

Sample ID	^{206}Pb (cps)	^{204}Pb (cps)	$\frac{^{238}U}{^{206}Pb}$ meas.	1 SE	$\frac{^{207}Pb}{^{206}Pb}$ meas.	1 SE	f_{206}	$1-f_{206}$	$\frac{^{206}Pb}{^{238}U}$ corr.	$\frac{^{206}Pb}{^{238}U}$ age (Ma)	1 SE
C269-C-8	18369	1005	0.75	0.02	0.830	0.00165	0.996	0.004	0.0060	38.5	238
C269-C-9	19408	989	1.04	0.02	0.822	0.00161	0.986	0.014	0.0139	88.9	128
C269-C-10	23714	1238	0.54	0.02	0.831	0.00179	0.996	0.004	0.0067	43.3	358
C269-C-11	14215	797	1.06	0.03	0.823	0.00239	0.986	0.014	0.0131	84.0	166
C269-C-12	92326	4833	3.72	0.05	0.819	0.00095	0.982	0.018	0.0049	31.3	24.7
C269-C-13	67586	3537	3.47	0.05	0.822	0.00092	0.985	0.015	0.0044	28.2	28.0
Session 4 - DPF 2											
T408-A-1	27354	1967	11.82	0.12	0.789	0.00157	0.900	0.100	0.0085	54.6	5.37
T408-A-2	18831	1590	9.55	0.17	0.798	0.00219	0.910	0.090	0.0094	60.5	11.6
T408-A-3	14346	1300	14.94	0.17	0.767	0.00237	0.873	0.127	0.0085	54.7	4.89
T408-A-4	11475	1189	17.62	0.19	0.740	0.00228	0.840	0.160	0.0091	58.2	3.87
T408-A-5	11422	1000	20.71	0.30	0.738	0.00264	0.838	0.162	0.0078	50.4	4.47
T408-A-6	12468	1002	18.78	0.23	0.733	0.00204	0.831	0.169	0.0090	57.6	4.12
T408-A-7	14376	1096	16.65	0.24	0.747	0.00233	0.849	0.151	0.0091	58.3	5.50
T408-A-8	31080	2037	12.35	0.14	0.776	0.00170	0.883	0.117	0.0095	60.8	5.82
T408-A-9	50338	3071	11.13	0.17	0.786	0.00151	0.896	0.104	0.0094	60.2	8.65
T408-A-10	22901	1585	16.15	0.23	0.748	0.00170	0.850	0.150	0.0093	59.6	5.58
T408-A-11	24556	1594	15.88	0.22	0.743	0.00196	0.844	0.156	0.0098	63.1	5.64
T408-A-12	54320	3224	8.21	0.07	0.783	0.00138	0.892	0.108	0.0131	83.9	6.72
T408-D-1	70543	4081	1.66	0.04	0.832	0.00108	0.999	0.001	0.0008	5.2	87.0
T408-D-2	8959	836	0.77	2.30	0.841	0.00274	1.011	-0.011	-0.0140	-90.7	10242
T408-D-3	23184	1526	0.76	0.03	0.836	0.00209	1.003	-0.003	-0.0044	-28.2	289
T408-D-4	4520	566	-0.30	0.18	0.826	0.00358	0.991	0.009	-0.0315	-206.7	7178
T408-D-5	16649	1260	3.13	0.04	0.790	0.00174	0.946	0.054	0.0173	110.6	25.2
T408-D-6	32735	2071	3.37	0.02	0.776	0.00132	0.928	0.072	0.0214	136.8	13.5
T408-D-7	174009	9080	13.95	0.07	0.771	0.00036	0.921	0.079	0.0057	36.5	2.17
T408-D-8	323300	16787	8.98	0.05	0.789	0.00069	0.943	0.057	0.0063	40.5	4.35
T408-D-9	144588	7991	0.68	0.00	0.820	0.00086	0.983	0.017	0.0247	157.2	63.2
T408-D-10	69029	4019	0.73	0.01	0.828	0.00089	0.994	0.006	0.0087	55.9	69.5
T408-D-11	46112	2715	0.75	0.01	0.829	0.00123	0.995	0.005	0.0064	40.8	85.7
T408-D-12	204994	11097	0.41	0.00	0.834	0.00083	1.001	-0.001	-0.0019	-12.4	130
T408-B-1	74519	4187	9.44	0.52	0.784	0.00289	0.956	0.044	0.0047	30.2	37.1
T408-B-2	3280	729	0.97	0.16	0.824	0.00512	1.008	-0.008	-0.0081	-52.4	1022
T408-B-3	4681	677	3.52	0.15	0.807	0.00342	0.985	0.015	0.0041	26.7	75.8
T408-B-4	5149	698	16.60	0.20	0.732	0.00380	0.888	0.112	0.0067	43.2	4.54
T408-B-5	5454	654	12.66	0.20	0.768	0.00311	0.936	0.064	0.0051	32.8	7.83
T408-B-6	6440	696	17.03	0.39	0.753	0.00304	0.916	0.084	0.0049	31.8	8.63
T408-B-7	4699	560	14.37	0.61	0.767	0.00424	0.934	0.066	0.0046	29.4	19.0

Table 7 (*continued*)

Sample ID	^{206}Pb (cps)	^{204}Pb (cps)	$\dfrac{^{238}U}{^{206}Pb}$ meas.	1 SE	$\dfrac{^{207}Pb}{^{206}Pb}$ meas.	1 SE	f_{206}	$1-f_{206}$	$\dfrac{^{206}Pb}{^{238}U}$ corr.	$\dfrac{^{206}Pb}{^{238}U}$ age (Ma)	1 SE
T408-B-8	4566	668	3.09	0.11	0.819	0.00364	1.001	-0.001	-0.0003	-2.0	74.5
T408-B-9	17322	1141	56.16	0.69	0.588	0.00262	0.702	0.298	0.0053	34.1	1.40
T408-B-10	12271	873	62.31	0.96	0.523	0.00231	0.618	0.382	0.0061	39.4	1.59
T408-B-11	12674	969	31.39	0.70	0.648	0.00363	0.779	0.221	0.0070	45.2	4.52
T408-B-12	5854	722	25.09	0.56	0.670	0.00311	0.808	0.192	0.0076	49.0	5.71
T408-B-13	6815	840	12.58	0.24	0.727	0.00254	0.882	0.118	0.0094	60.2	9.84
T408-B-14	4729	650	9.15	0.15	0.761	0.00305	0.926	0.074	0.0081	51.7	11.3
T408-B-15	4886	597	18.69	0.42	0.700	0.00483	0.847	0.153	0.0082	52.5	7.61
T408-C-1	10469	824	1.88	0.06	0.826	0.00255	0.981	0.019	0.0098	63.1	101
T408-C-2	20106	1324	4.39	0.11	0.809	0.00104	0.959	0.041	0.0093	59.6	35.0
T408-C-3	33925	2030	4.73	0.07	0.796	0.00137	0.943	0.057	0.0120	77.0	20.5
T408-C-4	34038	2057	5.19	0.07	0.799	0.00124	0.947	0.053	0.0103	65.9	15.6
T408-C-5	70771	3971	9.45	0.06	0.776	0.00125	0.917	0.083	0.0087	56.1	3.94
T408-C-6	64630	3676	9.48	0.09	0.770	0.00125	0.910	0.090	0.0095	60.8	6.07
T408-C-7	51226	2887	11.98	0.10	0.760	0.00116	0.898	0.102	0.0085	54.5	4.62
T408-C-8	30912	1883	17.90	0.14	0.724	0.00167	0.853	0.147	0.0082	52.9	2.83
T408-C-9	30432	1727	17.50	0.17	0.734	0.00117	0.865	0.135	0.0077	49.4	3.53
T408-C-10	24001	1649	17.24	0.12	0.735	0.00188	0.866	0.134	0.0078	49.9	2.67
T408-C-11	18975	1389	8.10	0.07	0.778	0.00190	0.920	0.080	0.0099	63.3	6.81
T408-C-12	28214	1868	8.78	0.09	0.785	0.00124	0.929	0.071	0.0081	51.7	7.22
T408-C-13	15661	1209	7.39	0.06	0.778	0.00189	0.921	0.079	0.0107	68.7	7.23
T408-C-14	19456	1493	9.96	0.15	0.756	0.00143	0.893	0.107	0.0107	68.7	9.47
T408-C-15	22667	1499	7.92	0.07	0.765	0.00122	0.904	0.096	0.0122	77.9	6.65
T408-C-16	21932	1510	5.38	0.06	0.789	0.00154	0.935	0.065	0.0121	77.7	14.1
T408-C-17	22272	1535	3.50	0.03	0.811	0.00182	0.962	0.038	0.0109	69.7	16.3
T408-C-18	20702	1459	2.73	0.03	0.814	0.00144	0.966	0.034	0.0123	78.9	25.7
T408-C-19	19780	1420	3.88	0.03	0.800	0.00162	0.948	0.052	0.0134	85.9	14.7
T408-C-20	14188	1120	0.67	0.03	0.835	0.00228	0.993	0.007	0.0106	68.1	361

Table 8
U-Pb laser ablation ICP-MS results for select fossil teeth from the Arroyo Chijuillita Member and the Dinosaur Park Formation, normalized using Durango apatite.

Arroyo Chijuillita Member, Nacimiento Fm

Sample ID	$\frac{^{238}U}{^{206}Pb}$ norm.	1 SE	$\frac{^{207}Pb}{^{206}Pb}$ meas.	1 SE	$\frac{^{206}Pb}{^{238}U}$ norm.	$\frac{^{206}Pb}{^{238}U}$ age (Ma)	1 SE
AL-C-1	0.06	0.00	0.853	0.00082	0.3257	1818	143
AL-C-2	9.51	0.13	0.802	0.00081	0.0086	54.9	1.10
AL-C-3	17.50	0.24	0.745	0.00072	0.0086	55.4	1.05
AL-C-4	14.90	0.21	0.734	0.00074	0.0110	70.6	1.35
AL-C-5	11.93	0.17	0.751	0.00099	0.0120	77.1	1.49
AL-C-6	11.84	0.17	0.770	0.00057	0.0102	65.6	1.26
AL-C-7	16.75	0.24	0.724	0.00108	0.0106	67.7	1.51
AL-C-8	24.39	0.34	0.679	0.00094	0.0095	60.8	1.20
AL-C-9	21.88	0.31	0.692	0.00115	0.0098	63.1	1.30
AL-C-10	30.88	0.43	0.632	0.00163	0.0093	60.0	1.19
AL-C-11	30.32	0.43	0.630	0.00130	0.0096	61.5	1.22
AL-C-12	28.99	0.42	0.650	0.00106	0.0092	59.1	1.36
AL-C-13	23.25	0.33	0.692	0.00118	0.0092	59.3	1.16
AL-C-14	20.74	0.29	0.717	0.00094	0.0089	57.2	1.15
AL-C-15	22.79	0.32	0.700	0.00102	0.0090	57.9	1.19
AL-C-16	27.59	0.39	0.666	0.00091	0.0090	57.5	1.21
AL-C-17	27.66	0.39	0.681	0.00096	0.0083	53.2	1.05
AL-C-18	23.67	0.33	0.708	0.00123	0.0083	53.0	1.01
AL-C-19	24.90	0.37	0.703	0.00114	0.0081	51.9	1.30
AL-C-20	23.35	0.33	0.707	0.00077	0.0084	54.2	1.10
AL-C-21	15.15	0.22	0.747	0.00080	0.0098	62.9	1.34
AL-C-22	13.13	0.18	0.805	0.00070	0.0059	38.2	0.74
AL-C-23	6.89	0.10	0.818	0.00058	0.0090	57.6	1.12
AL-C-24	6.38	0.09	0.818	0.00068	0.0098	63.0	1.45
AL-C-25	7.02	0.10	0.813	0.00040	0.0097	62.4	1.24
AL-C-26	10.73	0.15	0.802	0.00058	0.0076	48.9	0.94

Sample ID	$\frac{^{238}U}{^{206}Pb}$ norm.	1 SE	$\frac{^{207}Pb}{^{206}Pb}$ meas.	1 SE	$\frac{^{206}Pb}{^{238}U}$ norm.	1 SE	$\frac{^{206}Pb}{^{238}U}$ age (Ma)	1 SE
AL-B-1	4.22	0.23	0.826	0.00124	0.0033	0.0033	21.4	0.57
AL-B-2	3.59	0.19	0.832	0.00074	0.0019	0.0019	12.1	0.27
AL-B-3	8.80	0.47	0.810	0.00050	0.0039	0.0039	25.0	0.61
AL-B-4	12.36	0.64	0.795	0.00073	0.0043	0.0043	27.5	0.62
AL-B-5	6.64	0.35	0.819	0.00061	0.0035	0.0035	22.6	0.51
AL-B-6	2.51	0.13	0.830	0.00045	0.0039	0.0039	24.8	0.53
AL-B-7	2.20	0.12	0.833	0.00077	0.0026	0.0026	16.6	0.41
AL-B-8	6.30	0.33	0.819	0.00068	0.0036	0.0036	23.1	0.51
AL-B-9	8.25	0.43	0.815	0.00052	0.0034	0.0034	22.0	0.48
AL-B-10	12.05	0.62	0.805	0.00061	0.0033	0.0033	21.5	0.47
AL-B-11	15.26	0.78	0.793	0.00067	0.0037	0.0037	23.8	0.47
AL-B-12	14.36	0.74	0.778	0.00084	0.0052	0.0052	33.3	0.69
AL-B-13	8.99	0.46	0.807	0.00063	0.0043	0.0043	27.4	0.52
AL-B-14	12.11	0.62	0.800	0.00056	0.0039	0.0039	25.0	0.49
AL-B-15	21.80	1.12	0.740	0.00092	0.0056	0.0056	36.2	0.75
AL-B-16	3.90	0.20	0.829	0.00054	0.0027	0.0027	17.3	0.33
AL-B-17	2.33	0.12	0.832	0.00062	0.0028	0.0028	17.9	0.40
AL-B-18	2.11	0.11	0.830	0.00070	0.0042	0.0042	27.0	0.56
AL-B-19	1.74	0.09	0.832	0.00065	0.0035	0.0035	22.6	0.45
AL-B-20	1.77	0.09	0.831	0.00057	0.0047	0.0047	30.0	0.59
AL-B-21	1.99	0.10	0.832	0.00079	0.0035	0.0035	22.3	0.47
AL-B-22	2.02	0.10	0.831	0.00082	0.0039	0.0039	25.3	0.53
AL-B-23	2.30	0.12	0.832	0.00057	0.0030	0.0030	19.0	0.40
AL-B-24	2.57	0.13	0.830	0.00080	0.0033	0.0033	21.3	0.42
AL-B-25	4.70	0.26	0.821	0.00060	0.0043	0.0043	27.5	0.81
AL-B-26	4.49	0.23	0.829	0.00048	0.0023	0.0023	14.7	0.30

Table 8 (*continued*)

Dinosaur Park Formation

Sample ID	$\frac{238U}{206Pb}$ norm.	1 SE	$\frac{207Pb}{206Pb}$ meas.	1 SE	$\frac{206Pb}{238U}$ norm.	1 SE	$\frac{206Pb}{238U}$ age (Ma)	1 SE
T408-C-1	2.16	0.13	0.826	0.00255	0.0086	55.0	101
T408-C-2	5.02	0.28	0.809	0.00104	0.0081	52.0	35.0
T408-C-3	5.41	0.28	0.796	0.00137	0.0105	67.1	20.6
T408-C-4	5.94	0.31	0.799	0.00124	0.0090	57.5	15.6
T408-C-5	10.83	0.55	0.776	0.00125	0.0076	48.9	4.07
T408-C-6	10.86	0.55	0.770	0.00125	0.0083	53.0	6.18
T408-C-7	13.72	0.70	0.760	0.00116	0.0074	47.6	4.73
T408-C-8	20.50	1.04	0.724	0.00167	0.0072	46.1	2.99
T408-C-9	20.05	1.02	0.734	0.00117	0.0067	43.1	3.65
T408-C-10	19.75	1.00	0.735	0.00188	0.0068	43.5	2.82
T408-C-11	9.28	0.47	0.778	0.00190	0.0086	55.2	6.92
T408-C-12	10.05	0.51	0.785	0.00124	0.0070	45.1	7.28
T408-C-13	8.47	0.43	0.778	0.00189	0.0093	59.9	7.35
T408-C-14	11.41	0.60	0.756	0.00143	0.0093	59.9	9.57
T408-C-15	9.07	0.46	0.765	0.00122	0.0106	68.0	6.81
T408-C-16	6.16	0.32	0.789	0.00154	0.0106	67.8	14.2
T408-C-17	4.00	0.20	0.811	0.00182	0.0095	60.8	16.4
T408-C-18	3.13	0.16	0.814	0.00144	0.0107	68.8	25.7
T408-C-19	4.44	0.23	0.800	0.00162	0.0117	75.0	14.8
T408-C-20	0.76	0.05	0.835	0.00228	0.0093	59.4	361

Sample ID	$\frac{238U}{206Pb}$ norm.	1 SE	$\frac{207Pb}{206Pb}$ meas.	1 SE	$\frac{206Pb}{238U}$ norm.	1 SE	$\frac{206Pb}{238U}$ age (Ma)	1 SE
C269-D-1	3.43	0.17	0.814	0.00247	0.0092	59.1	38.9
C269-D-2	3.17	0.15	0.826	0.00160	0.0053	34.1	28.0
C269-D-3	6.72	0.32	0.798	0.00156	0.0077	49.3	11.4
C269-D-4	9.44	0.44	0.784	0.00143	0.0074	47.4	6.76
C269-D-5	10.86	0.51	0.775	0.00128	0.0074	47.7	4.40
C269-D-6	6.57	0.31	0.788	0.00114	0.0098	62.9	9.94
C269-D-7	6.78	0.32	0.795	0.00280	0.0083	53.0	11.1
C269-D-8	12.27	0.57	0.767	0.00102	0.0074	47.6	4.63
C269-D-9	19.05	0.89	0.745	0.00108	0.0062	40.1	2.66
C269-D-10	11.83	0.56	0.762	0.00139	0.0082	52.8	5.20
C269-D-11	16.09	0.75	0.744	0.00093	0.0075	48.1	2.86
C269-D-12	4.84	0.23	0.815	0.00135	0.0064	41.0	12.2
C269-D-13	3.64	0.18	0.817	0.00225	0.0077	49.6	31.8
T408-B-1	10.83	0.80	0.7838	0.00289	0.0041	26.3	37.1
T408-B-2	1.11	0.19	0.8240	0.00512	-0.0070	-45.6	-1021
T408-B-3	4.03	0.26	0.8068	0.00342	0.0036	23.3	75.8
T408-B-4	19.05	0.97	0.7320	0.00380	0.0059	37.6	4.61
T408-B-5	14.53	0.75	0.7683	0.00311	0.0044	28.6	7.86
T408-B-6	19.54	1.06	0.7532	0.00304	0.0043	27.7	8.65
T408-B-7	16.48	1.07	0.7673	0.00424	0.0040	25.7	19.0
T408-B-8	3.54	0.22	0.8188	0.00364	-0.0003	-1.8	-74.5
T408-B-9	64.45	3.28	0.5883	0.00262	0.0046	29.7	1.54
T408-B-10	71.50	3.70	0.5232	0.00231	0.0053	34.4	1.74
T408-B-11	36.02	1.95	0.6477	0.00363	0.0061	39.4	4.60
T408-B-12	28.79	1.56	0.6704	0.00311	0.0067	42.8	5.78
T408-B-13	14.44	0.77	0.7270	0.00254	0.0082	52.5	9.92
T408-B-14	10.50	0.55	0.7612	0.00305	0.0070	45.1	11.3
T408-B-15	21.44	1.16	0.7003	0.00483	0.0071	45.7	7.68

10. References

Ayliffe, L.K., Chivas, A.R. and Leakey, M.G. (1994) The retention of primary oxygen isotope compositions of fossil elephant skeletal phosphate. *Geochim. Cosmochim. Acta* **58**, 5291– 5298.

Baltz, E. H. (1967) Stratigraphy and regional tectonic implications of part of Upper Cretaceous and Tertiary rocks, east-central San Juan Basin, New Mexico. U.S. Govt. Print. Off. *Prof. Pap. 552*

Butler, R. F. and Lindsay E. H. (1985) Mineralogy of Magnetic Minerals and Revised Magnetic Polarity Stratigraphy of Continental Sediments, San Juan Basin, New Mexico. *J. Geol.* **93(5)**, 535-554.

Cant, D. J. and Stockmal G. S. (1989) The Alberta foreland basin: relationship between stratigraphy and Cordilleran terrane-accretion events. *Can. J. Earth Sci.s* **26(10)**, 1964-1975.

Chapin, C. E. (2012) Origin of the Colorado Mineral Belt. *Geosphere* **8(1)**, 28-43.

Chew, D. M., Sylvester, P. J. and Tubrett M.N. (2011) U–Pb and Th–Pb dating of apatite by LA-ICPMS. *Chem. Geol.* **280(1–2)**, 200-216.

Cifelli, R. L., Madsen S. K., and Larson E. M. (1996) Screenwashing and associated techniques for the recovery of microvertebrate fossils. *OK Geol. Surv. Spec. Publ.* **96-4**, 1-24.

Eberth, D. A. and Hamblin A. P. (1993) Tectonic, stratigraphic, and sedimentologic significance of a regional discontinuity in the upper Judith River Group (Belly River wedge) of southern Alberta, Saskatchewan, and northern Montana. *Can. J. Earth Sci.s* **30(1)**, 174-200.

Eberth, D., Roberts E., Deino A., Bowring S. and Ramezani J. (2013) Twenty-three years of radiometric dating at Dinosaur Provincial Park (Upper Cretaceous, Alberta, Canada). *J. Vertebr. Paleontol., Program and Abstracts*, 120.

Fan, M., Heller P., Allen S.D. and Hough B.G (2014) Middle Cenozoic uplift and concomitant drying in the central Rocky Mountains and adjacent Great Plains. *Geology* **42(6)**, 547–550.

Fassett, J. E. (2009) New geochronologic and stratigraphic evidence confirms the paleocene age of the dinosaur-bearing Ojo Alamo sandstone and animas formation in the San Juan Basin, New Mexico and Colorado. *Palaeontol. Electronica*, **12(1),** 3A, 150p.

Fassett J. E., Heaman L.M, and Simonetti A. (2012) Direct U-Pb dating of Cretaceous and Paleocene dinosaur bones, San Juan Basin, New Mexico. *Geology* **40(4)**, 260-261.

Ge S. and Garven G. (1992) Hydromechanical modeling of tectonically driven groundwater flow with application to the Arkoma foreland basin. *J. Geophys. Res.* **97(B6)**, 9119-9144.

Gradstein F.M., Ogg J.M., Schmitz M.D. and Ogg G.M. (2012) The Geologic Time Scale, Volume 2. Boston, Massachusetts, Elsevier, 1144 p.

Heaman L. M. and Kjarsgaard B. A. (2000) Timing of eastern North American kimberlite magmatism: Continental extension of the Great Meteor Hotspot Track? *Earth Planet. Sci. Lett.* **178**, 253–268.

Hearn Jr. B.C., Marvin R.F., Zartman R.E., and Naeser C.W. (1978) Ages of alkalic activity in north-central Montana; *U.S. Geol. Surv. Prof. Pap.* No. 1100, 60 p.

Heizler M. T., Mason A., Williamson T. E., Peppe D. J., Ramezani J., and Bowring S. A. (2013) ^{40}Ar/^{39}Ar Chronostratigraphy of Cretaceous and Paleocene strata in the San Juan Basin, New Mexico: Accuracy limitations of high precision measurements: In *Geol. Soc. Am., Abstracts with Programs*, **45(7)**, 289.

Herwartz D., Tutken T., Munker C., Jochum K. P., Stoll B. and Sander P.M. (2011) Timescales and mechanisms of REE and Hf uptake in fossil bones. *Geochim. Cosmochim. Acta* **75(1)**, 82-105.

Ingebritsen S. E. and Appold M. S. (2012). The physical hydrogeology of ore deposits. *Econ. Geol.* **107(4)**, 559-584.

Jaffey A. H., Flynn K. F., Glendenin L. E., Bentley W. C. and Essling A. M. (1971) Precision measurements of half-lives and specific activities of 235U and 238U. *Phys. Rev. C: Nucl. Phys.*, **C 4(5)**, 1,889-1,906.

Kocsis, L., Trueman C. N., Palmer M. R. (2010) Protracted diagenetic alteration of REE contents in fossil bioapatites: Direct evidence from Lu–Hf isotope systematics. *Geochim. Cosmochim. Acta* **74(21)**, 6077-6092.

Koenig A. E., Rogers R. R., Trueman C. N. (2009) Visualizing fossilisation using laser ablation–inductively coupled plasma–mass spectrometry maps of trace elements in Late Cretaceous bones. *Geology* **37(6)**, 511-514.

Koenig A. E., Lucas S. G., Neymark L. A., Heckert A. B., Sullivan R. M., Jasinski S. E., Fowler D. W. (2012) Direct U-Pb dating of Cretaceous and Paleocene dinosaur bones, San Juan Basin, New Mexico: COMMENT. *Geology* **40(4)**, 262-262.

Kohn M. J. (2008) Models of diffusion-limited uptake of trace elements in fossils and rates of fossilisation. *Geochim. Cosmochim. Acta* **72(15)**, 3758-3770.

Kohn M. J., Morris J., Olin P. (2013) Trace element concentrations in teeth – a modern Idaho baseline with implications for archeometry, forensics, and palaeontology. *J. Archeol. Sci.* **40(4)**, 1689-1699.

Kohn M. J. and Moses R. J. (2013) Trace element diffusivities in bone rule out simple diffusive uptake during fossilisation but explain in vivo uptake and release. *Proc. Natl. Acad. Sci. U.S.A.* **110(2)**, 419-424.

Kohn M. J., Schoeninger M. J. and Barker W. B. (1999) Altered states: effects of diagenesis on fossil tooth chemistry. *Geochim. Cosmochim. Acta* **63**, 2737–2747.

Koster E.H. (1987) Vertebrate taphonomy applied to the analysis of ancient fluvial systems. Recent developments in fluvial sedimentology. *Soc. Econ. Paleontol. Mineral. Special Publication*, **39**, 159-168.

Kowal-Linka M., Jochum K. P., Surmik D. (2014) LA-ICP-MS analysis of rare earth elements in marine reptile bones from the Middle Triassic bonebed (Upper Silesia, S Poland): Impact of long-lasting diagenesis, and factors controlling the uptake. *Chem. Geol.* **363**, 213-228.

Lehman T. M. (1987) Late Maastrichtian paleoenvironments and dinosaur biogeography in the western interior of North America. *Palaeogeogr. Palaeoclimatol. Palaeoecol.* **60**, 189-217.

Lindsay, E. H., et al. (1981) Magnetic polarity zonation and biostratigraphy of Late Cretaceous and Paleocene continental deposits, San Juan Basin, New Mexico. *Am. J. Sci.* **281(4)**: 390-435.

Lindsay, E. H., et al. (1978) Biostratigraphy and magnetostratigraphy of Paleocene terrestrial deposits, San Juan Basin, New Mexico. *Geology* **6(7)**: 425-429.

Lipman P.W. (1975) Evolution of the Platoro caldera complex and related volcanic rocks, southeastern San Juan Mountains, Colorado. *U.S. Geol. Surv. Prof. Pap.* **852**, 128 p.

Lipman P.W., Steven T.A., and Mehnert H.H. (1970) Volcanic history of the San Juan Mountains, Colorado, as indicated by potassium-argon dating: *Geol. Soc. Am. Bull.* **81**, 2329–2352.

Lipman, P. W., et al. (1986) Evolution of the Latir volcanic field, Northern New Mexico, and its relation to the Rio Grande Rift, as indicated by potassium-argon and fission track dating. *J. Geophys. Res. B: Solid Earth* **91(B6)**, 6329-6345.

Lipman, P. W. (2007) Incremental assembly and prolonged consolidation of Cordilleran magma chambers: Evidence from the Southern Rocky Mountain volcanic field. *Geosphere* **3(1)**, 42-70.

Lofgren D. L., Lillegraven J. A., Clemens W. A., Gingerich P. D., and Williamson T. E. (2004) Paleocene biochronology; the Puercan through Clarkforkian land mammal ages; pp. 43-105 in M. O. Woodburne (ed.), Late Cretaceous and Cenozoic mammals of North America. Columbia University Press, New York.

Ludwig K.R., (2008) Manual for Isoplot 3.7: *Berkeley Geochronology Center, Special Publication* No. 4. rev. August 26, 2008, 77 pp.

Ludwig K. R. (2012) Direct U-Pb dating of Cretaceous and Paleocene dinosaur bones, San Juan Basin, New Mexico: COMMENT. *Geology* **40(4)**, 258-258.

Mason I. P., Heizler M. T., and Williamson T. E. (2013a) $^{40}Ar/^{39}Ar$ sanidine chronostratigraphy of K-Pg boundary sediments of the San Juan Basin, NM. *NM Geology*.

Mason I. P., Heizler M. T., and Williamson T. E. (2013b) $^{40}Ar/^{39}Ar$ sanidine chronostratigraphy of K-Pg boundary sediments of the San Juan Basin, NM: In *Geol. Soc. Am., Rocky Mt. Section*, Abstract with Programs.

McIntosh W. C., Chapin C. E., Ratté J. C., Sutter J. F. (1992) Time-stratigraphic framework for the Eocene-Oligocene Mogollon-Datil volcanic field, southwest New Mexico. *Geol. Soc. Am. Bull.* **104(7)**: 851-871.

Millard A. R. and Hedges R. E. M. (1996). A diffusion-adsorption model of uranium uptake by archaeological bone. *Geochim. Cosmochim. Acta* **60(12)**, 2139-2152.

Mix H. T., Mulch A., Kent-Corson M. L., Chamberlain C. P. (2011) Cenozoic migration of topography in the North American Cordillera. *Geology* **39(1)**, 87-90.

Oliver J. (1986) Fluids expelled tectonically from orogenic belts: Their role in hydrocarbon migration and other geologic phenomenon. *Geology* **14**, 99-102.

Pan Y. and Fleet M. E. (2002) Compositions of the Apatite-Group Minerals: Substitution Mechanisms and Controlling Factors. *Rev. Mineral. Geochem.* **48(1)**, 13-49.

Pană, D. I. and van der Pluijm B. A. (2014) Orogenic pulses in the Alberta Rocky Mountains: Radiometric dating of major faults and comparison with the regional tectono-stratigraphic record. *Geol. Soc. Am. Bull.* **127**, 480-502.

Paton, C., et al. (2011) Iolite: Freeware for the visualisation and processing of mass spectrometric data. *J. Anal. At. Spectrom.* **26(12)**, 2508-2518.

Peppe D. J., Flynn A., Williamson T. E., Secord R., Heizler M. T., and Brusatte S. L. (2014) Early Paleocene terrestrial ecosystems in the San Juan Basin, New Mexico, USA. In *Geol. Soc. Am. - Abstract with Programs* **46(6)**, 422.

Renne P. R. and Goodwin M. B. (2012) Direct U-Pb dating of Cretaceous and Paleocene dinosaur bones, San Juan Basin, New Mexico: COMMENT. *Geology* **40(4)**, 259-259.

Romer R. L. (2001) Isotopically heterogeneous initial Pb and continuous 222Rn loss in fossils: The U-Pb systematics of Brachiosaurus brancai. *Geochim. Cosmochim. Acta* **65(22)**, 4201-4213.

Sano Y., Terada K., Ly C. V., Park E. J. (2006) Ion microprobe U-Pb dating of a dinosaur tooth. *Geochem. J.* **40(2)**, 171-179.

Sano Y. and Terada K. (1999) Direct ion microprobe U–Pb dating of fossil tooth of a Permian shark. *Earth Planet. Sci. Lett.* **174(1–2)**, 75-80.

Sano Y. and Terada K. (2001) In situ ion microprobe U-Pb dating and REE abundances of a carboniferous conodont. *Geophys. Res. Lett.* **28(5)**, 831-834.

Sikkink P. G. L. (1987) Lithofacies relationships and depositional environment of the Tertiary Ojo Alamo Sandstone and related strata, San Juan Basin, New Mexico and Colorado. *Geol. Soc. Am. Special Papers* **209**, 81-104.

Simonetti A., Buzon M. R., Creaser R. A. (2008). In-situ elemental and Sr isotope investigation of human tooth enamel by laser ablation-(MC)-ICP-MS: successes and pitfalls. *Archaeometry* **50(2)**, 371-385.

Simpson G. G. (1930) Allognathosuchus mooki, a new crocodile from the Puerco Formation. *Am. Mus. Novitates* **445**, 1-16.

Sinclair W. J., and Granger W. (1914) Paleocene deposits of the San Juan Basin, New Mexico. *Bull. Am. Mus. Nat. Hist.* **33**, 297-316.

Suarez C. A., Macpherson G. L., Gonzalez L. A., Grandstaff D. E. (2010) Heterogeneous rare earth element (REE) patterns and concentrations in a fossil bone: Implications for the use of REE in vertebrate taphonomy and fossilisation history. *Geochim. Cosmochim. Acta* **74(10)**, 2970-2988.

Toyoda K. and Tokonami M. (1990) Diffusion of rare-earth elements in fish teeth from deep-sea sediments. *Nature* **345(6276)**, 607-609.

Trueman C. N. (1999) Rare earth element geochemistry and taphonomy of terrestrial vertebrate assemblages. *PALAIOS* **14(6)**, 555-568.

Wallace S.R., and Bookstrom A.A., (1993) The Climax porphyry molybdenum system. *CO Sch. Mines Q.* **93(1)**, 35–41.

Williamson T. E. (1996) The beginning of the age of mammals in the San Juan Basin, New Mexico; biostratigraphy and evolution of Paleocene mammals of the Nacimiento Formation. *NM Mus. Nat. Hist. Sci. Bull.* **8**, 1-141.

Williamson T. E., and Lucas S. G. (1993) Paleocene vertebrate paleontology of the San Juan Basin, New Mexico. *NM Mus. Nat. Hist. Sci. Bull.* **2**, 105–135.

Williamson T. E. and Brusatte S. L. (2014) Small Theropod Teeth from the Late Cretaceous of the San Juan Basin, Northwestern New Mexico and Their Implications for Understanding Latest Cretaceous Dinosaur Evolution. *PLoS ONE* **9(4)**, 93190.

Appendix I: Geochemical similarity between Y and the REE

Introduction

In many geological systems, Y and the REE are thought to behave similarly; this appears to be the case for bioapatite as well. Both Y and the REE (and most other cations) substitute for Ca in the fluoroapatite structure (Fleet and Pan, 1995; Pan and Fleet, 2000), with preference for the Ca2 site. This preference varies from the LREE to the HREE, with the preference for the Ca2 site highest in the LREE and decreasing towards the HREE. Yttrium's site preference falls in the MREE-HREE range, between Dy and Er.

The similarity in geochemical behaviour between Y and the REE in fossil teeth is addressed, but in the interest of preserving space, not fully explored in the body of the thesis. Rare earth element patterns, a cornerstone for geochemical analysis even in bioapatite (e.g. Kowal-Linka et al., 2014), were also not presented. In this appendix, the similarity in behaviour between Y and the REE (Table 5 in Chapter 9) is more fully stated. Also, the REE patterns for teeth at varying stages of alteration are compared, in order to demonstrate that REE patterns are not the most useful indicator of the degree of alteration.

Methods

Trace element data were acquired and normalized using the method described in Chapter 4 of the thesis.

Results and Discussion

As stated in the main body of the thesis, the cross-sectional profile of all the REE is analogous to Y. In order to support this further, the profiles of Y, La, Pr, Eu, and Tm are plotted together for Pattern 1 sample T408-C (Figure 1a), Pattern 2 sample AL-C (Figure 1b), and Pattern 4 sample AL-B (Figure 1c). In

each case, the change in composition of Y across the cross-section is mirrored by the rare earth

elements with a high degree of fidelity. The assertion made in the main body of the thesis that the cross-

sectional profile of Y may be used represent those of the REE is thus well-supported.
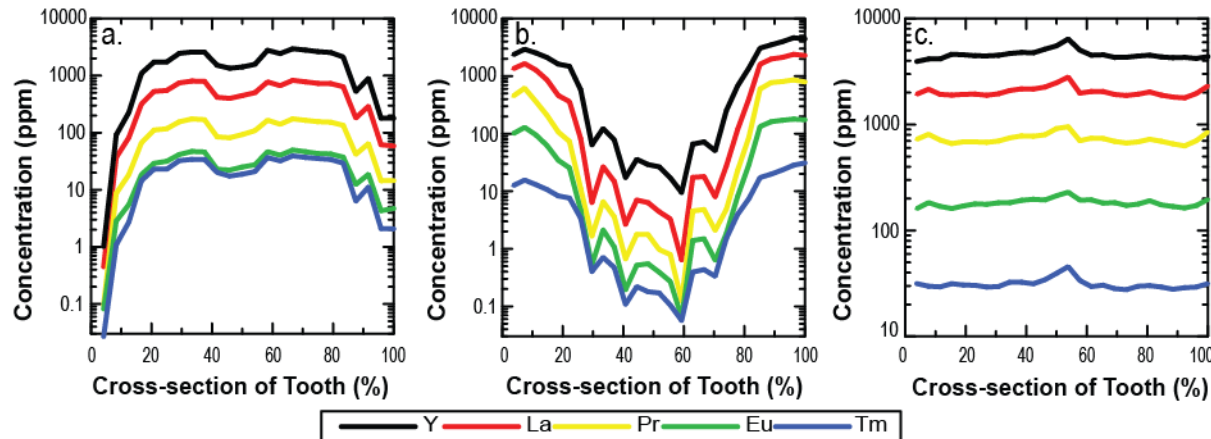

Figure 1: Cross-sectional profile of Y and select rare earth elements across fossil tooth a. T408-C, b. AL-C, c. AL-B.

These REE data were then normalized to Post-Archean Average Shale (PAAS; Taylor and

McLennan, 1985), and several analyses from across the cross-section of Pattern 1 sample T408-C (Figure

2a) and Pattern 2 sample AL-C (Figure 2b) were plotted. While there appears to be some difference in

REE pattern between the most-altered analyses of AL-C (green) and the least-altered analyses (red), the

differences are subtle. For T408-C, REE patterns are largely identical between the fossilisation-age and

the altered spots. It thus appears that for the purpose of this thesis, REE profiles are not the most useful

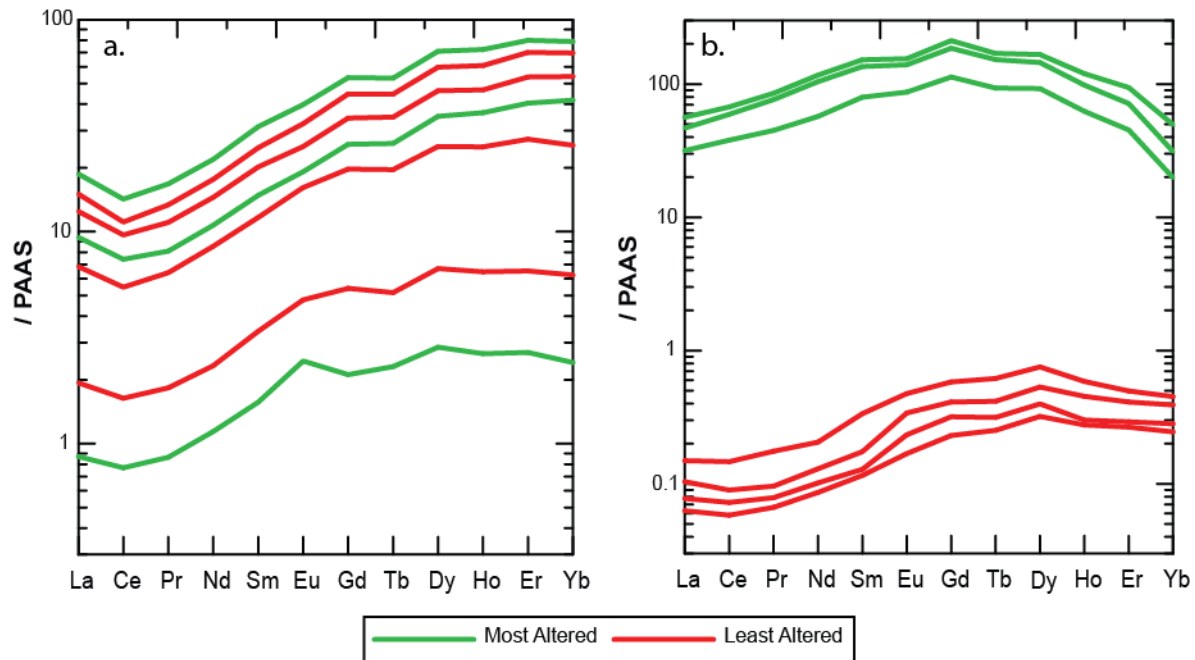metric for distinguishing altered from unaltered regions.

Figure 2: REE profiles for fossil tooth a. T408-C, and b. AL-C. Normalized to Post-Archean Average Shale (Taylor and McLennan, 1985).

References

Fleet M. E., Pan Y. (1995) Site preference of rare earth elements in fluorapatite. *Am. Mineral.* **329**, 3-4.

Kowal-Linka M., Jochum K. P., Surmik D. (2014) LA-ICP-MS analysis of rare earth elements in marine reptile bones from the Middle Triassic bonebed (Upper Silesia, S Poland): Impact of long-lasting diagenesis, and factors controlling the uptake. *Chem. Geol.* **363**, 213-228.

Pan Y. and Fleet M. E. (2002) Compositions of the Apatite-Group Minerals: Substitution Mechanisms and Controlling Factors. *Rev. Mineral. Geochem.* **48(1)**, 13-49.

Taylor S.R. and McLennan S.M. (1985) The Continental Crust; Its composition and evolution; an examination of the geochemical record preserved in sedimentary rocks. Blackwell, Oxford. 312.

Appendix II: Sr isotopes as paleodiet indicators

Introduction

In addition to endeavoring to date fossil teeth, some effort was made to evaluate the possibility of using Sr as a paleodiet indicator. Although there is little doubt among paleontologists that alligorids, crocodilians, and tyrannosaurs were carnivores, developing a robust geochemical method to determine paleodiet may help address questions of diet for animals whose diets are uncertain. In addition, variations in diet indicators may be related to migration habits, which are currently ill-constrained for extant animals.

The element Sr was chosen as the focus of this investigation because it is chemically similar to calcium, and Sr has been shown to enter into living bone in concentrations proportional to its concentration in dietary sources (e.g. Beard and Johnson, 1999). However, Sr has also been found to have a rapid diffusivity in bioapatite compared to other trace elements (> 1 x 10^{-12} cm^2/s for uptake in unfossilised bone; Kohn and Moses, 2013), which has the potential to destroy any *in vivo* Sr isotopic signature. In order to begin to evaluate this hypothesis, the cross-sections of three fresh teeth from American Alligators from the Toronto Zoo and three fossil teeth from the ~65.7 Ma Arroyo Chijuillita Member of the Nacimiento Formation, New Mexico, were analyzed.

Methods

Trace element data were acquired and normalized using the method described in Chapter 4 of the body of the text. Strontium isotope analyses were acquired in proximity to the trace element spots using a New Wave UP 213 nm laser Nu Plasma laser ablation ICP-MS; a spot size of 140 μm, a repetition rate of 10 Hz, and a fluence of approximately 4.68 J/cm^2 was used. Durango apatite was analyzed several times at the beginning and the end of each session, and after every ~10 sample analyses over

the course of the session. Blank corrections were run periodically. The resulting Sr isotopic data was normalized using an accepted value for Durango apatite of $^{87}Sr/^{86}Sr$ = 0.70634 (2 standard deviations = 0.00014; Yang et al., 2014). Normalized Sr isotopic data is reported in Table 1.

Unfossilised Teeth

Measurable differences in Sr/Ca ratios have been reported between the unfossilised bones of herbivores and carnivores (Burton et al., 1999); however biopurification, an organism's tendency to replace trace elements such as Sr in bioapatite with Ca, results in animal bones having somewhat lower Sr/Ca ratios than the plants and/or animals they eat. Complications arise from the fact that different plants have different Ca concentrations, which will affect the Sr/Ca ratio without a change in the plant/meat dietary ratio. The diversity in plant compositions is an issue for explaining the Sr/Ca composition of herbivore bone, and is a problem further compounded when dealing with carnivore bone (Burton et al., 1999). Thus, while the Sr/Ca ratio of living bone has been shown to reflect dietary Sr/Ca ratios, different diets can produce similar Sr/Ca ratios (Burton et al., 1999). It has also been suggested that diet is not the main control on trace element intake: soil and dust are thought to have the most significant effect on trace element intake (Kohn et al., 2013). If this is the case, the ability to make paleodiet interpretations may be compromised by the ingestion of soil and dust of unknown composition at an unknown rate (Kohn et al., 2013). However, this may favor the use of Sr as an indicator of migration.

The Sr isotopic composition may be used to further examine this point: if the Sr isotopic composition of teeth from the Toronto Zoo is indeed reflective of the composition of the ambient soil and dust, this composition should be similar to the isotopic composition measured in the Great Lakes drainage basin, particularly Lake Ontario. The $^{87}Sr/^{86}Sr$ ratios of the modern alligator teeth (Figure 1) have an average composition of 0.71244 +/- 0.00012 (Figure 2); this is less radiogenic than the 0.716

average reported for Lake Superior and Lake Huron, but more radiogenic than is reported for Lake Erie

and Lake Ontario ($^{87}Sr/^{86}Sr$ = ~ 0.710; Faure et al., 1967). This suggests that either the Sr composition of

Lake Ontario is not representative of soil and dust in the alligator pen of the Toronto Zoo, a food source

with a more radiogenic composition is impacting the Sr isotope composition, or this Sr composition is

reflective of the ambient composition of the alligators' previous habitat.
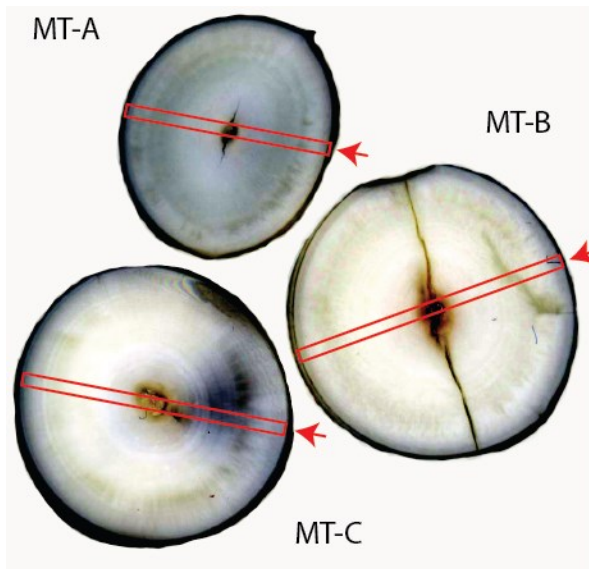
Figure 1: Enhanced photos of unfossilised American Alligator teeth, with analyzed transects in red.
Arrows indicate starting position.
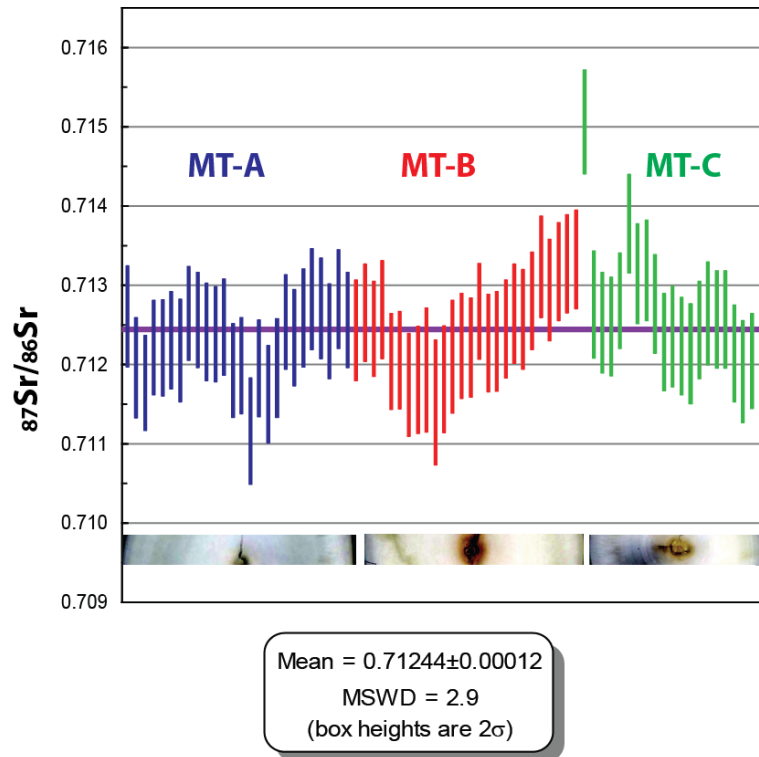
Figure 2: Weighted average of all analyses acquired along the pictured cross-sections of three unfossilised American Alligator teeth from the Toronto Zoo.

While it has been asserted that the $^{88}Sr/^{86}Sr$ ratios can be tied to trophic level (Knudson et al., 2010), the $^{87}Sr/^{86}Sr$ composition is often regarded as being most heavily influenced by the composition of the bedrock (Beard and Johnson, 1999; Knudson et al., 2010). The results of our investigation into this question thus far appear consistent with this conclusion, but additional study on the teeth of animals with a well-constrained diet that is available for analysis may yet yield a method to use $^{87}Sr/^{86}Sr$ ratios to determine diet.

Fossilised Teeth

Further complications to determining paleodiet or migration habits using $^{87}Sr/^{86}Sr$ ratios arise during diagenesis and fossilisation (e.g. Burton et al., 1999; Kohn and Moses, 2013). As discussed to some length in Chapter 6.4, the fossilisation process drastically alters the trace element composition and isotopic signature of bioapatite. It was found that the majority of fossil teeth will not preserve

fossilisation-age U-Pb isotopic signatures. This alteration was found to either occur from the edges of the tooth inward, presumably through diffusion, or along and in proximity to important cracks. Diffusion into a fossil is tracked using trace element cross-sectional profiles, where a steeper slope corresponds to a slower diffusion rate (e.g. Millard and Hedges, 1996; Trueman et al., 2011; Kohn and Moses, 2013).
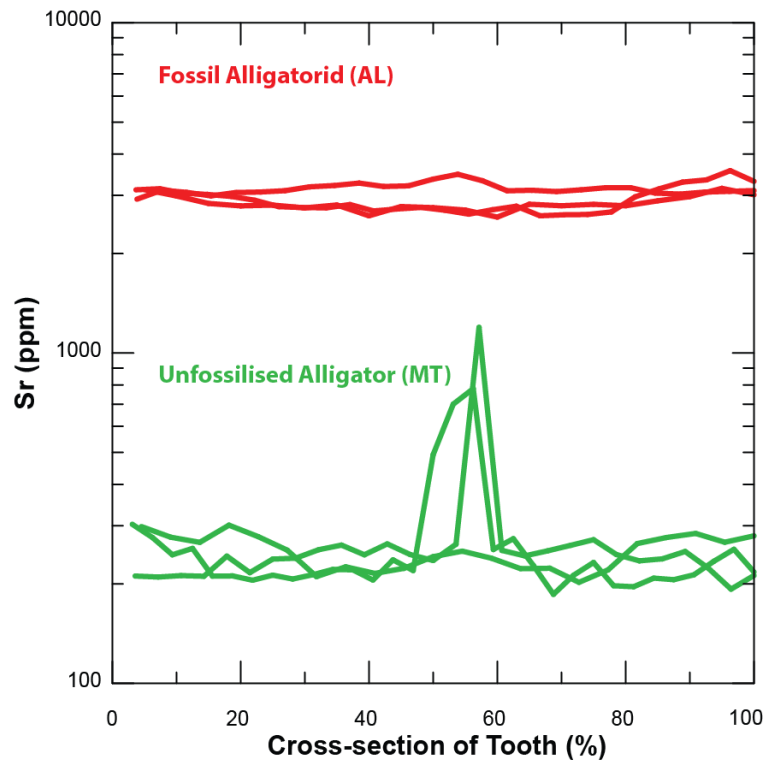
Figure 3: Elemental Sr concentration across the cross-section of the fossilised and unfossilised teeth.

The concentration of Sr in the fossil teeth analyzed is an order of magnitude greater than in the fresh alligator teeth provided by the Toronto Zoo (Figure 3). There are two possibilities: 1) an *in vivo* Sr composition is preserved in the fossilised teeth, and the variation in tooth Sr concentration reflects geographic and/or temporal changes in the abundance of Sr in the soil composition; 2) the Sr composition is overprinted during and possibly after fossilisation.

Experiments on fresh bone report that diffusion of Sr into bone is faster than Y, the REE, U, and Pb (Kohn and Moses, 2013). The tendency for disturbed U-Pb dates to be preserved (e.g. Romer, 2001)

indicates that U and Pb modification is occurring post-fossilisation, and by extension Sr modification

should have occurred as well. This is consistent with the generally flat Sr profiles measured in fossil

teeth; Sr profiles are consistently flatter than U or Pb profiles, suggesting that Sr enrichment occurs

more quickly. If this is the case, even tooth regions preserving a fossilisation-age U-Pb signature cannot

be assumed to have a fossilisation-age Sr composition. It therefore certainly cannot be assumed that the

tooth will preserve an *in vivo* Sr composition.
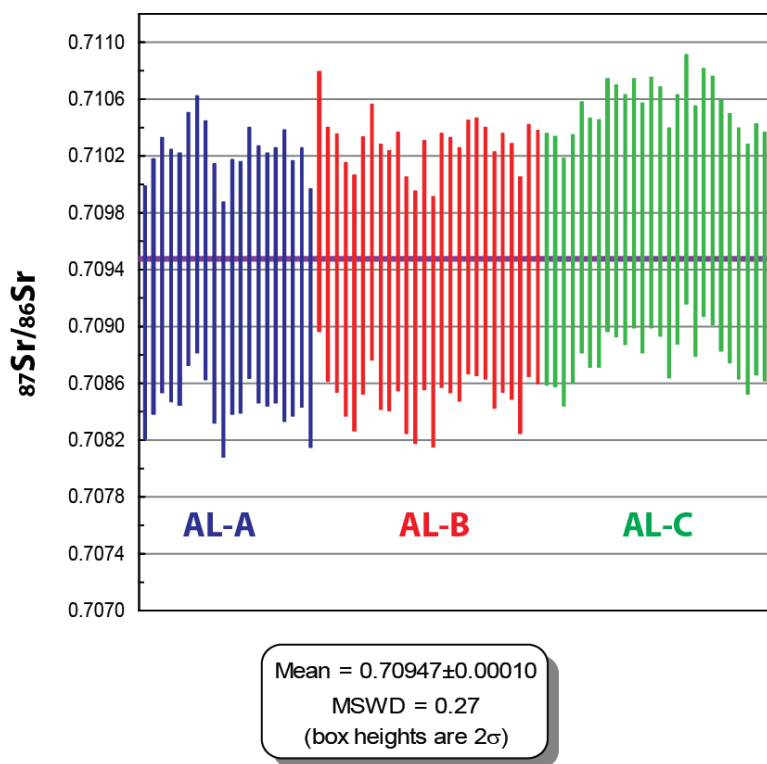
Figure 4: Weighted average of three fossilised alligatorid teeth from the ~65 Ma Nacimiento Formation, New Mexico.

The average Sr isotopic composition of the fossil teeth from the Nacimiento Formation is

$^{87}Sr/^{86}Sr$ = 0.70947 +/- 0.00010 (Figure 3). Unlike analyses from the unfossilised teeth, all analyses are

within uncertainty of this average, and little internal variation can be resolved. As the alligorids from the

Nacimiento Formation lived proximal to the Western Interior Seaway, the Sr isotopic composition of

their teeth before fossilisation would have been related to both the composition of the seawater, and

the composition of the bedrock of that time. Seawater $^{87}Sr/^{86}Sr$ during the late Cretaceous is estimated at 0.7075 (Veizer et al., 1999), less radiogenic than the signature preserved in the fossil teeth. This suggests at least the influence of a more radiogenic source(s); the bedrock beneath and around the San Juan Basin in New Mexico has units as young as the Cretaceous and as old as the Precambrian. While it may be that the Sr composition recorded in the teeth comes from a mixture of the Cretaceous bedrock and seawater, some more radiogenic source is needed to explain the measured compositions. The volcanics that, as discussed in the thesis in Chapter 6.4.4, likely caused significant overprinting in these teeth may be viable candidates; Sr isotopic compositions of 0.703-0.71447 have been measured in the ~25.1 Ma Amalia Tuff (Johnson et al., 1990).

In order to evaluate the meaning of the Sr isotopic composition of the unfossilised and fossilised teeth, more detailed investigation of their water source, ambient dust and bedrock, and food is necessary.

Table 1

Strontium isotopic composition measured by laser ablation ICP-MS along the cross-section of unfossilised American Alligator teeth and fossil teeth from the Arroyo Chijuillita Member, normalized to Durango apatite.

Sample ID	$^{87}Sr/^{86}Sr$	2 SE	Sample ID	$^{87}Sr/^{86}Sr$	2 SE	Sample ID	$^{87}Sr/^{86}Sr$	2 SE
MT-A-1	0.712595	0.000639	MT-B-1	0.712416	0.000636	MT-C-1	0.715054	0.000657
MT-A-2	0.711942	0.000638	MT-B-2	0.712636	0.000617	MT-C-2	0.712745	0.000675
MT-A-3	0.711752	0.000603	MT-B-3	0.712433	0.000603	MT-C-3	0.712515	0.000635
MT-A-4	0.712198	0.000598	MT-B-4	0.712675	0.000619	MT-C-4	0.712464	0.000625
MT-A-5	0.712197	0.000609	MT-B-5	0.712019	0.000607	MT-C-5	0.71279	0.000606
MT-A-6	0.712289	0.000614	MT-B-6	0.712038	0.000619	MT-C-6	0.713764	0.000621
MT-A-7	0.712161	0.000648	MT-B-7	0.711724	0.000649	MT-C-7	0.713135	0.00063
MT-A-8	0.71263	0.000595	MT-B-8	0.711787	0.000678	MT-C-8	0.713171	0.000636
MT-A-9	0.712546	0.000601	MT-B-9	0.711912	0.000783	MT-C-9	0.712749	0.000622
MT-A-10	0.712397	0.000616	MT-B-10	0.711501	0.00079	MT-C-10	0.712267	0.000616
MT-A-11	0.712368	0.0006	MT-B-11	0.711796	0.00068	MT-C-11	0.71234	0.000639
MT-A-12	0.712456	0.000606	MT-B-12	0.712082	0.000712	MT-C-12	0.712218	0.000616
MT-A-13	0.71191	0.000594	MT-B-13	0.712221	0.000666	MT-C-13	0.712116	0.000631
MT-A-14	0.711972	0.000609	MT-B-14	0.712195	0.000626	MT-C-14	0.712419	0.000617
MT-A-15	0.711141	0.000671	MT-B-15	0.712656	0.000607	MT-C-15	0.712627	0.000652
MT-A-16	0.711933	0.000612	MT-B-16	0.712254	0.000615	MT-C-16	0.712554	0.000614
MT-A-17	0.711607	0.000616	MT-B-17	0.712274	0.000629	MT-C-17	0.712555	0.000616
MT-A-18	0.711939	0.000624	MT-B-18	0.712433	0.00062	MT-C-18	0.712121	0.000612
MT-A-19	0.712523	0.000598	MT-B-19	0.712626	0.000626	MT-C-19	0.711894	0.000646
MT-A-20	0.712322	0.000611	MT-B-20	0.712554	0.000634	MT-C-20	0.712029	0.000599
MT-A-21	0.712574	0.000618	MT-B-21	0.71279	0.000616	MT-C-21	0.712626	0.000646
MT-A-22	0.712809	0.000637	MT-B-22	0.713221	0.000641			
MT-A-23	0.712694	0.000634	MT-B-23	0.712927	0.00064			
MT-A-24	0.712401	0.0006	MT-B-24	0.713159	0.000621			
MT-A-25	0.71281	0.000621	MT-B-25	0.713257	0.000621			
MT-A-26	0.712548	0.000602	MT-B-26	0.713311	0.000622			

Table 1 (*continued*)

Sample ID	$^{87}Sr/^{86}Sr$	2 SE	Sample ID	$^{87}Sr/^{86}Sr$	2 SE	Sample ID	$^{87}Sr/^{86}Sr$	2 SE
AL-A-1	0.709089	0.000895	AL-B-1	0.709874	0.000915	AL-C-1	0.709467	0.000888
AL-A-2	0.709272	0.0009	AL-B-2	0.709499	0.000895	AL-C-2	0.709449	0.000883
AL-A-3	0.709424	0.000901	AL-B-3	0.709439	0.000911	AL-C-3	0.709305	0.000872
AL-A-4	0.709351	0.00089	AL-B-4	0.709252	0.000894	AL-C-4	0.709469	0.000874
AL-A-5	0.709325	0.000891	AL-B-5	0.709158	0.000902	AL-C-5	0.709691	0.000884
AL-A-6	0.70961	0.000891	AL-B-6	0.709423	0.000906	AL-C-6	0.709583	0.000878
AL-A-7	0.709711	0.000907	AL-B-7	0.709658	0.000901	AL-C-7	0.709578	0.000872
AL-A-8	0.709531	0.000912	AL-B-8	0.709342	0.000935	AL-C-8	0.709849	0.00089
AL-A-9	0.709223	0.000913	AL-B-9	0.709314	0.000917	AL-C-9	0.709807	0.000888
AL-A-10	0.708969	0.000899	AL-B-10	0.709449	0.000913	AL-C-10	0.709745	0.000881
AL-A-11	0.70927	0.000897	AL-B-11	0.709143	0.000904	AL-C-11	0.709862	0.000879
AL-A-12	0.709268	0.000887	AL-B-12	0.709054	0.000889	AL-C-12	0.709687	0.00088
AL-A-13	0.70951	0.000886	AL-B-13	0.709422	0.00088	AL-C-13	0.709866	0.000883
AL-A-14	0.709358	0.000906	AL-B-14	0.709026	0.000883	AL-C-14	0.709802	0.000877
AL-A-15	0.709323	0.000891	AL-B-15	0.709458	0.000895	AL-C-15	0.709509	0.000881
AL-A-16	0.709352	0.000902	AL-B-16	0.709423	0.0009	AL-C-16	0.709747	0.000879
AL-A-17	0.709351	0.001029	AL-B-17	0.709359	0.000892	AL-C-17	0.710031	0.000879
AL-A-18	0.709261	0.0009	AL-B-18	0.709551	0.000893	AL-C-18	0.709663	0.000882
AL-A-19	0.709336	0.000914	AL-B-19	0.709555	0.000909	AL-C-19	0.709938	0.000874
AL-A-20	0.70905	0.000912	AL-B-20	0.709509	0.000887	AL-C-20	0.70988	0.000877
			AL-B-21	0.709321	0.000904	AL-C-21	0.709703	0.000884
			AL-B-22	0.70944	0.000911	AL-C-22	0.709612	0.00088
			AL-B-23	0.709379	0.000904	AL-C-23	0.709508	0.000885
			AL-B-24	0.709142	0.000904	AL-C-24	0.709397	0.000881
			AL-B-25	0.709527	0.000888	AL-C-25	0.709534	0.000886
			AL-B-26	0.709481	0.000895	AL-C-26	0.709484	0.000876

References

Beard B. L., Johnson C. M. (2000) Strontium isotope composition of skeletal material can determine the birth place and geographic mobility of humans and animals. *J. Forensic Sci.*, **45(5)**, 1049-1061.

Burton J. H., Price T., Middleton W. D. (1999) Correlation of Bone Ba/Ca and Sr/Ca due to Biological Purification of Calcium. *J. Archaeolog. Sci.* **609**, 26(6).

Faure G., Jones L. M., Eastin R., and Christner M. (1967) Strontium isotope composition and trace element concentrations in Lake Huron and its principal tributaries. Prof. Pap. W-107.

Johnson C.M., Lipman P.W., and Czamanske G.K. (1990) H, O, Sr, Nd, and Pb isotope geochemistry of the Latir volcanic field and cogenetic intrusions, New Mexico, and relations between evolution of a continental magmatic center and modifications of the lithosphere. *Contrib. Mineral. Petrol.* **104(1)**, 99-124.

Knudson KJ, Williams HM, Buikstra JE, Tomczak PD, Gordon GW, Anbar AD (2010) Introducing d88/86Sr analysis in archaeology: a demonstration of the utility of strontium isotope fractionation in paleodietary studies. *J. Archaeolog. Sci.* **37(9)**, 2352-2364.

Kohn M. J., Morris J., Olin P. (2013) Trace element concentrations in teeth – a modern Idaho baseline with implications for archeometry, forensics, and palaeontology. *J. Archaeolog. Sci.* **40(4)**, 1689-1699.

Kohn M. J. and Moses R. J. (2013) Trace element diffusivities in bone rule out simple diffusive uptake during fossilisation but explain in vivo uptake and release. *Proc. Natl. Acad. Sci. USA* **110(2)**, 419-424.

Romer R. L. (2001) Isotopically heterogeneous initial Pb and continuous 222Rn loss in fossils: The U-Pb systematics of Brachiosaurus brancai. *Geochim. Cosmochim. Acta* **65(22)**, 4201-4213.

Trueman CN, Kocsis L, Palmer MR, Dewdney C (2011) Fractionation of rare earth elements within bone mineral: A natural cation exchange system. *Palaeogeogr. Palaeoclimatol. Palaeoecol.* **310**, no. Special Issue: Fossil bones and teeth: preservation or alteration of biogenic compositions?, 124-132.

Millard A. R. and Hedges R. E. M. (1996). A diffusion-adsorption model of uranium uptake by archaeological bone. *Geochim. Cosmochim. Acta* **60(12)**, 2139-2152.

Veizer J., Ala D., Azmy K, Bruckschen P, Buhl D, Bruhn F, Carden G.A.F., Diener A, Ebneth S, Godderis Y, Torsten Jasper, Korte C, Pawellek F, Podlaha O.G., Strauss H. (1999) 87Sr/86Sr, δ13C and δ18O evolution of Phanerozoic seawater. *Chem. Geol.* **161(1–3)**, 59-88.

Yang Y., Wu F., Yang J., Chew D. M., Xie L., Chu Z., & ... Huang C. (2014) Sr and Nd isotopic compositions of apatite reference materials used in U–Th–Pb geochronology. *Chem. Geol.* **385**, 35-55.

Appendix III: Possible *in vivo* signatures

Introduction

It is apparent from this study, and much previous work (e.g. Trueman et al., 1999; Koenig et al., 2009; Herwartz et al., 2011; Kowal-Linka et al., 2014), that the trace element composition of fossil teeth is disturbed both during fossilisation and post-fossilisation. Some studies have concluded that fossils record an early diagenetic signature (e.g. Trueman et al, 1999), and others that that the post-fossilisation signal dominates (e.g. Kowal-Linka et al, 2014). Some have suggested that there may be geochemical indicators, such as Sr or Ba concentrations, that may be used as proxies for rapid recrystallization, and thus the possibility of recording *in vivo* signatures (Koenig et al, 2009), while others find this unlikely (Hinz and Kohn, 2010). It has also been suggested that certain parts of the fossil are more resistant to further over-printing than others, such as the bone-dentine and enamel-dentine boundary (Kohn, 2008). Although it was not a focus of this thesis, the identification of *in vivo* geochemical signatures was considered.

Methods

Trace element data were acquired and normalized using the method described in the Chapter 4 of the body of the text. Data is reported in Chapter 9, Table 5.

Results

Most fossil teeth from the Nacimiento Formation were found to have significantly elevated concentrations of most trace elements compared to unfossilised teeth (Figure 1). Strontium is present in fossil teeth at about 10x the concentration measured in unfossilised teeth. Lead is between 3 and 1000x more abundant in fossil teeth than unfossilised teeth; Uranium is more elevated by 300 to 30 000x. The elements Ti, Rb and Zn were found to be present at similar concentrations in both fossilised and

unfossilised teeth (Figure 2). Rare earth elements are largely below detection limits in unfossilised teeth, although some significant analyses were acquired using the high resolution laser ablation ICP-MS at the Arctic Resources Lab at the University of Alberta. Concentrations of Y and all rare earth elements are extremely low (on the ppb scale), several order of magnitude lower than in fossilised teeth.
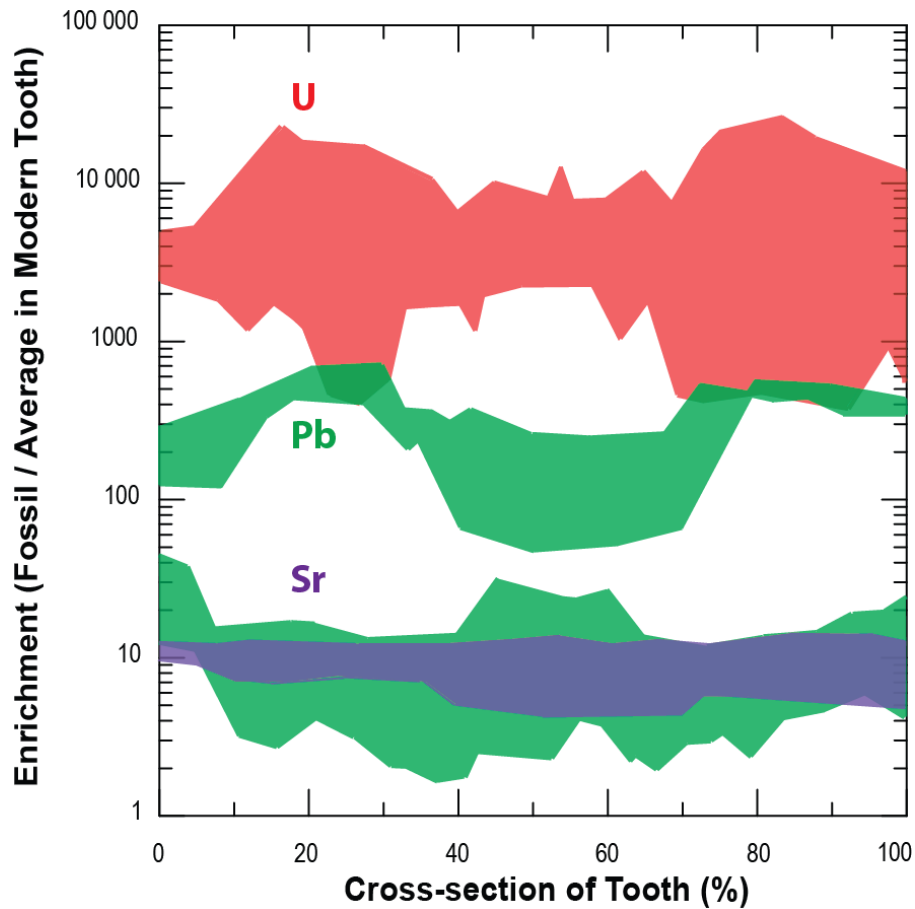
Figure 1: Enrichment of select trace elements in fossil teeth from the Nacimiento Formation above concentrations found in unfossilised alligator teeth from the Toronto Zoo.

Discussion

Although the possibility that some elements, such as Sr, might record an *in vivo* signature that is significantly more elevated than modern samples because of the environment in which they lived, this is considered unlikely (see Appendix II). Unfossilised teeth from geographically disparate areas record very similar Sr concentrations (Kohn et al., 2013; this study), suggesting that the major control on Sr

partitioning into a living tooth is biological. Biopurification would effectively act to limit the amount of Sr

and other trace elements that would remain in a living tooth (Burton et al., 1999).
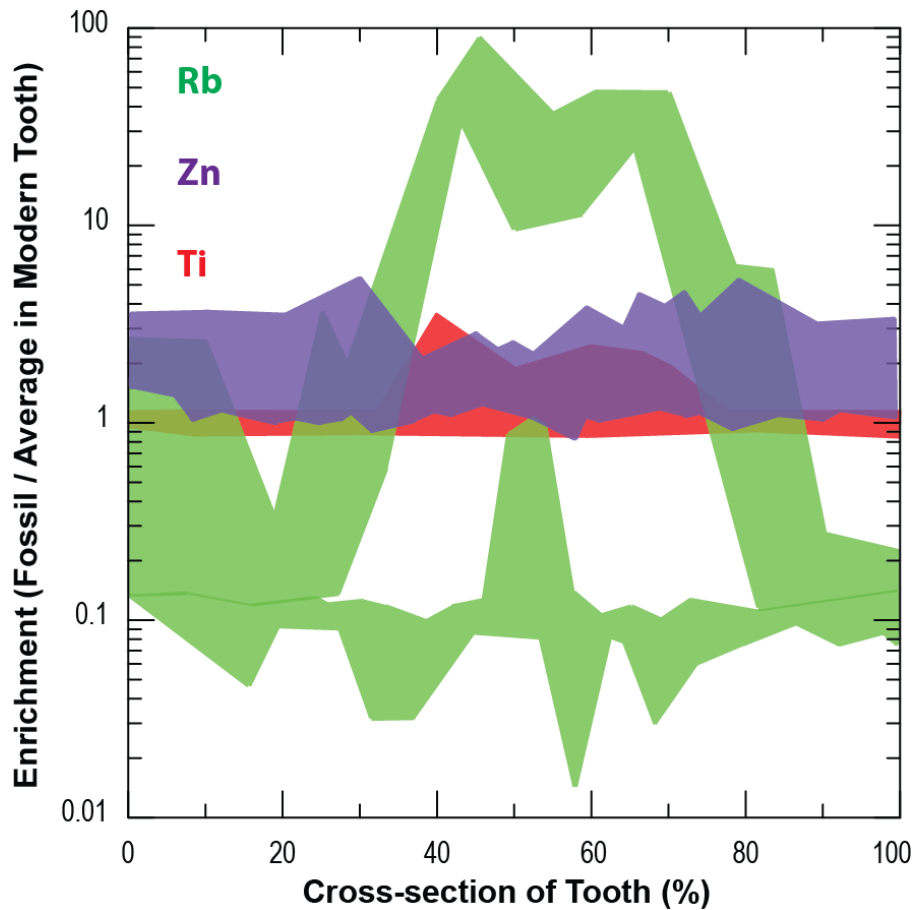
Figure 2: Enrichment of Ti, Zn, and Rb in fossil teeth from the Arroyo Chijuillita Member above concentrations found in unfossilised alligator teeth from the Toronto Zoo.

The most likely candidates for preserving an *in vivo* signature are thus the elements that have

similar concentrations in fossilised and unfossilised teeth: Ti, Rb, and Zn (Figure 2). The similarity in

concentration measured in [48]Ti was found to be due to interference from Ar and Ca. Rubidium is highly

incompatible in apatite, and is thus below detection limits for most teeth samples, fossilised or

unfossilised. However, for Zn, there is no apparent candidates for molecular interference, and

concentrations are relatively elevated at about 30 – 35 ppm for the less altered teeth from the Arroyo

Chijuillita Member (Figure 2). Concentrations of Zn in the Pattern 1 and 3 Dinosaur Park Formation teeth

are similar to concentrations in the Arroyo Chijuillita Member teeth and the unfossilised teeth.

However, most Dinosaur Park Formation teeth have experienced depletion in trace elements (see

Chapter 6.4.1); as with Sr, this has resulted in Zn concentrations below *in vivo* levels (Figure 3).
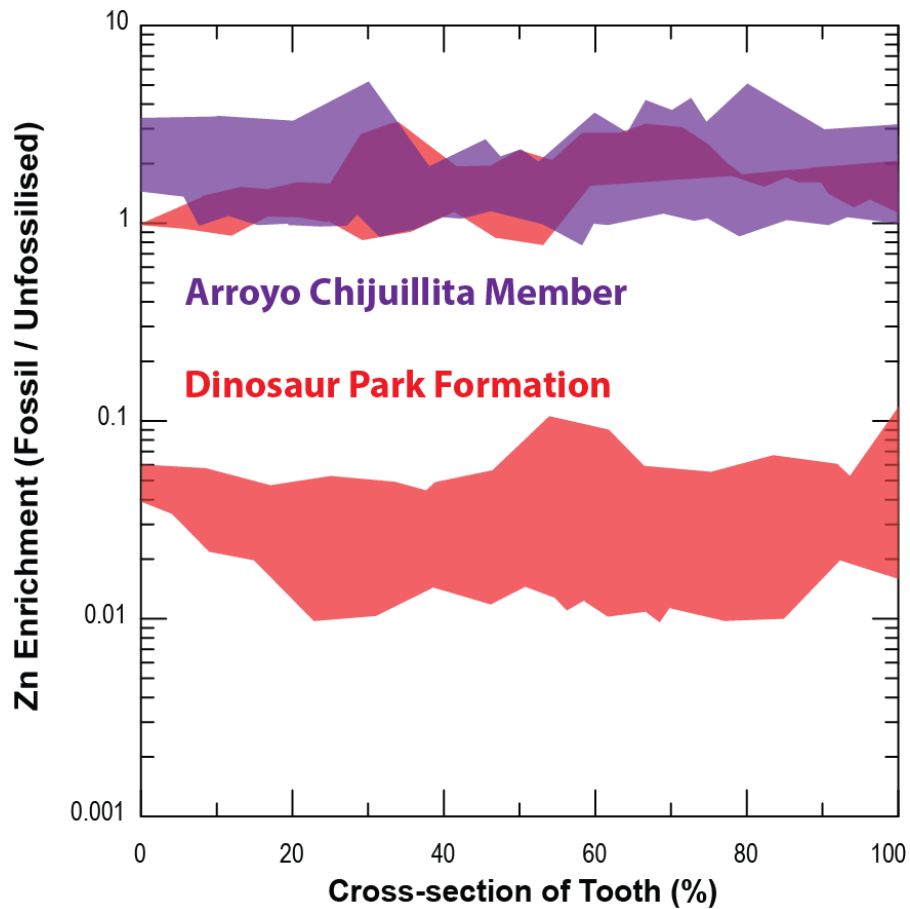
Figure 3: Zn enrichment in fossil teeth from the Arroyo Chijuillita Member of the Nacimiento Formation and the Dinosaur Park Formation, over the average Zn concentration measured in the unfossilised teeth from the Toronto Zoo.

Experiments on trace element uptake in living bone (Kohn and Moses, 2013) suggest that Zn

should be incorporated into bone via recrystallization during diagenesis at rates similar to Pb, or rates

intermediate between Pb and Sr (Kohn and Moses, 2013). Diffusion to the recrystallization front and

incorporation into the bioapatite structure could be affected by concentration in the host sediments,

diagenetic fluids, or post-diagenetic fluids, or compatibility in the crystallographic structure. The lack of

Zn enrichment during and after fossilisation could be the result of a severe Zn depletion in the host sediments, the diagenetic fluid, and any post-diagenetic fluid that would have interacted with the tooth. However, it is unlikely that Zn would be so entirely absent from the host sediment or diagenetic fluids, while the more exotic rare earth elements, U, Pb, Y, etc. are present in significant enough quantities through time to generate significant enrichment.

A crystallographic limit on Zn uptake may be a possibility, because unlike Sr, which can substitute entirely for Ca in both Ca sites, Zn has a maximum solubility in the apatite structure of $Ca_9Zn_1(PO_4)_6F_2$ (Pan and Fleet, 2002). This maximum solubility is thus at 6.25 cation units, or 62 500 ppm, significantly greater than the concentration measured in the fossilised and unfossilised samples (25 – 40 ppm). However, the maximum solubility of Zn in hydroxlapatite and fluoroapatite under realistic diagenetic conditions has not been addressed, thus it is possible that a significantly lower crystallographic limit for Zn in bioapatite exists under the relevant conditions. Bioapatite might be expected to take in less Zn than Sr, based on the lower maximum site occupancy of Zn (6.25 cation units) compared to Sr (62.5 cation units).

The similarity in concentration between Zn in many fossil teeth and Zn in unfossilised teeth suggests that fossilisation and post-fossilisation overprinting of the *in vivo* signature has not occurred. However, at present, there is no apparent explanation for why uptake of Zn should not occur during diagenesis and in a more pronounced way during alteration.

References

Burton J. H., Price T., Middleton W. D. (1999) Correlation of Bone Ba/Ca and Sr/Ca due to Biological Purification of Calcium. *J. Archaeolog. Sci.* **609**, 26(6).

Herwartz D., Tutken T., Munker C., Jochum K. P., Stoll B. and Sander P.M. (2011) Timescales and mechanisms of REE and Hf uptake in fossil bones. *Geochim. Cosmochim. Acta* **75(1)**, 82-105.

Hinz E. A., Kohn M. J. (2010). The effect of tissue structure and soil chemistry on trace element uptake in fossils. *Geochim. Cosmochim. Acta* **74**, 3213-3231.

Koenig A. E., Rogers R. R., Trueman C. N. (2009) Visualizing fossilisation using laser ablation–inductively coupled plasma–mass spectrometry maps of trace elements in Late Cretaceous bones. *Geology* **37(6)**, 511-514.

Kowal-Linka M., Jochum K. P., Surmik D. (2014) LA-ICP-MS analysis of rare earth elements in marine reptile bones from the Middle Triassic bonebed (Upper Silesia, S Poland): Impact of long-lasting diagenesis, and factors controlling the uptake. *Chem. Geol.* **363**, 213-228.

Kohn M. J. and Moses R. J. (2013) Trace element diffusivities in bone rule out simple diffusive uptake during fossilisation but explain in vivo uptake and release. *Proc. Natl. Acad. Sci. USA* **110(2)**, 419-424.

Kohn M. J., Morris J., Olin P. (2013) Trace element concentrations in teeth – a modern Idaho baseline with implications for archeometry, forensics, and palaeontology. *J. Archaeolog. Sci.* **40(4)**, 1689-1699.

Kohn M. J. (2008) Models of diffusion-limited uptake of trace elements in fossils and rates of fossilisation. *Geochim. Cosmochim. Acta* **72(15)**, 3758-3770.

Pan Y. and Fleet M. E. (2002) Compositions of the Apatite-Group Minerals: Substitution Mechanisms and Controlling Factors. *Rev. Mineral. Geochem.* **48(1)**, 13-49.

Trueman C. N. (1999) Rare earth element geochemistry and taphonomy of terrestrial vertebrate assemblages. *PALAIOS* **14(6)**, 555-568.

Appendix IV: Additional teeth

Introduction

Fourteen of the seventeen fossil teeth analyzed for this thesis are included in the body of the work, and another (AL-D) is used in the body of the thesis to verify the LA ICP-MS results by comparing them to corresponding IDTIMS results. The two teeth that were not included in the final paper are a Tyrannosaurus Rex tooth from the Naashoibito Member (TR1), and a ceratopsid tooth from the De-na-zin Member, Kirtland Formation (CE1), both from the San Juan Basin of New Mexico (Figure 1). Over the course of the project, the focus shifted from looking for fossilisation-age signatures in individual teeth to describing fossilisation and alteration using several teeth from the same unit. In this new context, these two teeth that are from neither the Dinosaur Park Formation, Alberta, nor the Arroyo Chijuillita Member of the Nacimiento Formation, New Mexico no longer fit the scope of the project.
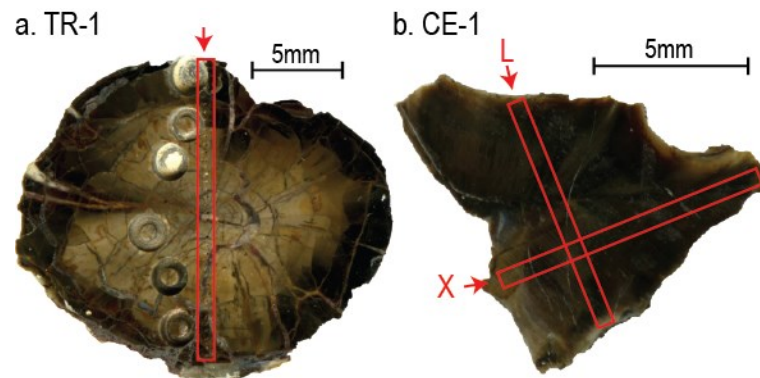
Figure 1: Photos of a. TR-1 from the Naashoibito Member, New Mexico, and b. CE-1 from the De-na-zin Member of the Kirtland Formation, New Mexico. Red bars outline the analyzed sections, with arrows indicating the start. 'X' represent the cross-section, and 'L' represents the longitudinal section in CE-1.

The age of the Naashoibito Member is disputed, with maximum age estimates ranging between ~73 Ma and ~65.5 Ma, but mammalian biostratigraphic correlation and detrital sanidine dates at the base of the Naashoibito Member led Williamson and Brusatte (2014) to suggest an age for the unit between 66.3 Ma and latest Cretaceous. This is consistent with the retrieval of a Tyrannosaur Rex tooth

from this unit. Unlike the Naashoibito Member, ash beds allow for constraints on the age of the De-na-zin Member of the Kirtland Formation: single crystal ^{40}Ar/^{39}Ar dating of sanidine produces a date of 73.04±0.25 Ma, representing the age of the top of the De-na-zin Member (Fassett, 2009), with the maximum age of the bottom of the unit thought to be 74.3 Ma (Williamson and Brusatte, 2014).

Methods

Trace element and U-Pb isotopic data were acquired and normalized using the method described in the Chapter 4 of the body of the text.

Results

Trace element data for TR1 and CE1 are reported in Table 1. Concentrations of Sr, U and Pb for TR1 and CE1 are within the range measured in teeth from the Arroyo Chijuillita Member, with similar cross-sectional profiles (Table 1). Yttrium concentrations vary between 10 – 1000 ppm for TR1 (Figure 2) and 1 – 1000 ppm for CE1 (Figure 3). Anomalous analyses plot significantly below (Figure 2) and above (Figure 3) adjacent analyses, suggesting that veins in the teeth of a different material were accidentally sampled in some places. This is supported by the presence of visible veins in TR1 (Figure 1a).

Yttrium profiles are used in the body of this thesis to evaluate the potential that a fossil will preserve a fossilisation-age U-Pb signature. The presence of Y high gradients (a change in Y concentration over several orders of magnitude) along the cross-sections of TR1 and CE1 places these teeth in the Pattern 2 category (Figure 2, 3). On this basis, these teeth would be expected to preserve the age of fossilisation in some portion of the tooth, although the scatter in the Y profile may suggest localized alteration.
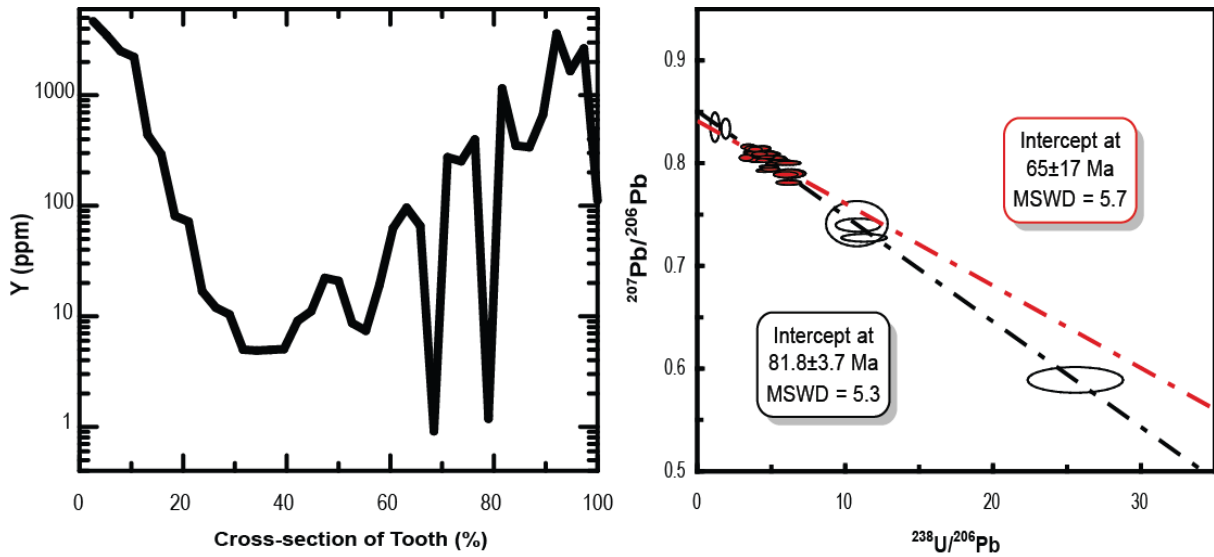
Figure 2: Cross-sectional Y profile for sample TR1 from the Naashoibito member, San Juan Basin, New Mexico, and associated Tera-Wasserburg plot of U-Pb analyses.

U-Pb isotopic data for the Durango standard analysed during each session are reported in Table 2, and unnormalized U-Pb data for each tooth are reported in Table 3. The majority of normalized U-Pb analyses acquired on sample TR1 plot in a small $^{238}U/^{206}Pb$ range of about 3 to 6, and a small $^{207}Pb/^{206}Pb$ range of about 0.78 to 0.81. These analyses produce a date of 65±17 Ma (n=41, MSWD = 5.7; Figure 2), which is consistent with the age of the Naashoibito Member; however, this date is less precise than the successful dating attempts reported in the body of the thesis. No justifiable selection of these points will produce a more precise age. Anomalous U-Pb analyses have a much larger compositional range: $^{238}U/^{206}Pb$ ratios vary between about 0 and 25, and $^{207}Pb/^{206}Pb$ ratios range between about 0.85 and 0.57. These analyses represent a sampling of the same veining represented by anomalous trace element analyses. The date produced by the inclusion of these anomalous analyses is 81.8±3.7 Ma (n=47, MSWD=5.3; Figure 2), significantly older than both the age of the host unit and the age of the first known Tyrannosaurus Rex.
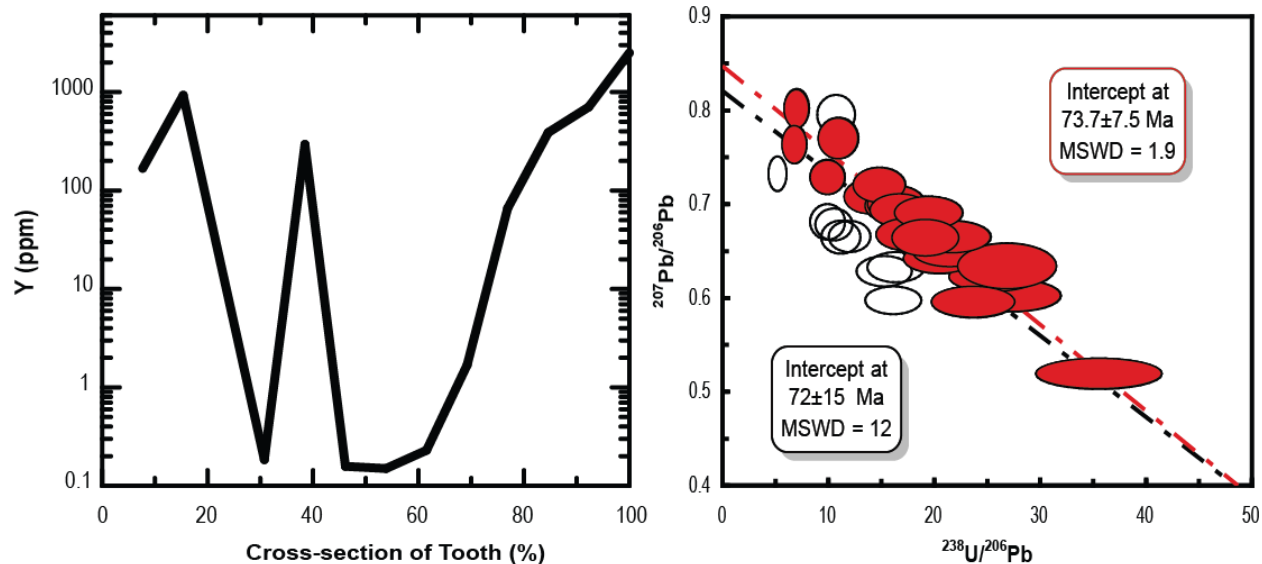
Figure 3: Cross-sectional Y profile for sample CE1 from the De-na-zin member of the Kirtland Formation, San Juan Basin, New Mexico, and associated Tera-Wasserburg plot of U-Pb analyses.

Sample CE1 shows more range in U-Pb composition: ^{238}U/^{206}Pb ratios vary between about 5 and 35, and ^{207}Pb/^{206}Pb ratios vary between about 0.81 and 0.5. When all analyses are considered together, a date of 72±15 Ma results (n=31, MSWD=12; Figure 3), however a selection which includes all but two analyses along the cross-section, and several consecutive analyses from the longitudinal section produces a more precise date of 73.7±7.5 Ma (n=22, MSWD=1.9; Figure 3). Both dates are consistent with the age of the host unit.

Discussion

According to the model proposed in this thesis, the high Y gradient preserved along the cross-section of these teeth (Pattern 2) suggests that these samples should preserve fossilisation-age signatures; the dates derived from these teeth broadly support this supposition. However, both dates, TR1 especially, are associated with very elevated uncertainties. For TR1, the high uncertainties originate from the lack of significant spread in the U-Pb data; a characteristic that is likely inherent to the system at the time of fossilisation. Low U uptake during fossilisation would produce little spread in ^{238}U/^{206}Pb

114

ratios. For CE1, which preserves meaningful spread in the U-Pb isotopic data (Figure 3), the high

uncertainties are derived from significant scatter about the 73.7 Ma reference line, possibly with a

secondary trend at lower $^{238}U/^{206}Pb$ and $^{207}Pb/^{206}Pb$ ratios. Most of the analyses significantly off the 73.7

Ma reference line are at the edges of the sample and in one discreet region of the longitudinal section,

suggesting the action of an alteration event at the edges, and possibly along an unidentified vein or

more porous region.

The anomalous U-Pb analyses in TR1 produce a date older than the host unit and any known

Tyrannosaurus Rex by about 16 Ma years, suggesting against the ~82.4 Ma date representing an age of

fossilisation. It has been reported that older dates can be produced when the fossil has been affected by

fluids with an older Pb composition (Romer, 2001). The 65±17 Ma date of the majority of the analyses is

within uncertainty of the 82.4±3.6 Ma date produced when anomalous analyses are included into the

calculation, which may imply that the entire tooth has been affected thus. However, without analyzing

other teeth from this unit, it is difficult to characterize the nature of the fossilisation and post-

fossilisation processes that this tooth might have experienced.

While the model presented in this thesis is broadly supported by these two additional teeth, the

high uncertainties in the dates provide a measure of caution. The restricted nature of post-fossilisation

alteration, as indicated by the Y profile, does not necessarily mean that a fossilisation-age signature will

be preserved with high precision. The scatter observed in the Y profile is likely reflective of the

heterogeneous nature of the samples, and may be a qualitative indicator of the likelihood that scatter

will also occur in the U-Pb isotopic data.

Additional processes clearly contribute to obscuring a precise date, and these processes proved

difficult to constrain when looking at single teeth. In the body of this thesis, widely variable processes

were found to occur in the Dinosaur Park Formation, Alberta, and the Arroyo Chijuillita Member, New

Mexico; it thus cannot be assumed that fossils in the Naashoibito Member or De-na-zin Member, New

Mexico, will have experienced a similar history to either of these units. Analyzing additional teeth from

the Naashoibito Member and the De-na-zin Member would thus be required to explain its fossilisation

and post-fossilisation history.

Table 1
Trace element concentrations in ppm measured by laser ablation ICP-MS along the cross-section of fossil tooth samples.

Sample ID	Ti	V	Cr	Mn	Fe	Ni	Cu	Zn	Rb	Sr	Y	Zr	La	Ce
Naashoibito Member														
TRI-1	36.1	17.4	1.42	1621	6577	0.58	4.77	25.2	0.357	2606	4662.6	103.2	679.9	1237.8
TRI-2	28.7	17.6	0.49	1756	600	0.27	1.66	20.6	0.094	2674	3473.2	96.8	233.1	285.4
TRI-3	26.3	17.3	0.57	1718	599	0.17	0.80	19.2	0.084	2465	2510.3	106.6	67.9	62.7
TRI-4	26.1	17.7	0.86	1799	570	0.48	1.50	18.7	0.07	2558	2212.1	117.3	29.7	20.8
TRI-5	24.6	11.2	1.47	1952	6417	0.46	1.19	10.3	0.161	1829	438.9	84.4	3.3	1.9
TRI-6	33.1	12.6	0.8	1955	9178	0.55	0.21	15.9	0.107	2301	291.7	154.6	11.0	3.2
TRI-7	31.7	11.8	0.84	1939	10656	0.70	-	15.2	0.046	2158	80.9	166.4	3.8	1.3
TRI-8	27.9	11.0	0.58	1930	9488	0.39	0.63	13.8	-	2132	71.8	144.4	2.4	0.5
TRI-9	12.1	7.1	0.87	1739	2130	0.40	0.17	11.7	0.042	2113	16.9	80.8	0.2	0.1
TRI-10	10.4	8.8	0.47	1791	2010	0.21	0.15	12.0	-	2170	12.0	74.0	0.2	0.1
TRI-11	93.3	11.5	0.53	1965	32312	0.84	0.19	14.3	-	2081	10.4	310.8	0.1	0.0
TRI-12	39.2	6.9	0.7	1869	13840	0.41	0.12	8.9	-	1616	5.0	125.5	0.1	0.0
TRI-13	14.1	7.0	0.51	2096	4185	0.39	0.19	10.2	-	1905	4.9	79.2	0.1	0.1
TRI-14	11.4	7.7	1.29	2112	3304	0.36	0.16	10.8	0.05	1862	5.0	69.3	0.3	0.5
TRI-15	12.4	7.1	0.72	1699	4560	0.25	0.18	8.0	-	1755	5.1	75.4	0.5	0.1
TRI-16	15.8	9.2	1.1	2151	6108	0.46	0.77	10.3	0.213	1756	9.1	62.8	1.6	0.3
TRI-17	13.9	10.0	1.32	1842	3065	0.38	0.37	10.0	0.26	1776	11.1	63.7	2.3	0.4
TRI-18	16.2	14.8	0.72	1701	3958	0.28	2.96	10.0	0.419	1828	22.2	54.2	8.4	1.3
TRI-19	12.1	19.7	0.74	2004	7669	0.29	0.33	10.2	0.058	1724	20.9	52.9	9.3	1.5
TRI-20	136.7	28.7	1.84	3340	103211	0.93	18.06	5.1	3.17	503	8.7	87.4	14.7	2.4
TRI-21	126.5	15.0	2.21	7138	22040	0.65	4.67	2.3	5.23	447	7.4	31.9	14.3	3.5
TRI-22	19.9	9.6	1.11	2193	17111	0.38	3.57	10.1	-	1638	19.2	56.1	9.3	2.4
TRI-23	27.3	6.3	0.79	2067	9642	0.51	0.30	9.6	-	1718	62.9	62.2	36.0	17.1
TRI-24	23.5	6.1	0.73	1729	5917	0.26	0.29	9.2	0.175	1771	95.9	35.6	62.9	36.2
TRI-25	99.1	26.5	2.42	7136	22270	3.63	0.66	5.0	5.91	422	65.5	61.1	75.2	39.3
TRI-26	18.0	3.8	1.18	1300	4456	0.24	0.47	7.3	0.806	1395	274.2	18.5	149.1	136.4
TRI-27	35.3	6.6	0.69	1947	14638	0.74	2.25	10.8	0.185	1639	253.0	51.6	138.1	127.5
TRI-28	13.8	4.9	0.84	1397	2979	0.26	1.03	12.2	0.064	1772	397.2	25.0	182.0	187.5
TRI-29	16.4	4.4	0.51	1656	4036	0.40	0.23	11.9	2.91	1853	1149.0	25.7	142.4	112.6
TRI-30	16.1	4.9	0.75	1774	7505	0.27	0.20	13.4	3.93	1773	349.8	27.8	35.3	24.2
TRI-31	10.1	5.2	0.59	1651	548	0.27	0.23	14.9	0.123	2023	338.2	31.6	21.5	7.4
TRI-32	10.5	5.4	0.5	1682	6656	0.29	0.12	16.9	1.79	2005	664.0	27.8	151.2	83.4
TRI-33	45.7	7.4	-	1538	14274	0.47	0.38	18.5	0.72	2077	3607.1	87.8	1474.7	1948.9
TRI-34	314.4	71.6	2.82	1830	432532	2.58	15.46	16.9	6.53	1021	1654.9	163.8	603.4	1073.1
TRI-35	18.1	7.8	0.75	1494	4166	0.18	0.29	18.4	2.75	2042	2646.6	40.7	282.6	183.5
TRI-36	8.7	2.9	1.69	27041	5138	0.76	2.34	1.7	0.798	473	111.7	8.2	35.8	65.0

Table 1 (*continued*)

Naashoibito Member

Sample ID	Pr	Nd	Sm	Eu	Gd	Tb	Dy	Ho	Er	Tm	Yb	Lu	Pb	Th	U
TR1-1	125.19	652.8	169.8	46.1	327.2	53.6	423.5	102.2	296.4	38.3	224.9	34.9	29.39	0.82	32.35
TR1-2	33.00	173.9	46.2	14.69	122.2	22.88	215.0	60.4	199.7	28.6	180.3	30.2	23.74	0.51	31.77
TR1-3	6.40	34.87	9.55	3.72	38.60	8.94	107.2	36.9	141.6	22.8	155.1	26.7	24.22	1.30	32.79
TR1-4	1.96	10.60	2.83	1.34	16.62	4.71	69.0	27.6	118.4	20.7	148.1	26.4	24.48	1.22	32.27
TR1-5	0.14	0.76	0.181	0.09	1.24	0.44	8.38	4.40	23.30	4.62	37.52	7.14	17.79	0.57	32.48
TR1-6	0.21	0.80	0.097	0.05	0.68	0.16	3.05	1.79	10.28	2.16	18.18	3.67	22.07	0.24	29.33
TR1-7	0.09	0.35	-	0.02	0.18	0.04	0.61	0.37	2.34	0.55	4.66	1.03	20.32	0.91	30
TR1-8	0.03	0.10	-	0.01	0.10	0.02	0.42	0.30	2.02	0.47	4.42	0.93	20.81	0.21	28.99
TR1-9	0.01	-	-	-	-	-	0.06	0.05	0.43	0.12	1.24	0.27	18.75	0.76	25.88
TR1-10	0.01	0.03	-	-	-	-	0.04	0.04	0.32	0.07	0.92	0.22	18.13	0.87	25.55
TR1-11	0.01	-	-	-	0.02	0.00	0.04	0.04	0.25	0.07	0.77	0.21	26.89	2.19	25.38
TR1-12	-	0.02	-	-	-	0.00	0.03	0.02	0.13	0.04	0.43	0.11	15.56	0.28	27.66
TR1-13	0.01	0.02	-	-	0.02	0.00	0.03	0.02	0.10	0.04	0.39	0.10	18.38	0.06	25.5
TR1-14	0.02	0.06	-	0.01	-	0.00	0.05	0.02	0.11	0.03	0.40	0.09	17.72	0.87	27.03
TR1-15	0.01	0.04	-	-	-	-	0.06	0.02	0.13	0.02	0.26	0.06	17.18	0.06	26.58
TR1-16	0.02	0.10	-	-	0.08	0.01	0.13	0.05	0.20	0.03	0.30	0.06	15.72	0.54	27.23
TR1-17	0.03	0.08	-	0.01	0.08	0.01	0.13	0.06	0.23	0.04	0.33	0.07	16.37	0.46	26.62
TR1-18	0.06	0.25	-	0.02	0.13	0.02	0.29	0.12	0.47	0.07	0.50	0.09	15.73	0.75	31.63
TR1-19	0.08	0.28	-	0.02	0.18	0.01	0.25	0.11	0.44	0.06	0.45	0.10	16.40	0.23	43.05
TR1-20	0.15	0.51	0.081	0.03	0.11	0.01	0.11	0.03	0.13	0.02	0.14	0.02	50.21	1.00	105.7
TR1-21	0.21	0.77	0.121	0.03	0.10	0.02	0.13	0.03	0.12	0.02	0.13	0.02	17.35	1.49	46.74
TR1-22	0.11	0.48	0.065	0.04	0.24	0.04	0.34	0.13	0.44	0.06	0.33	0.08	19.68	0.71	26.02
TR1-23	1.19	4.74	0.701	0.28	2.23	0.27	2.08	0.60	1.74	0.20	1.07	0.19	15.81	0.58	24.96
TR1-24	2.76	11.34	1.737	0.66	4.68	0.56	4.10	1.08	2.95	0.33	1.68	0.28	12.93	0.98	25.52
TR1-25	2.58	9.75	1.122	0.40	3.05	0.32	2.23	0.67	1.80	0.20	1.02	0.15	18.81	0.93	17.81
TR1-26	13.28	58.11	11.18	3.62	23.81	3.11	20.04	4.49	11.28	1.20	5.44	0.80	12.25	0.32	23.28
TR1-27	12.56	55.70	11.09	3.51	23.47	2.97	19.54	4.28	10.52	1.10	5.25	0.77	15.46	0.12	23.19
TR1-28	19.68	89.25	18.88	6.12	37.95	5.17	34.45	7.39	18.31	1.96	9.28	1.32	13.74	0.41	23.21
TR1-29	11.42	52.04	10.43	3.37	27.05	4.52	41.91	13.37	47.37	6.81	41.76	7.18	16.82	0.87	22.17
TR1-30	2.37	10.51	2.12	0.67	5.58	0.96	9.52	3.41	13.36	2.07	13.83	2.61	16.17	0.50	25.01
TR1-31	0.52	2.27	0.35	0.14	1.84	0.39	5.09	2.42	11.12	1.89	13.58	2.65	18.65	1.80	27.27
TR1-32	6.33	26.34	3.66	1.28	13.67	2.08	21.06	7.47	27.71	4.10	25.78	4.77	19.98	0.15	29.81
TR1-33	180.8	822.5	173.4	49.2	297.3	43.2	305.8	70.8	192.8	23.6	128.7	19.2	20.68	1.02	27.03
TR1-34	115.0	533.7	121.9	36.4	180.9	26.1	176.7	37.8	97.9	11.7	62.7	9.1	154.7	0.90	47.58
TR1-35	17.4	79.0	15.4	5.1	50.3	9.1	93.8	31.9	112.1	16.6	101.7	17.5	21.65	0.77	32.57
TR1-36	8.04	37.59	9.43	2.88	13.37	2.19	15.23	3.19	8.56	1.06	6.59	0.94	2.35	0.82	5.84

Table 1 (*continued*)

Sample ID	Ti	V	Cr	Mn	Fe	Ni	Cu	Zn	Rb	Sr	Y	Zr	La	Ce
De-na-zin Member														
CEIL-1	103.6	23.42	29	6630	1674	2.2	9.57	53.6	-	2435	550	3.06	147	296
CEIL-2	99	58.2	29.55	5901	1823	2.59	2.09	42.5	-	2655	94.5	0.645	24.7	44.4
CEIL-3	96.2	42.7	30.3	6450	1563	2.3	10	45.5	-	2240	15.03	0.228	3.15	5.96
CEIL-4	96	41.18	12.13	8890	984	2.76	7.08	63.3	-	2085	0.083	0.022	0.0407	0.028
CEIL-5	99.5	50.1	29.3	6540	1264	2.27	53.3	45.7	-	2351	13.3	0.337	2.44	4.7
CEIL-6	98.2	55.6	37.3	5730	2120	2.04	3.29	33.3	-	2540	76.1	0.99	18.5	30.9
CEIL-7	96.3	58.8	35.7	5790	1260	1.74	30.6	30.2	-	2565	98	1.4	26.3	46
CEIL-8	97.8	78.2	41.2	6050	1537	1.71	10.8	30.9	-	2603	44	0.59	11.8	20.4
CEIL-9	98.1	68.5	31.2	6090	1037	1.63	42.8	29.5	-	2580	215	2.1	56.1	102.3
CEIL-10	95.1	47.48	27.71	6180	790	1.34	27.8	29.1	-	2563	256	1.051	62.2	121.6
CEIL-11	96.8	48.9	18.2	6190	953	1.55	23.1	28	-	2580	136.5	0.99	36.2	64.8
CEIL-12	97.1	53.88	10.43	5964	831	1.47	17	28.4	0.17	2547	86.2	0.79	21.9	35.6
CEIL-13	99.1	62.5	16.52	6570	1630	1.68	5.47	30.2	-	2546	11.2	0.161	2.49	3.9
CEIL-14	97.3	70.2	22.1	6550	1454	-	-	33.5	-	2430	-	-	-	-
CEIL-15	95.6	42.5	18.06	6980	1543	1.81	11.8	28.6	-	2441	0.0382	0.076	0.0241	-
CEIL-16	98.9	44.9	29.7	7000	897	-	17.2	27.5	-	2439	-	-	-	-
CEIL-17	99.8	30.8	57.9	7440	951	-	18.4	26.1	-	2610	-	-	-	-
CEIL-18	100.5	33.2	74.9	7410	955	1.315	28.8	28.8	0.083	2570	238	0.85	53.9	107
CEIL-19	101.6	61.5	38.1	7490	1191	2.34	49.9	36	0.35	2659	1010	5.4	284	579
CEIX-1	97.5	2.19	1.45	926	283	1.3	9.9	61.2	0.32	2130	168	1.71	45	122
CEIX-2	99.1	22.2	27	5890	1588	1.55	28	47.6	-	2597	928	4.09	245	583
CEIX-3	96.4	52.2	5	9426	963	3.9	13.96	111.8	-	1538	-	-	0.044	0.045
CEIX-4	99.2	112.8	8.18	8670	781	2.33	26.4	113.9	-	1434	0.185	-	0.046	-
CEIX-5	100.2	43.5	7.43	5710	2110	1.25	15.6	37.9	-	2554	294	1.57	85.4	174
CEIX-6	100.5	85.3	7.02	8430	1056	2.22	17.66	72.7	-	1589	0.158	0.044	0.069	0.063
CEIX-7	97.3	151	15.07	5420	3250	4.14	2.64	47.1	-	2524	0.15	0.079	0.024	0.021
CEIX-8	97.3	59.2	6.66	6240	1140	2.93	1.66	37.1	-	2480	0.23	0.074	0.0371	0.016
CEIX-9	100.1	87	14.16	6490	1492	3.05	0.827	35.2	-	2483	1.69	0.084	0.51	0.93
CEIX-10	99.1	50.4	19.44	6317	1250	1.41	10.9	33.07	-	2511	66	0.34	17.3	33.3
CEIX-11	96.7	45.6	25.8	6240	1233	1.53	25.3	38	-	2631	388	1.396	111.8	231.4
CEIX-12	100.5	36.8	58.2	6360	912	1.31	37	41.4	-	2756	706	2.09	195.8	417
CEIX-13	101.5	14.4	12.4	5570	792	1.05	41.3	34.8	0.33	3037	2500	7.7	791	1900

Table 1 (*continued*)

De-na-zin Member

Sample ID	Pr	Nd	Sm	Eu	Gd	Tb	Dy	Ho	Er	Tm	Yb	Lu	Pb	Th	U
CEIL-1	41	196	56	11.9	73	10.9	65	11.9	31.1	3.92	23.2	3.73	51	-	181
CEIL-2	5.37	25.2	5.66	1.44	8.8	1.34	9.34	2.15	6.12	0.811	4.76	0.714	16.47	-	102.1
CEIL-3	0.736	3.54	0.86	0.311	1.26	0.2	1.53	0.298	1	0.133	0.875	0.12	22.6	-	214
CEIL-4	-	0.027	-	0.083	0.01	0.0029	-	-	-	-	-	-	31.17	-	289
CEIL-5	0.61	2.66	0.74	0.201	0.94	0.143	1.21	0.305	0.88	0.123	0.69	0.122	18.7	-	207
CEIL-6	3.64	17.34	3.84	0.96	6.63	0.923	7.07	1.64	5.1	0.659	3.93	0.598	16.9	-	149
CEIL-7	5.2	25.7	5.8	1.49	10	1.42	10	2.07	5.4	0.65	3.7	0.52	17.8	-	116
CEIL-8	2.36	11	2.67	0.7	4.6	0.65	4.1	0.9	2.53	0.292	1.66	0.232	17.4	-	131
CEIL-9	12.34	58.3	14.2	3.49	22.6	3.33	22	4.47	11.85	1.43	8.11	1.1	11.53	-	55.2
CEIL-10	15.5	75.2	18.8	4.51	28.3	4.29	28.4	5.37	13.19	1.62	8.54	1.223	11.02	-	46.5
CEIL-11	7.92	37	8.24	2.13	13.7	1.99	14.1	2.97	8.13	1.039	5.96	0.823	10.89	-	61.9
CEIL-12	4.09	19.4	3.99	1.08	6.96	1.07	7.71	1.71	5.15	0.65	3.99	0.53	10.46	-	66.6
CEIL-13	0.42	2.02	0.42	0.19	0.74	0.121	0.89	0.194	0.61	0.087	0.47	0.081	16.3	-	133.6
CEIL-14	-	-	-	-	-	-	-	-	-	-	-	-	16.2	-	118.1
CEIL-15	-	-	-	0.0746	0.018	-	-	-	-	-	-	-	8.95	-	38.96
CEIL-16	-	-	-	-	-	-	-	-	-	-	-	-	7.51	-	21.2
CEIL-17	-	-	-	-	-	-	-	-	-	-	-	-	8.53	-	9.99
CEIL-18	13.6	64.7	17	4.16	27	3.95	24.7	4.42	10.4	1.29	6.5	0.88	9.49	-	28.4
CEIL-19	77	370	98	22.3	145	20.2	116	20.2	46.9	5.24	28.5	4	11.26	-	53.4
CEIX-1	15.8	68	21	4.9	27	4.2	25	3.9	8.3	0.93	4.7	0.61	15.9	0.17	10.1
CEIX-2	86	403	120	25.4	149	22.4	130	21	51.9	6.21	35.9	5.51	25.4	0.0267	126.8
CEIX-3	-	-	-	0.12	-	-	-	-	-	-	-	-	9.75	-	145.7
CEIX-4	-	-	-	0.11	-	-	-	-	-	-	-	-	6.48	-	171.5
CEIX-5	22.3	104.6	26.2	6.06	39.4	5.62	35	6.55	15.88	1.939	10.66	1.399	12.53	-	73.9
CEIX-6	-	-	-	0.134	-	-	-	-	-	-	-	-	6.89	-	162.4
CEIX-7	-	-	-	0.041	-	-	-	-	-	-	-	-	17.8	-	160.2
CEIX-8	-	-	-	0.078	-	-	-	-	-	-	-	-	5.62	-	117.3
CEIX-9	0.112	0.45	0.165	0.093	0.156	0.024	0.167	0.0191	0.094	-	-	-	13.77	-	103.2
CEIX-10	3.95	18.5	4.43	1.19	7.41	1.14	7.2	1.45	3.62	0.48	2.64	0.365	12.32	-	101.9
CEIX-11	30.24	143.1	37.7	9.19	56.6	8.01	47.3	8.13	18.26	2.07	10.99	1.367	11.12	-	68
CEIX-12	55	266	70.9	16.81	104.5	14.77	86.9	14.96	31.8	3.37	17.26	2.18	11.64	-	68.7
CEIX-13	270	1340	389	79	485	68.5	390	64.5	147	17.1	92	14.1	30.6	1.26	52.1

Table 2
U-Pb laser ablation ICP-MS results for Durango apatite standard for each session.

Sample ID	^{206}Pb (cps)	^{204}Pb (cps)	$\frac{^{238}U}{^{206}Pb}$ meas.	1 SE	$\frac{^{207}Pb}{^{206}Pb}$ meas.	1 SE	f_{206}	$1-f_{206}$	$\frac{^{206}Pb}{^{238}U}$ corr.	$\frac{^{206}Pb}{^{238}U}$ age (Ma)	1 SE
Session 1 - Naashoibito Member											
Durango-1	27809	1950	124.04	1.23	0.221	0.0025	0.385	0.615	0.00496	31.9	0.5
Durango-2	27451	1899	125.91	1.14	0.210	0.0027	0.209	0.791	0.00628	40.4	0.5
Durango-3	34049	2423	117.18	0.86	0.207	0.0014	0.206	0.794	0.00678	43.6	0.4
Durango-4	35528	2214	122.12	0.76	0.204	0.0013	0.202	0.798	0.00654	42.0	0.3
Durango-5	36433	2115	122.08	1.11	0.205	0.0014	0.203	0.797	0.00653	42.0	0.5
Durango-6	43748	2621	124.20	0.91	0.207	0.0021	0.206	0.794	0.00640	41.1	0.4
Durango-7	32798	2181	122.15	1.50	0.207	0.0030	0.206	0.794	0.00650	41.8	0.6
Durango-8	32141	2094	125.00	0.96	0.203	0.0012	0.200	0.800	0.00640	41.1	0.4
Durango-9	38032	2336	124.56	0.63	0.204	0.0008	0.202	0.798	0.00641	41.2	0.3
Session 2 - De-na-zin Member											
Durango-1	1000	555	106.71	2.16	0.412	0.0090	0.462	0.538	0.00504	32.4	1.22
Durango-2	4309	614	141.14	0.95	0.227	0.0034	0.228	0.772	0.00547	35.2	0.31
Durango-3	4389	525	141.27	1.19	0.233	0.0029	0.235	0.765	0.00542	34.8	0.38
Durango-4	4338	662	141.24	1.08	0.229	0.0040	0.230	0.770	0.00545	35.0	0.35
Durango-5	4366	692	140.59	1.10	0.226	0.0048	0.227	0.773	0.00550	35.3	0.36
Durango-6	4193	660	142.05	1.25	0.237	0.0046	0.241	0.759	0.00534	34.4	0.40
Durango-7	4840	582	138.65	1.42	0.198	0.0027	0.192	0.808	0.00583	37.5	0.47
Durango-8	4609	539	146.14	1.38	0.183	0.0025	0.172	0.828	0.00566	36.4	0.41
Durango-9	4919	497	144.31	1.24	0.185	0.0033	0.174	0.826	0.00572	36.8	0.38
Durango-10	4977	905	134.24	1.26	0.188	0.0026	0.179	0.821	0.00612	39.3	0.45
Durango-11	4264	202	149.55	1.13	0.219	0.0043	0.218	0.782	0.00523	33.6	0.32
Durango-12	4277	290	146.05	0.76	0.225	0.0024	0.226	0.774	0.00530	34.1	0.23
Durango-13	4220	277	147.58	1.20	0.219	0.0035	0.218	0.782	0.00530	34.1	0.35
Durango-14	4065	284	150.34	1.22	0.218	0.0032	0.217	0.783	0.00521	33.5	0.35
Durango-15	4082	433	144.33	1.44	0.226	0.0047	0.227	0.773	0.00535	34.4	0.44
Durango-16	3957	369	147.08	1.30	0.219	0.0035	0.218	0.782	0.00532	34.2	0.39
Durango-17	3955	370	147.42	1.18	0.225	0.0042	0.225	0.775	0.00526	33.8	0.35
Durango-18	4045	323	149.60	1.26	0.228	0.0067	0.230	0.770	0.00515	33.1	0.36
Durango-19	3893	343	149.98	1.08	0.226	0.0039	0.226	0.774	0.00516	33.2	0.31

Table 3
U-Pb laser ablation ICP-MS results for the cross-sections of fossil Tyrannosaurus Rex tooth TR1 from the Naashoibito Member, San Juan Basin, and ceratopsid tooth CE1 from the De-na-zin Member, San Juan Basin.

Sample ID	^{206}Pb (cps)	^{204}Pb (cps)	$\frac{^{238}U}{^{206}Pb}$ meas.	1 SE	$\frac{^{207}Pb}{^{206}Pb}$ meas.	1 SE	f_{206}	$1\text{-}f_{206}$	$\frac{^{206}Pb}{^{238}U}$ corr.	$\frac{^{206}Pb}{^{238}U}$ age (Ma)	1 SE
Session 1 - **Naashoibito Member**											
TR1-1	255691	13403	2.80	0.08	0.816	0.00086	0.956	0.044	0.0162	103.5	61.8
TR1-2	148474	7997	3.04	0.07	0.810	0.00090	0.948	0.052	0.0173	110.5	46.0
TR1-3	133171	4911	3.30	0.12	0.808	0.00175	0.946	0.054	0.0168	107.1	70.3
TR1-4	168020	8857	3.00	0.10	0.811	0.00063	0.949	0.051	0.0176	112.3	68.8
TR1-5	133481	7004	3.04	0.09	0.809	0.00077	0.946	0.054	0.0178	113.9	58.1
TR1-6	169272	8725	3.05	0.07	0.809	0.00076	0.946	0.054	0.0178	113.7	46.9
TR1-7	151555	7837	3.23	0.06	0.804	0.00095	0.940	0.060	0.0187	119.5	38.8
TR1-8	154588	7718	3.34	0.09	0.805	0.00078	0.942	0.058	0.0177	113.2	50.2
TR1-9	166063	8440	3.25	0.04	0.808	0.00062	0.946	0.054	0.0168	107.5	25.2
TR1-10	141922	7182	3.36	0.10	0.803	0.00048	0.939	0.061	0.0184	117.5	55.4
TR1-11	144557	7323	3.00	0.09	0.805	0.00070	0.941	0.059	0.0196	125.0	66.2
TR1-12	146790	7410	3.06	0.05	0.804	0.00058	0.941	0.059	0.0195	124.4	34.0
TR1-13	151755	7695	3.12	0.05	0.803	0.00076	0.940	0.060	0.0195	124.5	33.2
TR1-14	135986	6682	3.67	0.06	0.793	0.00049	0.927	0.073	0.0201	128.3	26.1
TR1-15	116958	5783	3.95	0.05	0.794	0.00074	0.928	0.072	0.0182	116.5	22.1
TR1-16	118986	5818	4.87	0.11	0.781	0.00084	0.912	0.088	0.0179	114.1	28.7
TR1-17	176557	8629	5.19	0.18	0.790	0.00150	0.923	0.077	0.0152	97.0	42.6
TR1-18	113252	5498	12.87	1.87	0.788	0.00434	0.921	0.079	0.0108	69.1	71.8
TR1-19	300568	15447	2.72	0.08	0.805	0.00117	0.942	0.058	0.0218	138.9	71.8
TR1-20	153968	7805	3.89	0.08	0.797	0.00048	0.931	0.069	0.0179	114.2	32.4
TR1-21	115091	5930	3.79	0.09	0.803	0.00070	0.939	0.061	0.0163	104.1	40.3
TR1-22	136303	6906	3.63	0.06	0.803	0.00071	0.939	0.061	0.0168	107.6	26.6
TR1-23	130130	6591	4.25	0.08	0.800	0.00049	0.935	0.065	0.0152	97.4	27.7
TR1-24	112573	8939	8.57	0.55	0.741	0.00900	0.862	0.138	0.0161	102.7	46.9
TR1-25	26262	1292	4.97	0.18	0.790	0.00179	0.923	0.077	0.0155	99.3	46.6
TR1-26	113882	5773	4.27	0.07	0.804	0.00066	0.941	0.059	0.0138	88.6	25.2
TR1-27	112087	5649	4.51	0.08	0.802	0.00072	0.937	0.063	0.0139	88.8	23.6
TR1-28	94627	4678	4.87	0.15	0.800	0.00075	0.936	0.064	0.0132	84.5	39.8
TR1-29	5367	303	0.95	0.09	0.835	0.00582	0.979	0.021	0.0220	140.1	598
TR1-30	162291	8292	3.49	0.08	0.812	0.00093	0.950	0.050	0.0142	90.9	39.8
TR1-31	149258	7586	4.18	0.08	0.805	0.00074	0.942	0.058	0.0138	88.5	30.4
TR1-32	117818	5983	3.78	0.11	0.808	0.00082	0.946	0.054	0.0143	91.7	47.7
TR1-33	134007	6766	3.76	0.21	0.809	0.00056	0.947	0.053	0.0142	90.6	92.9
TR1-34	169054	8589	3.62	0.03	0.811	0.00049	0.949	0.051	0.0140	89.8	16.1
TR1-35	53088	2387	8.64	0.28	0.740	0.00265	0.861	0.139	0.0161	103.2	23.4
TR1-36	163173	8022	4.77	0.14	0.789	0.00116	0.922	0.078	0.0164	104.5	40.1
TR1-37	117371	5235	8.96	0.26	0.727	0.00153	0.845	0.155	0.0173	110.4	20.8
TR1-38	7109	262	1.53	0.06	0.834	0.00393	0.977	0.023	0.0149	95.1	172
TR1-39	144024	7411	3.50	0.04	0.815	0.00082	0.954	0.046	0.0132	84.8	20.8

Table 3 (*continued*)

Sample ID	^{206}Pb (cps)	^{204}Pb (cps)	$\frac{^{238}U}{^{206}Pb}$ meas.	1 SE	$\frac{^{207}Pb}{^{206}Pb}$ meas.	1 SE	f_{206}	$1-f_{206}$	$\frac{^{206}Pb}{^{238}U}$ corr.	$\frac{^{206}Pb}{^{238}U}$ age (Ma)	1 SE
Session 1 - Naashoibito Member											
TR1-40	129755	6646	3.63	0.09	0.811	0.00070	0.949	0.051	0.0142	90.7	45.7
TR1-41	128881	6629	3.05	0.04	0.810	0.00068	0.948	0.052	0.0172	109.7	30.3
TR1-42	142378	7333	2.94	0.04	0.815	0.00093	0.954	0.046	0.0157	100.5	32.0
TR1-43	114664	5827	3.85	0.05	0.809	0.00077	0.947	0.053	0.0137	87.8	19.9
TR1-44	144014	7273	3.75	0.04	0.806	0.00060	0.943	0.057	0.0151	96.7	19.9
TR1-45	152193	7731	3.37	0.05	0.809	0.00080	0.947	0.053	0.0157	100.7	27.1
TR1-46	35878	1320	20.31	0.43	0.589	0.00511	0.673	0.327	0.0161	102.9	6.6
TR1-47	125620	6387	3.15	0.04	0.814	0.00090	0.953	0.047	0.0151	96.6	23.1
TR1-48	124393	6199	3.50	0.05	0.809	0.00075	0.947	0.053	0.0153	97.7	25.7
Session 2 - De-na-zin Member											
CE1L-1	731490	33160	13.13	0.09	0.708	0.00094	0.834	0.166	0.0127	81.1	3.36
CE1L-2	433549	18247	20.03	0.17	0.656	0.00115	0.767	0.233	0.0116	74.4	2.72
CE1L-3	289817	11384	27.43	0.20	0.603	0.00172	0.700	0.300	0.0109	70.1	1.67
CE1L-4	339857	15342	25.63	0.12	0.623	0.00088	0.726	0.274	0.0107	68.6	1.15
CE1L-5	238083	10617	20.50	0.07	0.653	0.00082	0.763	0.237	0.0115	74.0	1.00
CE1L-6	381791	17402	16.15	0.21	0.699	0.00134	0.822	0.178	0.0110	70.8	5.05
CE1L-7	208831	9308	16.37	0.09	0.633	0.00087	0.738	0.262	0.0160	102.2	2.05
CE1L-8	194011	8665	15.27	0.31	0.629	0.00102	0.733	0.267	0.0175	111.7	8.30
CE1L-9	145258	7077	10.51	0.12	0.678	0.00074	0.796	0.204	0.0194	123.9	6.85
CE1L-10	148232	7179	11.99	0.04	0.666	0.00067	0.780	0.220	0.0184	117.3	1.83
CE1L-11	145734	7244	20.51	0.13	0.642	0.00063	0.750	0.250	0.0122	78.0	1.91
CE1L-12	307307	14782	16.42	0.11	0.701	0.00159	0.824	0.176	0.0107	68.7	2.63
CE1L-13	211789	10623	14.82	0.11	0.721	0.00103	0.849	0.151	0.0102	65.2	3.07
CE1L-14	113312	6505	10.72	0.12	0.795	0.00163	0.944	0.056	0.0053	33.8	6.60
CE1L-15	117189	6837	7.00	0.06	0.802	0.00122	0.952	0.048	0.0068	43.7	8.08
CE1L-16	145346	8359	6.80	0.07	0.764	0.00166	0.904	0.096	0.0141	90.4	9.49
CE1L-17	179920	9257	9.91	0.10	0.681	0.00183	0.799	0.201	0.0202	129.2	6.35
CE1L-18	201126	9270	11.17	0.08	0.665	0.00135	0.779	0.221	0.0198	126.4	4.24
CE1X-1	99422	5323	5.18	0.05	0.732	0.00088	0.864	0.136	0.0262	166.8	10.9
CE1X-2	504980	22669	16.73	0.18	0.694	0.00078	0.815	0.185	0.0110	70.7	4.21
CE1X-3	280691	10938	23.70	0.25	0.596	0.00165	0.692	0.308	0.0130	83.3	2.80
CE1X-4	179457	6327	35.54	0.44	0.519	0.00208	0.595	0.405	0.0114	73.0	2.22
CE1X-5	234041	10335	21.49	0.12	0.650	0.00091	0.760	0.240	0.0112	71.7	1.62
CE1X-6	217181	9857	17.41	0.15	0.668	0.00092	0.783	0.217	0.0125	80.0	3.17
CE1X-7	231602	9976	26.85	0.62	0.634	0.00383	0.740	0.260	0.0097	62.1	5.48
CE1X-8	154808	7178	21.74	0.20	0.665	0.00095	0.779	0.221	0.0102	65.1	2.75
CE1X-9	105083	6282	10.95	0.22	0.770	0.00222	0.912	0.088	0.0080	51.5	11.6
CE1X-10	339888	15586	19.46	0.18	0.691	0.00076	0.812	0.188	0.0097	62.1	2.98
CE1X-11	213344	10246	19.18	0.13	0.664	0.00214	0.778	0.222	0.0116	74.1	2.28
CE1X-12	203327	8635	16.12	0.07	0.598	0.00044	0.694	0.306	0.0190	121.2	1.80
CE1X-13	331848	16016	9.92	0.04	0.729	0.00084	0.860	0.140	0.0141	90.4	2.71

References

Fassett, J. E. (2009) New geochronologic and stratigraphic evidence confirms the paleocene age of the dinosaur-bearing Ojo Alamo sandstone and animas formation in the San Juan Basin, New Mexico and Colorado. *Palaeontol. Electronica* **12(1),** 3A, 150p.

Romer R. L. (2001) Isotopically heterogeneous initial Pb and continuous 222Rn loss in fossils: The U-Pb systematics of Brachiosaurus brancai. *Geochim. Cosmochim. Acta* **65(22)**, 4201-4213.

Williamson T. E. and Brusatte S. L. (2014) Small Theropod Teeth from the Late Cretaceous of the San Juan Basin, Northwestern New Mexico and Their Implications for Understanding Latest Cretaceous Dinosaur Evolution. *PLoS ONE* **9(4)**, 93190.